

A Thesis for the Degree of Ph.D. in Engineering

Design of a Retrofitted Pilot-controlled System
to Conduct Flight-deck Interval Management

February 2020

Graduate School of Science and Technology
Keio University

Timo Mario Riedel

ABSTRACT

This thesis explores Flight-deck Interval Management (FIM), an airborne self-spacing technology to ensure the safe and efficient operation of aircraft in highly utilized airspace by speed control. Leading research on FIM was conducted by the National Aeronautics and Space Administration (NASA), who proposed the current control logic ASTAR, and designed the dedicated avionics for FIM. However, industry demand and the wish to demonstrate the technology earlier called for a paradigm change from a fully automated, to a retrofitted, pilot-controlled system. In early 2017, NASA concluded their research on FIM with a flight test that revealed that the current control logic issues too many speed commands, and thereby causes too much workload for the pilots. Therefore, it was recommended to explore alternative control logics to achieve operational implementation.

The aim and originality of this thesis is in the proposal, optimization, and testing of a new, easy-to-integrate control logic, called IM-SP, that uses an original two-staged rule-based speed plan modification concept, which employs performance and pilot workload related decision factors. Focus was given on the reduction of speed commands and other findings made by NASA during their test. Optimization was achieved using evolutionary algorithms, and a flight simulator evaluation, involving airline and test pilots, was conducted. It is envisioned that the results of this thesis will provide the FIM research community with tools and ideas to bring FIM toward operational implementation, so that the time and performance goals of global and national airspace improvement initiatives are met.

Chapter 1 introduces the current research matter, motivation for the topic, and the thesis structure.

Chapter 2 explains the concepts and history of FIM in further detail and gives a description of the ASTAR control logic along an in-depth analysis of the issues found in the ATD-1 flight test. Further, other models and concepts important to this thesis are presented.

Chapter 3 shows the research results of multiple feasibility studies using large-scale Monte Carlo simulations of aircraft using ASTAR based FIM on arrivals in Tokyo International Airport. These simulations were used to investigate the spacing performance and speed control behavior of ASTAR and to ensure arrival route compatibility under local environmental conditions.

Chapter 4 introduces the IM-SP concept and describes its design principles and two-staged selection-algorithm. Two benchmark studies are shown, comparing the performance of ASTAR to IM-SP.

Chapter 5 describes an optimization study of IM-SP, using Particle Swarm Optimization to improve the selection logic for an improved spacing performance, user friendliness and ecology. Two distinctive results, a spacing performance optimal, and a fuel performance improved solution, are shown in detail.

Chapter 6 presents the setup and results of the flight simulator evaluation in which airline and certified test pilots evaluated FIM, ASTAR and IM-SP in an Airbus A320 flight simulator, recreating the ATD-1 flight test environment. Pilots' comments are provided and further observations are presented

Chapter 7 concludes this paper with a summary of the research achievements and an outlook on future research tasks, including potential enhancements for FIM.

ACKNOWLEDGEMENT

The following thesis is the result of three years research at Keio University in Yokohama, Japan. By looking at my name you might have (correctly) guessed that I am not Japanese, in fact I am German, and boy do I look German, actually so much that I was regularly invited to appear on Japanese television to represent my home country and portray German characters. Nevertheless, whenever I attended a conference, I took pleasure in turning the tables and starting my presentations with the words “My name is Timo and as you can obviously see: I come from Japan.” The usual reaction was a mixture of confusion and laughter, but at least I had everyone’s attention.

Jokes aside, the reason why I am mentioning this is that these three years actually mark the second part and conclusion of a six and a half years stay in Japan, that all started with a scholarship to explore the Japanese language and society and should finish in me obtaining my doctoral degree in this beautiful country.

Needless to say, this time has become a very memorable, and, for the most time, very enjoyable part of my life. Therefore, I feel it is appropriate not only to thank those persons that have had an impact on this thesis, but also those that supported and encouraged me throughout this time and without I wouldn’t be where I am today. This is to you:

First, I would like to thank my thesis advisor Prof. Masaki Takahashi for his insight and support throughout this thesis. I think I was lucky to have an advisor like him who would accommodate my needs as a privately-financed student and who I would get along with very well.

I highly appreciate that he often asked for and valued my opinion on aeronautical and operational matters in our group meetings. Last, I would like to thank him for his patience, as we always spoke Japanese, language was surely one additional challenge in supervising a foreign student, but I always felt welcomed and never felt that there was a barrier of any sort.

Further, I would like to thank my co-referees: Prof. Miwa Nakanishi, whose lecture in Human Factors I attended and who kindly invited me to participate in her aviation accident analysis discussions. Prof. Genya Ishigami, who was my first contact at Keio University and introduced me to Prof. Takahashi. And Prof. Masayuki Kohiyama, who also attended my mid-term presentation. I’d like to thank all of them for taking the time to review my thesis and for their helpful feedback.

Next, I would like to thank my supervisor at the Electronic Navigation Research Institute (ENRI), Dr. Eri Itoh, for her tremendous support throughout this thesis. It is thanks to her consultation that I found my research topic and was able to become an intern at ENRI. It is without questions that

without her help this thesis would not exist in this form and therefore I am extremely grateful for her efforts and encouragement.

I would also like to thank the other co-authors of my journal papers: Prof. Tomoaki Tatsukawa of the Tokyo University of Science for his help with the K Computer; and Dr. Thomas Feuerle and Paul Frost of the Technische Universität Braunschweig for their help in realizing the flight simulator experiment. And of course, all the pilots who participated in the experiment itself.

Further I would like to thank Prof. Jorg Entzinger of the University of Tokyo for his ongoing advises and friendship since my time as an intern at the Japanese Aerospace Exploration Agency (JAXA). At JAXA I would like to especially thank my former colleagues Kohei Funabiki, Masayuki Katow and Gen Tsuchiya for their support.

I would also like to express my gratitude to my former advisors at the University of Applied Sciences Gelsenkirchen, Prof. Jürgen Dunker and Prof. Klaus Fricke for their never-ending support and encouragement to pursue a doctoral degree.

This thesis could not have been made without the generous financial support of various organizations, especially the Rotary Yoneyama Memorial Foundation and the members of the Kawasaki North Rotary Club. Further, the Keio University's Office of Student Affairs, their International Student's branch, and the Keio Leading-edge Laboratory of Science and Technology. And also the Japan Student Services Organization (JASSO) and the JGC-S Scholarship Foundation.

No one can maintain sanity throughout a PhD without great friends and words can hardly describe how thankful I am to Michael Elting for his friendship and the unforgettable memories we made. If there wasn't "Unser Donnerstag" I would never have been able to survive "Dieses Land".

Further, I would like to thank Yusuke Naora for his friendship and outgoing personality and for showing me his hometown Izumo. I am always amazed how well he knows and understands me.

I also like to express my thanks to the team of "my office", that is the Starbucks in Shimokitazawa, where I basically learned most of my Japanese, worked a lot on my thesis or studied in my "free time". (Don't you think you will ever have free time during a PhD.)

Last, I would like to thank my parents, Stephie and Uli, simply for being there and for not changing at all. (Drehstromrechner kommt, irgendwann, ganz bestimmt!)

Concluding, it has been a true pleasure to work on Flight-deck Interval Management for the past three years and I would like to express my deepest appreciation for the FIM community, the people at the NASA Langley Research Center, and especially Brian Baxley and Kurt Swieringa for their encouraging support, and for developing such an outstanding technology over the almost past two decades. It is this much a single person can contribute in the given time frame, but it is aspired that this thesis encourages future research on the topic and hopefully the IM-SP concept will be picked up by the FIM community and finds its way into future iterations of FIM.

~Always follow your dreams

Tokyo, February 2020

Timo Mario Riedel

TABLE OF CONTENT

1. Introduction	1
1.1. Motivation.....	2
1.2. Thesis Structure.....	3
2. Theory of Flight-deck Interval Management	5
2.1. Overview	5
2.1.1. Separation and Spacing	5
2.1.2. History	7
2.1.3. Working Principle.....	8
2.1.4. FIM Procedures	9
2.1.5. Advantages.....	9
2.1.6. Disadvantages	9
2.2. Minimum Operational Performance Standards (MOPS-FIM)	10
2.3. Airborne Spacing for Terminal Arrival Routes (ASTAR)	11
2.3.1. Control Law	11
2.3.2. Graphical User Interface (GUI)	14
2.4. ATD-1 Flight Test	15
2.5. Other Concepts.....	18
2.5.1. Continuous Descent Operations (CDO)	18
2.5.2. Base of Aircraft Data (BADA)	19
3. Feasibility Study toward Tokyo International Airport	20
3.1. Introduction.....	20
3.2. Simulation Environment.....	20
3.2.1. SPICA.....	20
3.2.2. K Computer	21
3.2.3. Arrival Scenarios to Tokyo International Airport	21
3.2.4. Wind Conditions.....	24
3.2.5. Aircraft.....	24
3.2.6. Initial Conditions	25
3.2.7. Evaluated Data and Number of Simulations.....	25
3.3. Results	25
3.3.1. En-route Scenario	26
3.3.2. Night Scenario	27

3.3.3. Approach Scenario	28
3.3.4. End Speed Logic.....	29
3.3.5. Chained Operation	31
3.4. Discussion	32
3.4.1. Wind Effects	32
3.4.2. Effect of Runway Proximity on the Spacing Performance	33
3.4.3. Reasons for High Numbers in Speed Commands and Reversals	33
3.5. Conclusion of Chapter 3.....	34
4. Interval Management – Speed Planning	35
4.1. Introduction.....	35
4.2. Speed Plan Definitions.....	35
4.2.1. Time Required Map.....	35
4.2.2. Action Point Concept	37
4.3. Speed Plan Modifications.....	37
4.3.1. Planned Speed Changes	37
4.3.2. Additional Speed Changes.....	38
4.4. Algorithm Considerations.....	39
4.5. Proposed Algorithm.....	40
4.5.1. First Stage – Time-based Preselection.....	41
4.5.2. Second Stage – Cost Function	41
4.5.3. Attributes	42
4.5.4. Speed Plan Optimization	45
4.5.5. System Initiation and Continuous Operation	45
4.6. Simulation Scenario I.....	48
4.6.1. Routing.....	48
4.6.2. FIM Operation	49
4.6.3. Number of Simulations	50
4.6.4. Nominal Values	50
4.6.5. Results	52
4.7. Simulation Scenario II.....	60
4.7.1. Routing.....	60
4.7.2. FIM Operation	61
4.7.3. Number of Simulations	61
4.7.4. Nominal Values	61
4.7.5. Results	62
4.8. Discussion	64
4.8.1. Spacing Performance or the Linear Error Pattern	64

4.8.2. Application of Speed Constraints.....	65
4.8.3. Fuel Burn	65
4.9. Conclusion of Chapter 4.....	66
5. Optimization of IM-SP	67
5.1. Introduction.....	67
5.2. Particle Swarm Optimization (PSO).....	68
5.2.1. Overview.....	68
5.2.2. Speed-constrained Multi-objective Particle Swarm Optimization (SMPSO)	68
5.3. Optimization Problem.....	69
5.3.1. Decision Variable.....	69
5.3.2. Objective Function	70
5.3.3. Block Diagram	71
5.3.4. SMPSO Settings.....	71
5.4. Weight Factor Vector Analysis	72
5.4.1. Arrival Expedition Margin vs. Time-To-Go	73
5.4.2. Time-To-React	75
5.4.3. Action Point Distance	76
5.4.4. Action Point Type.....	77
5.4.5. Analysis Summary.....	78
5.5. Multi-objective Optimization	78
5.5.1. SMPSO Optimization Results	78
5.5.2. Speed Profile Characteristics.....	81
5.5.3. Full Dataset Results	83
5.6. Discussion	86
5.6.1. Optimal Setting.....	86
5.6.2. Synergetic Effects of q_{AEM} and the Penalty Attributes	87
5.7. Conclusion of Chapter 5.....	88
6. Flight Simulator Evaluation	89
6.1. Introduction.....	89
6.2. Simulator	89
6.3. GUI Design.....	91
6.3.1. ASTAR	91
6.3.2. IM-SP	92
6.4. Test Plan.....	95
6.4.1. Operational Procedures	95
6.4.2. Routing and Error Setups	95

6.4.3. Participants	96
6.4.4. Pilot Briefing.....	96
6.4.5. Test Sequence.....	97
6.5. Results	97
6.5.1. Quantitative Results	97
6.5.2. Qualitative Survey.....	101
6.5.3. Reaction Times.....	105
6.5.4. Model Verification Trial.....	106
6.6. Discussion	107
6.6.1. Simulator Characteristic	107
6.6.2. Deceleration Rate.....	107
6.6.3. Use of the EFB Page.....	108
6.6.4. GUI Recommendations.....	108
6.6.5. Consideration of Aircraft Type Specific Parameters	109
6.6.6. Training Procedures for FIM	109
6.7. Conclusion of Chapter 6.....	110
7. Conclusion.....	111
7.1. Research Summary.....	111
7.2. Other Contributions and Findings.....	111
7.3. Future Research	112
7.3.1. Numerical Testing	112
7.3.2. HITL Testing.....	112
7.3.3. FIM Avionics and GUI Design.....	113
7.3.4. Long-term Vision	113
Bibliography.....	114
Appendix A (Equations)	120
Appendix B (Error Patterns).....	126
Appendix C (Approach Plate RJTT ILS X RWY 34L) ⁽⁵⁰⁾	129
Appendix D (Index)	130

LIST OF FIGURES

Figure 1.1 Structure of this thesis.....	4
Figure 2.1 Spacing example for capacity planning.....	6
Figure 2.2 Spacing performance for different IM concepts.....	6
Figure 2.3 Location of the FIM relevant instruments on an Airbus A320 flight deck.....	7
Figure 2.4 Glareshield panel of the Airbus A320 showing the FCU in the center ⁽³⁸⁾	8
Figure 2.5 PFD (left) and ND (right) on an Airbus A320 ⁽³⁸⁾	8
Figure 2.6 Time-based spacing concept for aircraft on merging tracks.....	10
Figure 2.7 Block diagram of the ASTAR TBO law ⁽¹⁴⁾	12
Figure 2.8 Block diagram of the ASTAR TBO ground speed compensation ⁽¹⁴⁾	13
Figure 2.9 Overview of the ASTAR ATD-1 EFB page GUI ⁽¹⁷⁾	14
Figure 2.10 Overview of the ASTAR ATD-1 CGD page GUI ⁽¹⁷⁾	14
Figure 2.11 Boxplots of the Cross clearances spacing performance ⁽¹⁷⁾	16
Figure 2.12 Boxplots of the Achieve stage spacing performance ⁽¹⁷⁾	16
Figure 2.13 Comparison between continuous, here fixed FPA, and stepwise descents.....	18
Figure 3.1 Routing for the en-route scenario with Terminal Entry STONE ⁽⁴⁴⁾	22
Figure 3.2 Routing for the en-route scenario with Terminal Entry ADDUM ⁽⁴⁴⁾	22
Figure 3.3 Routing for the night scenario with termination point KAIHO ⁽⁴⁴⁾	23
Figure 3.4 Routing for the approach scenarios depending on the runway in use ⁽⁴⁴⁾	24
Figure 3.5 Spacing performance for the en-route scenarios.....	26
Figure 3.6 Spacing performance for the night time scenario.....	27
Figure 3.7 Spacing performance for the approach scenarios, divided by active runway.....	28
Figure 3.8 Speed command behavior for different ESL tolerances ⁽⁴⁴⁾	29
Figure 3.9 Progression of SD and commands depending on the end speed tolerance ⁽⁴⁴⁾	30
Figure 3.10 Spacing performance for chained FIM operations, by example of RWY 23 ⁽⁴⁵⁾	31
Figure 3.11 Spacing performance for the STONE winter scenario, divided by start point ⁽⁴⁴⁾	32
Figure 3.12 Characteristics of the ASTAR algorithm that increase speed commands ⁽⁴⁵⁾	33
Figure 4.1 Speed envelope and nominal speed for a Boeing 787-8 ⁽⁴⁸⁾	36
Figure 4.2 Principle for modifications made to planned speed changes ⁽⁴⁸⁾	37
Figure 4.3 Principle for the addition of unplanned speed changes ⁽⁴⁸⁾	38

Figure 4.4 Solutions to mitigate a spacing error of 5 s to within ± 0.5 s ⁽⁴⁸⁾	39
Figure 4.5 Flow of the IM-SP selection algorithm ⁽⁴⁸⁾	40
Figure 4.6 Flowchart for the IM-SP system initiation process ⁽⁴⁸⁾	46
Figure 4.7 Flowchart for the IM-SP continuous operation mode ⁽⁴⁸⁾	47
Figure 4.8 Lateral flight path for Scenario I ⁽⁴⁸⁾	48
Figure 4.9 Vertical flight path for Scenario I ⁽⁴⁸⁾	49
Figure 4.10 Reference speed profile for Scenario I.....	49
Figure 4.11 Detailed comparison of the "SPICA Low+" simulation ⁽⁴⁸⁾	54
Figure 4.12 Boxplot for all simulations of Scenario I ⁽⁴⁸⁾	56
Figure 4.13 Boxplot for all simulations, grouped by pattern, direction, and amplification ⁽⁴⁸⁾	57
Figure 4.14 Median difference in commands and accelerations by error pattern ⁽⁴⁸⁾	59
Figure 4.15 Lateral flight path for Scenario II ⁽⁴⁹⁾	60
Figure 4.16 Vertical flight path for Scenario II ⁽⁴⁹⁾	60
Figure 4.17 Reference speed profile for Scenario II ⁽⁴⁹⁾	61
Figure 4.18 Boxplot for all simulations of Scenario II ⁽⁴⁹⁾	63
Figure 4.19 Saturated speed profile (AEM = 0) ⁽⁴⁸⁾	65
Figure 5.1 Block diagram of the IM-SP algorithm ⁽⁵¹⁾	71
Figure 5.2 Overall results depending on q_{AEM} (equivalent to $1 - q_{TTG}$) ⁽⁵¹⁾	73
Figure 5.3 Backloading phenomenon observed with low q_{AEM} values ⁽⁵¹⁾	74
Figure 5.4 Overall results depending on q_{TTR} ⁽⁵¹⁾	75
Figure 5.5 Overall results depending on q_{APD} ⁽⁵¹⁾	76
Figure 5.6 Overall results depending on q_{Type} ⁽⁵¹⁾	77
Figure 5.7 Optimization results – final error vs. fuel burn ⁽⁵¹⁾	79
Figure 5.8 Optimization results – command difference vs. fuel burn ⁽⁵¹⁾	80
Figure 5.9 Optimization results – critical commands vs. fuel burn ⁽⁵¹⁾	80
Figure 5.10 Comparison for T+ and F+ on the "SHTLE High+" setup ⁽⁵¹⁾	81
Figure 5.11 Comparison for T+ and F+ on the "SHTLE High-" setup ⁽⁵¹⁾	82
Figure 5.12 Boxplot for the objective functions divided by setting ⁽⁵¹⁾	84
Figure 5.13 Boxplot for the non-objective functions divided by setting ⁽⁵¹⁾	85
Figure 6.1 Overview of the Airbus A320 simulator at the IFF ⁽⁵⁹⁾	90
Figure 6.2 Position of the CGD on the Captain's side ⁽⁵⁹⁾	90
Figure 6.3 CGD layout for ASTAR (GUI A) ⁽⁵⁹⁾	91
Figure 6.4 Reverse video on GUI A to indicate a speed command update.....	91

Figure 6.5 CGD layout for IM-SP (GUI B) ⁽⁵⁹⁾	92
Figure 6.6 GUI B indicating an upcoming speed change ⁽⁵⁹⁾	93
Figure 6.7 GUI B during a speed change ⁽⁵⁹⁾	93
Figure 6.8 GUI B indicating a speed plan change that requires immediate crew reaction	94
Figure 6.9 Graphical representation of the speed plan on the EFB page of GUI B ⁽⁵⁹⁾	94
Figure 6.10 Error propagation of the selected setups ⁽⁵⁹⁾	96
Figure 6.11 Maximum speed placard of an Airbus A320 ⁽³⁸⁾	102
Figure 6.12 Flight data record for GUI A ⁽⁵⁹⁾	104
Figure 6.13 Flight data record for GUI B ⁽⁵⁹⁾	104
Figure 6.14 Comparison of the Δ CAS progression for GUI A and GUI B ⁽⁵⁹⁾	104
Figure 6.15 Boxplot of the command input time differences, grouped by GUI ⁽⁵⁹⁾	105
Figure 6.16 Final error for the model verification trials, grouped by configuration ⁽⁵⁹⁾	106

LIST OF TABLES

Table 2.1 Spacing performance for the Cross clearance trials ⁽¹⁷⁾	16
Table 2.2 Spacing performance after the Achieve stage ⁽¹⁷⁾	16
Table 2.3 Survey responses for Cross-Merge operation ⁽¹⁷⁾	17
Table 3.1 Results for the en-route scenarios	26
Table 3.2 Results for the night scenario	27
Table 3.3 Results for the approach scenarios.....	28
Table 3.4 Mean Final spacing error with and without an ESL for each scenario	29
Table 3.5 SD of the final spacing error with and without an ESL for each scenario	29
Table 3.6 Total number of speed commands issued with and without an ESL for each scenario	30
Table 3.7 Speed commands issued within less than 60s with and without an ESL for each scenario.....	30
Table 3.8 Wind conditions and GS at the initial waypoint for the STONE - Winter scenario ⁽¹⁷⁾	32
Table 4.1 Action Points list for the nominal profile ⁽⁴⁸⁾	36
Table 4.2 Attributes and weight factors used in the IM-SP cost function ⁽⁴⁸⁾	44
Table 4.3 Nominal values for Scenario I	50
Table 4.4 Design differences of ASTAR and IM-SP (as used in this simulation).....	52
Table 4.5 Results for the "SPICA Low+" simulation ⁽⁴⁸⁾	52
Table 4.6 Speed plan modification history of IM-SP ⁽⁴⁸⁾	55
Table 4.7 Overall results for ASTAR (A13) ⁽⁴⁸⁾	58
Table 4.8 Overall results for ASTAR Limited (LTD) ⁽⁴⁸⁾	58
Table 4.9 Overall results for IM-SP (SP) ⁽⁴⁸⁾	58
Table 4.10 Nominal values for Scenario II ⁽⁴⁹⁾	62
Table 4.11 Overall results for ASTAR ⁽⁴⁸⁾	64
Table 4.12 Overall results for IM-SP ⁽⁴⁸⁾	64
Table 5.1 SMPSO Settings.....	72
Table 5.2 Weight factor settings by profile ⁽⁵¹⁾	79
Table 5.3 Objective function results by profile ⁽⁵¹⁾	79
Table 5.4 Overall results for the original settings (Orig.) ⁽⁵¹⁾	83
Table 5.5 Overall results for the time optimal setting (T+) ⁽⁵¹⁾	83
Table 5.6 Overall results for the fuel improved setting (F+) ⁽⁵¹⁾	83

Table 6.1 Selected setups for the flight simulator evaluation	95
Table 6.2 Summary of the questionnaire responses ⁽⁵⁹⁾	98
Table 6.3 Reaction times and input time differences, grouped by GUI ⁽⁵⁹⁾	105

NOMENCLATURE

General

ANSP	Air Navigation Service Provider
ASPA	Airborne Spacing
ASTAR	Airborne Spacing for Terminal Arrival Routes
ATC	Air Traffic Control
ATCo	Air Traffic Controller
ATM	Air Traffic Management
BADA	Base of Aircraft Data
FIM	Flight-deck Interval Management
GIM	Ground-based Interval Management
GUI	Graphical User Interface
HITL	Human-in-the-Loop
IM	Interval Management
IM-SP	Interval Management - Speed Planning
ISA	International Standard Atmosphere
MSL	Mean Sea Level
NAS	National Airspace System
RJTT, HND	Tokyo International Airport – Haneda Airport
SD, σ	Standard Deviation
TGT	Target
TMA	Traffic Management Advisor

Organizations and Projects

ATD-1	Air Traffic Management Technology Demonstration 1
CARATS	Collaborative Actions for Renovation of Air Traffic Systems
ENRI	Electronic Navigation Research Institute
FAA	Federal Aviation Administration
IATA	International Air Transport Association
IFF	Institute for Flight Guidance – Technische Universität Braunschweig
ICAO	International Civil Aviation Organization
JCAB	Japan Civil Aviation Bureau
NASA	National Aeronautics and Space Administration

Organizations and Projects (continued)

NextGen	The Next Generation Air Transportation System
SESAR	Single European Sky ATM Research

Aircraft Systems and Instrumentation

A/P	Autopilot
A/THR	Autothrust, Autothrottle
CGD	Configurable Graphics Display
CPDLC	Controller Pilot Data Link Communications
EFB	Electronic Flight Bag
ELI	Early/Late-Indicator
FCU	Flight Control Unit
FMS	Flight Management System
FSI	Fast/Slow-Indicator
MCP	Mode Control Panel
ND	Navigation Display
PFD	Primary Flight Display

Aircraft Operations

CAS	Calibrated Airspeed
CCS	Constant CAS Segment
CDO	Continuous Descent Operation
CRS	Course
FAF	Final Approach Fix
FAS	Final Approach Speed
FL	Flight Level
FPA	Flight-Path Angle
GS	Ground Speed
IAF	Intermediate Approach Fix
IFR	Instrument Flight Rules
ILS	Instrument Landing System
PF	Pilot Flying
PM	Pilot Monitoring
ROCD	Rate of Climb / Descend
RWY	Runway

Aircraft Operations (continued)

SOP	Standard Operating Procedure
STAR	Standard Terminal Arrival Route
TAS	True Airspeed
TOD	Top of Descent
UTC	Coordinated Universal Time
V _{FE}	Velocity – Maximum Flap Extension
V _{LS}	Velocity – Lowest Selectable
W _x	Wind

Arrival Times

ATA	Actual Time of Arrival
ETA	Estimated Time of Arrival
IAT	Inter-Arrival Time
RTA	Required Time of Arrival
STA	Scheduled Time of Arrival

FIM Related Definitions (Chapter 2 & 3)

ABP	Achieve-by Point
ASG	Assigned Spacing Goal
CTD	Constant Time Delay
DTG	Distance-To-Go
ESL	End Speed Logic
FDMS	Flight Deck-based Merging and Spacing
IMAC	Interval Management Alternative Clearances
MOPS	Minimal Operation Performance Standards
OWN	Ownship
PTP	Planned Termination Point
SPICA	Spacing Time Intervals of Arrival Aircraft Conducting ASPA IM
TBO	Trajectory Based Operation
TTF	Traffic-To-Follow
TTG	Time-To-Go
$e(t)$	Spacing Error Term
Δ	Nominal Spacing (equivalent to ASG)

IM-SP Related Definitions (Chapter 4)

A13	ASTAR (Version 13 – Intended Implementation, speed constraints lifted)
AEM	Arrival Expedition Margin
AP	Action Point
APC	Action Point Dataset (Candidates)
APD	Action Point Distance
APM	Action Point Dataset (Modifications)
LTD	ASTAR (Limited Implementation, speed constraints enforced)
RPD	Reference Profile Deviation
RSE, $e()$ *	Remaining Spacing Error
TTN	Time-To-Next Command
TTR	Time-To-React
c_x	Constants
d_x	Distances
i	Modification Intervals
q_x	Attribute Weight (Cost Function)
r	Modification Ranges
s_x	Attribute Cost (Cost Function)
S_x	Total Cost (Cost Function)

Optimization (Chapter 5)

MOEA	Multi-objective Evolutionary Algorithm
OMOPSO	Optimized Multi-objective Particle Swarm Optimization
PSO	Particle Swarm Optimization
SMPSO	Speed-constrained Multi-objective Particle Swarm Optimization
F+	Fuel improved setting
T+	Time optimal setting
c_x	Constants
f_x	Objective Function
p_x	Particle Position
r_x	Random Number
v_x	Particle Velocity

Optimization (continued)

δ_j	Dimensional Maximum Velocity
χ	Velocity Constriction Coefficient
φ	Sum of Constants
ω	Particle Inertia

Flight Crew Licenses (Chapter 6)

CPL	Commercial Pilot License
IR	Instrument Rating
ME	Multi Engine
MPL	Multi-Crew Pilot License

Units

ft	Feet (1 ft = 0.3048 m)
kt	Knot (1 kt = 1 NM/h)
NM	Nautical Mile (1 NM = 1.852 km)

1. INTRODUCTION

Over the last decade the demand for air travel, especially in the Asia-Pacific region, has been constantly increasing, and independent ⁽¹⁾ as well as makers' market forecasts ^(2,3) project this demand to double within the next 20 years.

At the same time, an interesting transition on the airline market could be observed: With the rise of low-cost carriers, Point-to-Point operation, using smaller aircraft, has become more common in contrast to the Hub-and-Spoke system often used by legacy carriers ⁽²⁾. And even here, fleet preferences have changed, moving away from high-capacity four-engine wide-body aircraft, like the Boeing 747 or the Airbus A380, to more fuel-efficient two-engine, sometimes even narrow-body, alternatives, thus spreading previous demand onto more flights.

Consequentially, the total number of aircraft worldwide is projected to grow at almost the same rate as the total demand. However, handling this demand poses an enormous challenge to regions in which the airspace is congested, or at airports that are already at their capacity. Accordingly, new strategies to handle the additional traffic and more sophisticated technologies to assist pilots, air traffic controllers, and all other stakeholders alike, are required to ensure safe, efficient and environmentally friendly operations.

With this in mind, the International Civil Aviation Organization (ICAO) has defined multiple working areas in its Global Air Navigation Plan (GANP) ⁽⁴⁾, and local initiatives like NextGen in the USA ⁽⁵⁾, SESAR in Europe ⁽⁶⁾, and CARATS in Japan ⁽⁷⁾ adapted these for the modernization of their respective national airspace system (NAS).

One of these working areas is the application of Airborne Spacing (ASPA) and within its scope, Interval Management (IM). The GANP defines IM as the "precise management of intervals between aircraft with common or merging trajectories" ⁽⁴⁾, en-route and in the terminal area. In other words, IM enables the highest utilization of airways and runways, without compromising safety margins, nor wasting capacity through excess spacing.

Technically, this can be realized in two ways: In a conventional ground-to-air manner, called Ground-based Interval Management (GIM), in which, similar to nowadays operation, an Air Traffic Controller (ATCo) gives speed advisories, expressed as Calibrated Airspeed (CAS), to the pilots via voice communication or Controller Pilot Data Link Communications (CPDLC), however here assisted by advanced IM software ⁽⁸⁾; Or, more sophisticated, in an air-to-air manner, called Flight-deck Interval Management (FIM) ^(9,10), in which dedicated avionics and systems within the flight deck provide the pilots directly with the necessary guidance to achieve the spacing target.

Envisioned to be implemented by 2024 ⁽⁴⁾, studies have shown that FIM, compared to current non-IM software assisted ATCo guided arrivals, could potentially increase airport capacity by up to five aircraft per hour and runway ^(9,11,12). Nevertheless, currently FIM and its avionics are still at

development stage, leaving just four more years to be on schedule.

Frontier research on FIM has been conducted by the National Aeronautics and Space Administration (NASA) ⁽¹³⁻²²⁾ who invented “Airborne Spacing for Terminal Arrival Routes” (ASTAR) ⁽¹⁴⁻¹⁶⁾, a control law for FIM, that quickly evolved to become the gold standard, and served as the base for follow-up research worldwide ⁽²³⁻²⁷⁾.

NASA’s research on FIM and ASTAR was later integrated into their Air Traffic Management Technology Demonstration (ATD-1) project ⁽¹³⁾ that reached its peak in a series of flight tests in early 2017 ⁽¹⁷⁻²⁰⁾. The tests successfully demonstrated the capability of FIM to accomplish the self-spacing task, but also revealed shortcomings with the speed control behavior; Most noteworthy, the amount of IM speed commands and speed reversals (a speed command opposing the intention of a previous command) were deemed as “too high” from a pilot’s standpoint ⁽¹⁷⁻¹⁹⁾.

Therefore, NASA specifically recommended to address this aspect and to explore alternative control law techniques before operational implementation ⁽¹⁸⁾.

While an alternative control law, using Model Predictive Control, has been explored in parallel to the flight test ^(28,29), this approach showed issues with a high computation time demand, and resulting profiles also displayed a high frequency of speed changes, impeding its feasibility for a retrofitted implementation.

Since the flight test also marked the conclusion of the ATD-1 project, and the FIM technology and research responsibility was handed over to the Federal Aviation Administration (FAA) ⁽³⁰⁾, the above-mentioned issues are yet unresolved.

The studies in this thesis address the findings and recommendations made by NASA respectively. Numerical simulations using the ASTAR algorithm were made to better understand the system and its behavior. Following, a new control logic, called “Interval Management – Speed Planning” (IM-SP), was proposed to reduce the necessary amount of speed commands, while ensuring sufficient spacing performance. This new logic was then further optimized to enhance its performance and improve imperfections found in the first iteration. In parallel, a Human-in-the-Loop (HITL) flight simulator experiment was conducted to confirm if the envisioned improvements are actually perceived by the pilots and to gain further insight for the ongoing development of FIM and IM-SP, that can only be obtained in a realistic application environment.

It is aspired that this thesis will propose a solution to the above-mentioned findings of the ATD-1 flight test, give ideas for future research on the original and new control logic, and to further the advancement of FIM on its way toward operational implementation.

1.1. Motivation

Given the issues described in the introduction and with the GANP’s implementation goal in mind, FIM is a very current topic, and further, as avionics certification is usually a lengthy process, if an

impact was to be made before the initial implementation of FIM, now is arguably the only time.

Thanks to the meticulous research work of NASA, the research problem, i.e., reduction of speed commands, was also very well defined, but also emphasized the importance to approach the problem from a human-centered, here pilot's, perspective to ensure actual operational feasibility. As this thesis was developed in Japan, there is also a strong local interest in solutions like FIM, which can be explained by the example of the current developments at the Tokyo International Airport (ICAO: RJTT, IATA: HND). With the Olympic Games 2020 to be hosted in Tokyo, considerations were made how to increase the capacity of the already congested airport for the expected increase in demand, especially during daytime hours. While options like building a fifth runway were considered, ultimately new arrival routes, that utilize the current runway configuration better, have been chosen and are currently being tested⁽³¹⁾. However, infrastructural changes like these are costly, lengthy and depending on the location, simply not possible.

For those situations, FIM offers a solution that is independent of local circumstances or equipment available and can easily be integrated into the current environment. Accordingly, while examples here are presented for the example of RJTT, this research is in no way limited to national interest, and results are applicable worldwide.

1.2. Thesis Structure

This thesis is divided into eight chapters, sorted in (chrono-)logical order, as shown in Figure 1.1.

Chapter 1 gave an overview of the current research matter, motivation for the topic and the thesis structure.

Chapter 2 explains the concepts and history of FIM in further detail. A description of ASTAR's control logic and an in-depth analysis of the issues found in the ATD-1 flight test are given. Further, other models and concepts important to this thesis are explained in detail.

Chapter 3 shows the research results of multiple feasibility studies using large-scale Monte Carlo simulations of aircraft using ASTAR based FIM on arrivals in Tokyo International Airport. These simulations were used to investigate the spacing performance and speed control behavior of ASTAR based FIM and ensure arrival route compatibility under local environmental conditions.

Chapter 4 introduces the initial version of IM-SP with its design principles and underlying algorithms explained in full detail. Two benchmark studies are provided, comparing the performance of ASTAR to IM-SP, including a detailed example to show the algorithms' differences.

Chapter 5 takes the initial version of IM-SP through an optimization study using evolutionary algorithms to improve the control logic for its spacing performance, user friendliness and ecology. Further a benchmark study, comparing two new, user-priority dependent, settings to the results of the initial study, is presented.

Chapter 6 presents the setup and results of a HITL study in which airline and certified test pilots

evaluated FIM, ASTAR and IM-SP in an Airbus A320 flight simulator, recreating the ATD-1 flight test environment. Pilot's comments are provided for each logic and further observations are presented.

Chapter 7 concludes this paper with a summary of the research achievements and an outlook on future research tasks, including potential enhancements for FIM.

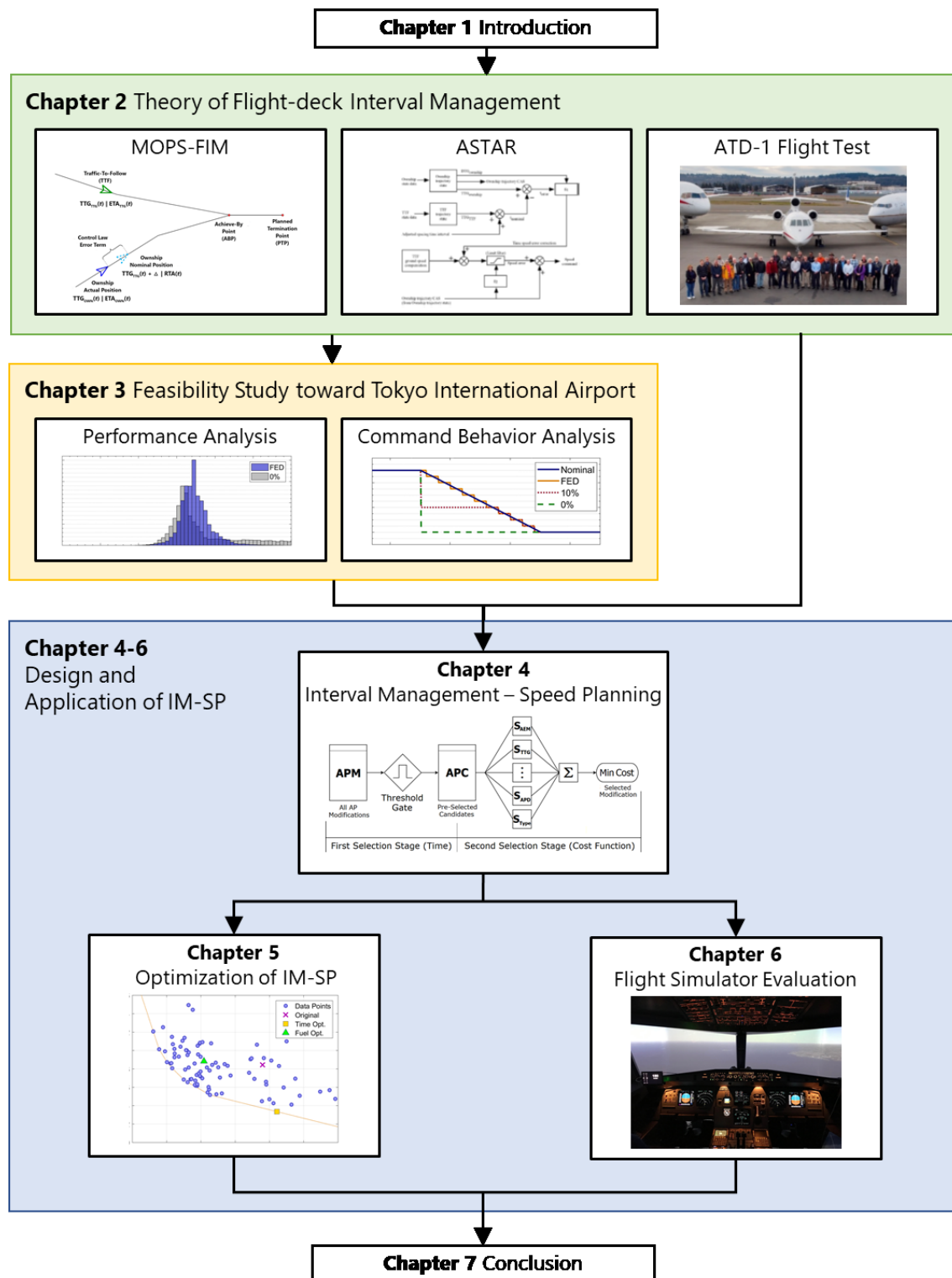


Figure 1.1 Structure of this thesis

2. THEORY OF FLIGHT-DECK INTERVAL MANAGEMENT

2.1. Overview

2.1.1. Separation and Spacing

Ensuring sufficient separation between aircraft is a vital task for the safe conduct of flight, whether it is for small general aviation airplanes or large transport aircraft. The difference for the latter is that virtually all scheduled air traffic operates under Instrument Flight Rules (IFR). In IFR operation, independent from actual instrument meteorological conditions being present or not, separation is provided by and within the responsibility of Air Traffic Control (ATC).

When necessary, ATC advises pilots via voice communication or CPDLC to change their altitude, track, or speed to provide separation in all dimensions. The required minima for each are defined in ICAO Doc. 4444⁽³²⁾ and depend on various factors, e.g., if aircraft are on crossing, merging or identical tracks, the available avionics and radar equipment, or the aircrafts' wake vortex category.

In IM, the longitudinal separation, that is the in-trail spacing between aircraft, is of special significance and additional consideration must be given to the wake vortex category pairing of the aircraft, which might require for more spacing than just given by minimum radar separation⁽³²⁾.

Separation minima are usually provided in distance, but might also be given in time. The latter is often used for (runway) capacity planning. For example, if an aircraft pairing requires a longitudinal separation of 4 nautical miles (NM), and the trailing aircraft has a Final Approach Speed (FAS) of 144 knots (kt), the time-based separation is 100 s.

If aircraft were able to achieve and maintain this spacing without fail, this would result in a theoretical runway capacity of 36 aircraft per hour, assuming the same conditions for each aircraft pairing. However, in a realistic operational environment this performance cannot be achieved and the Actual Time of Arrival (ATA) can vary heavily from the Scheduled (STA) or Estimated Time of Arrival (ETA).

Multiple studies to measure the actual distribution and standard deviation (SD, σ) of the time between arrivals, called the Inter-Arrival Time (IAT), were conducted in the 1970's and research has widely adopted a SD of 18 s for baseline operations as referenced in (11) and (33).

Since then, advancements in ATC supporting technology, namely the start of en-route metering, assisted by a Traffic Management Advisor (TMA)⁽¹³⁾, allowed the SD to be reduced to its current benchmark value of 16.5 s^(11,12).

In capacity planning, practices have been adopted to ensure that 95% of all arriving traffic do not fall below minimum separation^(11,33). In other words, in only 5% of all cases may the ATCo be put into a situation where he/she has to intervene to prevent a "loss of separation". An example, assuming a normal distribution for the IAT^(11,12), the use of a TMA ($\sigma = 16.5$ s) and an aircraft pairing with a minimum separation of 100 s, as used above, is shown in Figure 2.1.

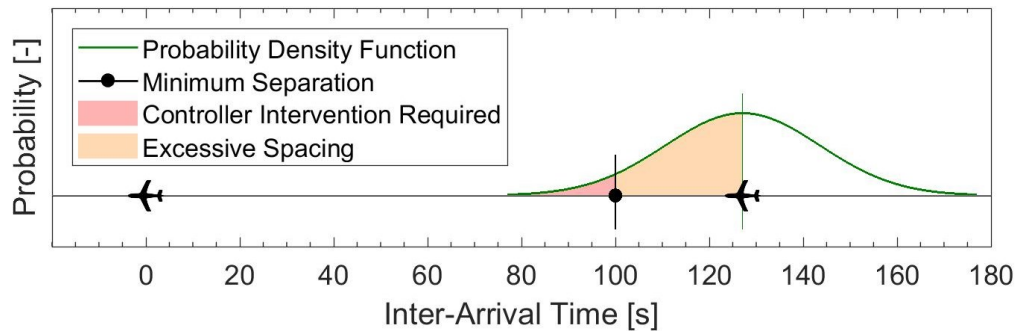


Figure 2.1 Spacing example for capacity planning

As mentioned before, ideally aircraft would be scheduled to arrive exactly at the minimum separation (100 s, black dot), however, here, in order to ensure that controller intervention is limited to an average 5% (red area) aircraft have to be scheduled with an additional, i.e., excessive, spacing ($\Delta\mu$) of 27.1 s (amber area).

It is this excessive spacing, that IM concepts try to reduce by providing means to achieve more consistent IATs with smaller SDs. Simulations have estimated ⁽¹²⁾ and performance standards require ⁽⁹⁾ that GIM systems achieve a SD of 12 s, while FIM systems achieve an even lower value of 5 s. Accordingly the excessive spacing could be reduced to 19.7 s (improvement of -7.4 s) for GIM and to 8.2 s (-18.9 s) for FIM, as shown in Figure 2.2.

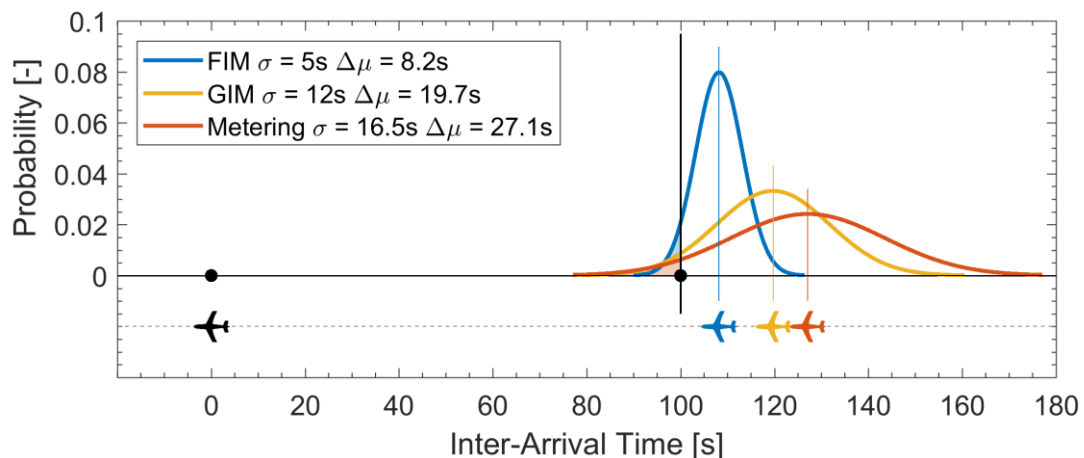


Figure 2.2 Spacing performance for different IM concepts

In this example, the capacity could be increased from the benchmark 28 aircraft per hour for Metering (shown in red), to 30 for GIM (orange) and 33 for FIM (blue). For pairings with lower separation minima, even higher capacities would be possible. As suggested in Ref. (12) it is also practical to trade part of the increased capacity for higher margins of safety and schedule 99% of all arriving FIM aircraft above minimum separation. In this case the excessive spacing would be at 11.5 s with a capacity of 32 aircraft per hour.

Reasons for FIM to achieve these low SDs are further explained in Subsection 2.1.5.

2.1.2. History

Early ideas for interval management and self-spacing date back to the time of the IAT measurement trials in the late 1970's^(12,33,34). It wasn't however until the advancement of more sophisticated, data link capable, avionics, like Automatic Dependent Surveillance – Broadcast (ADS-B), that the concept gained new research interest⁽¹⁴⁾.

An immediate predecessor to FIM and the first actually demonstrated airborne self-spacing application was Flight Deck-based Merging and Spacing (FDMS)⁽³⁵⁻³⁷⁾, which was promoted by the United Parcel Service (UPS) for their cargo fleet operation. However, FDMS had partially different concepts and required ground support from UPS's airline operation center. Hence it was limited to the fleet of UPS and specific airport and arrivals. By contrast, FIM provides a universal, operator and airport independent solution.

Early development phases of FIM intended for full flight deck integration, i.e., information is displayed on the Primary Flight Display (PFD) or Navigation Display (ND), and full interconnection with the autopilot (A/P) and autothrottle (A/THR) system is provided, so that FIM could work fully automatically. However, this would limit FIM to new flight deck and aircraft designs, and additionally would require for a lengthy and costly certification process. Considering the average time between aircraft generations or the re-design of a type and its associated flight deck of up to 20 or more years, it might take decades before the majority of aircraft are equipped with FIM. Therefore, desires to demonstrate and make the FIM system available earlier, called for an inexpensive, easily retrofittable solution⁽¹⁴⁾.

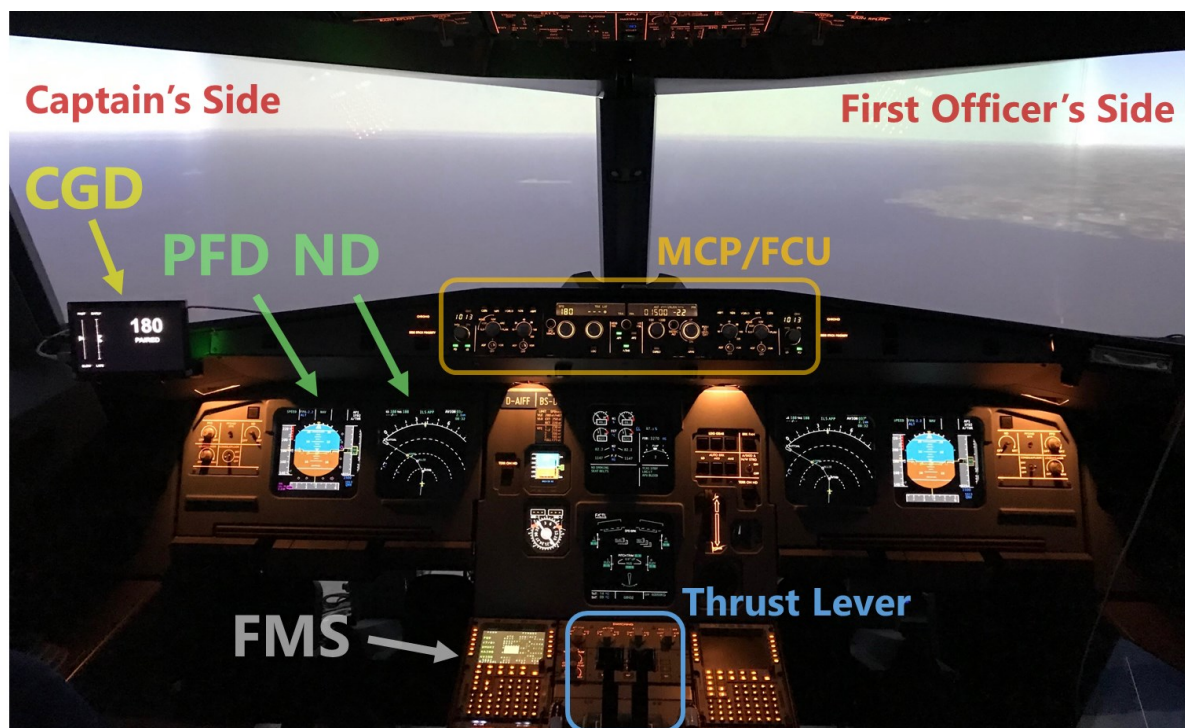


Figure 2.3 Location of the FIM relevant instruments on an Airbus A320 flight deck



Figure 2.4 Glareshield panel of the Airbus A320 showing the FCU in the center ⁽³⁸⁾
 (© Cockpit Revolution, used with permission)

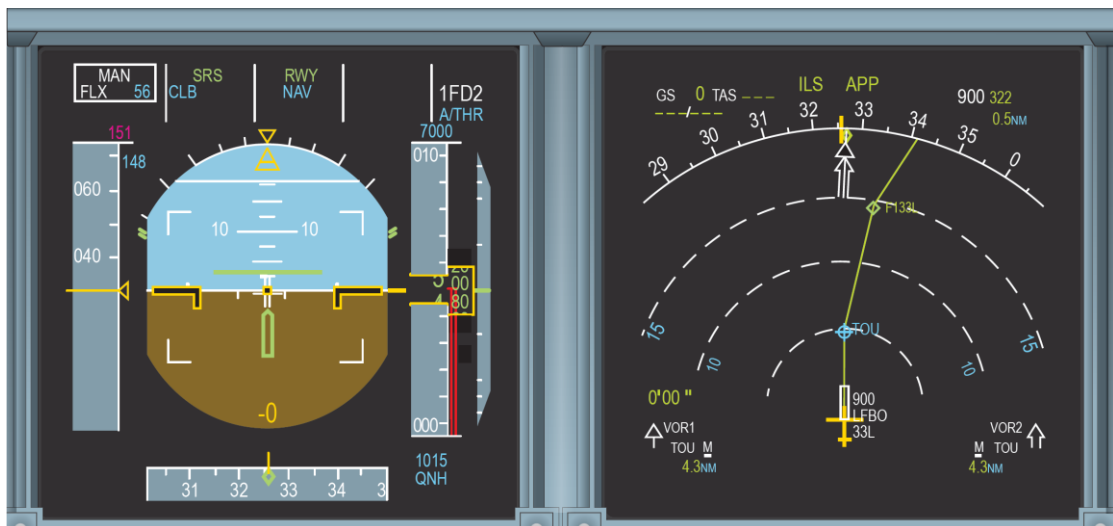


Figure 2.5 PFD (left) and ND (right) on an Airbus A320 ⁽³⁸⁾
 (© Cockpit Revolution, used with permission)

Accordingly, in its current version FIM is implemented as a federated, i.e., retrofitted, system. Here the core software runs as an application on an Electronic Flight Bag (EFB) and a dedicated display, called the Configurable Graphics Display (CGD), is positioned in the pilots' field of view for command information. This implementation requires pilots to set the IM speed commands manually, usually by manipulating the autopilot's Mode Control Panel (MCP) / Flight Control Unit (FCU), or setting the speed in the Flight Management System (FMS), or more rarely by directly setting an appropriate thrust. Therefore, FIM logics (Section 2.3) and their corresponding Graphical User Interfaces (GUI, Sections 2.4 and 6.3) have been modified for this type of operation.

2.1.3. Working Principle

In principle, FIM uses means similar to those of ATC to monitor and manage the spacing situation:

FIM aircraft scan their surrounding via ADS-B In for other aircraft transmitting via ADS-B Out to get information like the other aircrafts' current altitude and position, and derivative information like their ground speed (GS) and course. A target aircraft, namely the Traffic-To-Follow (TTF), is selected, for example by its flight number, to set the aircraft pairing. Further, a common waypoint at which the spacing situation is to be achieved, hence called the Achieve-by Point (ABP), is defined and a spacing goal is assigned.

A trajectory generator now computes the remaining flight time, called the Time-To-Go (TTG), to the ABP for both aircraft based on their route and speed. These values are then put into an error term (explained in detail in Section 2.2) to obtain the spacing error.

Depending on its value, FIM, i.e., its underlying control law (Section 2.3), will then issue a speed command, displayed on both the EFB and CGD, similar to a command received by ATC, to resolve the spacing error.

2.1.4. FIM Procedures

Aircraft capable of FIM operation receive their TTF information and assigned spacing goal from ATC, followed by a clearance to commence FIM operation. The information is then copied by the pilots into the FIM application on the EFB.

Once the system is set up and FIM operation starts, the ATCo will also get an indication on his screen that the aircraft is now in self-spacing operation. From this point on pilots continue to fly according to the speed commanded by the FIM system. Note however, that even during this type of operation the ATCo is still legally responsible to provide separation from other aircraft.

FIM operation is terminated when the aircraft reaches the Planned Termination Point (PTP), or when requested by the pilots or ATCo, from where on typical ATC guidance is resumed.

2.1.5. Advantages

The rationale for FIM is obvious in its higher efficiency and safety (as shown in Subsection 2.1.1); and reasons for FIM to achieve more consistent IATs can be attributed to the concept in itself:

Airborne self-spacing allows to remove the ground station from the communication chain, i.e., a situation that requires a speed change must no longer first be detected by the ground station, be processed, and then be communicated by ATC to the pilots. Therefore, latencies and communication delay are reduced.

Further, data pertaining the own aircraft is readily available and not limited to the information shared via a transponder or ADS-B⁽³⁹⁾ allowing for a better trajectory calculation.

Implications of the above are also a reduction in required pilot-controller interaction, thus reducing the workload for the ATCo.

2.1.6. Disadvantages

Contrarily, moving the separation task to the flight deck also entails an increase in workload for the pilots and the need for additional training on FIM avionics and procedures.

It is however anticipated that the increased workload will be limited to a permissible level and that the benefits of FIM will outweigh the disadvantages, including the initial acquisition costs.

2.2. Minimum Operational Performance Standards (MOPS-FIM)

Requirements, definitions, modes of operation and calculation models for FIM are defined in the Minimum Operational Performance Standards (MOPS-FIM, RTCA DO-361)⁽⁹⁾. The MOPS have been drafted in close alignment to the development of ASTAR (Section 2.3), and the initial and current version of MOPS-FIM was published in 2015.

Figure 2.6 depicts the time-based spacing concept for merging traffic; the most important concept for this thesis. Here the leading aircraft, TTF, shown in green, and the trailing FIM aircraft, called the Ownship (OWN), shown in blue, are on different tracks toward the ABP.

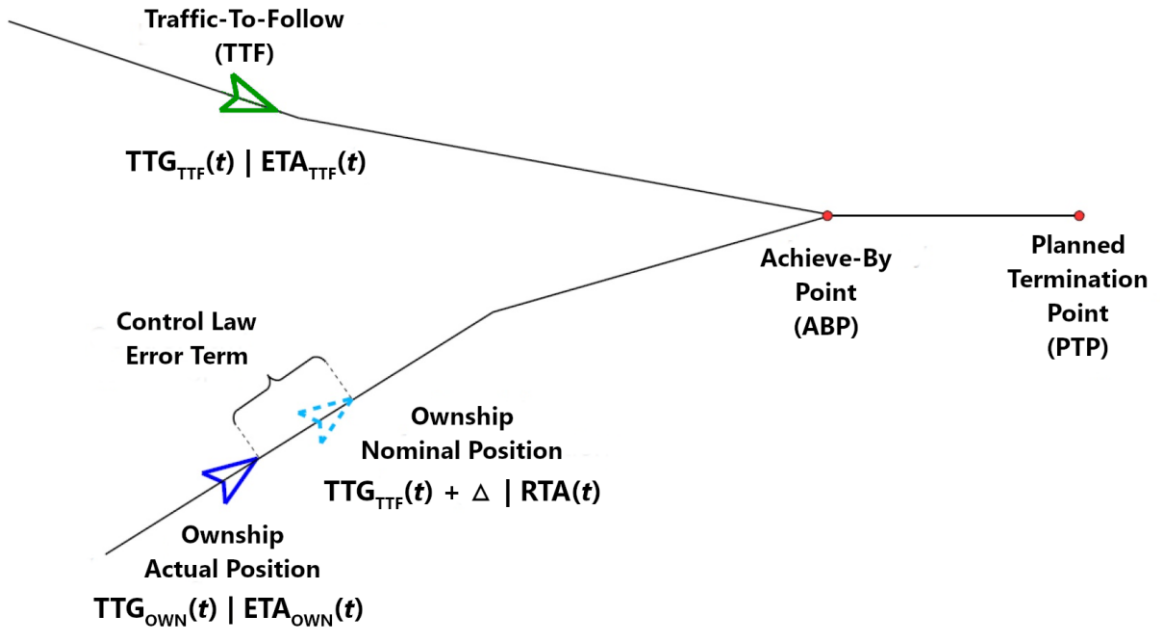


Figure 2.6 Time-based spacing concept for aircraft on merging tracks

At the time t each aircraft has the remaining flight time, or Time-To-Go: $TTG(t)$. In nominal, i.e., ideal, spacing conditions the Ownship would be exactly the Assigned Spacing Goal (ASG, Δ) behind the aircraft, giving:

$$TTG_{\text{NOM}}(t) = TTG_{\text{TTF}}(t) + \Delta. \quad (2.1)$$

By comparing the actual TTG of the Ownship to the nominal TTG, one can get the time-based spacing error $e(t)$ as defined by MOPS-FIM:

$$e(t) = TTG_{\text{OWN}}(t) - (TTG_{\text{TTF}}(t) + \Delta). \quad (2.2)$$

Accordingly, a positive spacing error indicates that the aircraft is late, i.e., spacing is excessive, and conversely a negative error implies that the aircraft is early, i.e., spacing is insufficient.

Alternatively, the terms can also be expressed by the (absolute) ETA, instead of the (relative) TTG, by adding the current time, giving

$$ETA(t) = TTG(t) + Current\ Time(t), \quad (2.3)$$

and for Equation 2.2:

$$e(t) = ETA_{OWN}(t) - (ETA_{TF}(t) + \Delta). \quad (2.4)$$

The equivalent for the nominal TTG in Equation 2.1 is called the Required Time of Arrival (RTA), giving:

$$RTA(t) = ETA_{TF}(t) + \Delta \quad (2.5)$$

so that the error term in Equation 2.4 can be shortened to:

$$e(t) = ETA_{OWN}(t) - RTA(t). \quad (2.6)$$

MOPS-FIM requires the spacing error to be calculated at least once per second. This value is then used as an input variable of the respective FIM control logic.

Other equations defined in MOPS-FIM, that have been used throughout this thesis are shown in Appendix A. The equations describe the horizontal path and turn generation from waypoints, given in geodetic coordinates (latitude and longitude), and the trajectory calculation, i.e., the progression of position, altitude and velocity along the flight path.

In MOPS-FIM, aircraft are generally regarded as point-masses and for accelerated or decelerated flight, a constant CAS change rate of ± 0.5 kt/s is assumed in all phases of flight.

Atmospheric and performance calculations were based on a different model, described in Subsection 2.5.1.

2.3. Airborne Spacing for Terminal Arrival Routes (ASTAR)

2.3.1. Control Law

Airborne Spacing for Terminal Arrival Routes (ASTAR) has been developed at NASA's Langley Research Center since 2002, with its latest version, called ASTAR13, being published in 2015^(14,15). During this time ASTAR has been adapted numerous times to accommodate to changes in the FIM environment, e.g., the switch from an integrated to a federated implementation, the requirements set in MOPS-FIM, and the technology available for the ATD-1 flight test.

ASTAR uses two different control laws, depending on if aircraft are on merging tracks (as shown in Figure 2.6) or already on the same track (in-trail).

For the former, ASTAR uses a Trajectory-based Operation (TBO) control law, further described and depicted in Figure 2.7 below, that is the subject of this thesis.

The in-trail law is a Constant Time-delay (CTD) station keeping law, that, simplified, mimics the speed profile of the TTF, plus a spacing error dependent shift.

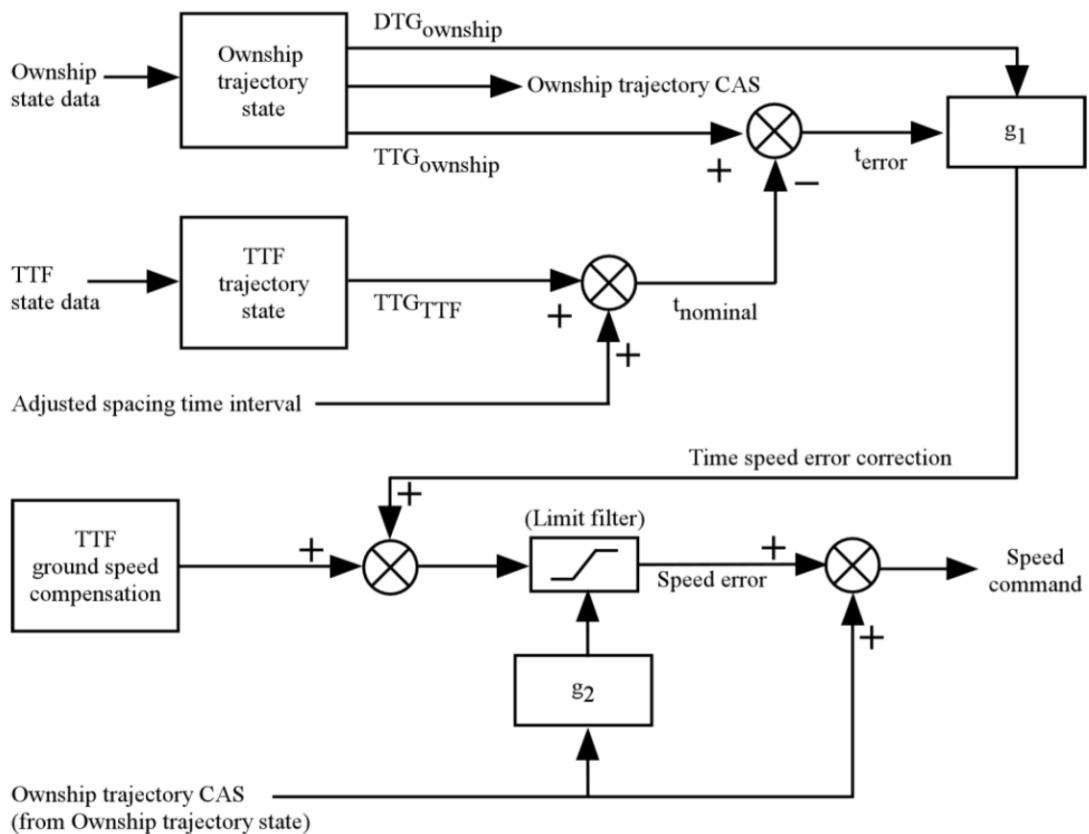


Figure 2.7 Block diagram of the ASTAR TBO law ⁽¹⁴⁾

ASTAR's TBO control law works on a feed-forward principle; The input parameters are the Ownship's and TTF's state data and a ground speed compensation block, shown in Figure 2.8. From the trajectory state of both aircraft their respective TTG is taken and compared as described in Equation 2.4 to obtain the spacing error. The spacing error is then multiplied by a gain factor (g_1), dependent on the remaining flight distance, called Distance-To-Go (DTG), of the Ownship. The time speed error correction term is then added to the ground speed compensation and put into a limit filter. This limit filter's boundaries are set to ± 0.15 (g_2) times the Ownship's trajectory, i.e., nominal, CAS. The obtained speed error is then added to the nominal CAS to obtain the speed command.

In summary, ASTAR advises a speed command within $\pm 15\%$ of the currently planned CAS.

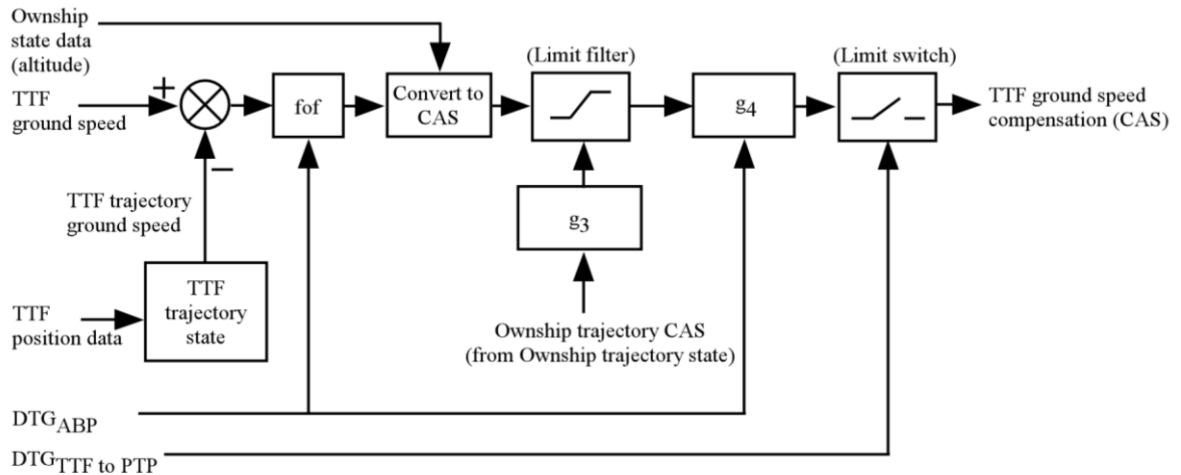


Figure 2.8 Block diagram of the ASTAR TBO ground speed compensation⁽¹⁴⁾

The ground speed compensation in ASTAR was introduced with the purpose to prevent aircraft from closing in to each other too quickly during early stages of FIM operation. Accordingly, it is only used to slow down the aircraft. It was developed to resemble ATC's practice to slow down aircraft below their nominal speed when farther away from the airport and thus is meant to increase ATC acceptability, not spacing performance⁽¹⁴⁾.

The primary input parameters are the TTF's planned, i.e. nominal, ground speed and its actual ground speed. These two values are compared and passed on to a first-order low pass filter. The filter's time constant is modulated by the Ownship DTG to the ABP. The ground speed is then converted to a CAS value, using the Ownship's altitude data, and put through a limit filter to limit its values to 0 to -0.15 times the value of the Ownship's nominal CAS. This value is then modulated by the gain parameter g_4 , again dependent on the Ownships's DTG to the ABP, and finally put through a cutoff switch, which is opened, meaning the ground speed compensations becomes 0, once the TTF has crossed the PTP.

With respect to the federated implementation, speed commands in ASTAR are quantized in either 5 kt or 10 kt steps to reduce the total amount of speed commands and avoid frequent speed manipulation. For example, if the current nominal CAS is 250 kt and the TBO logic has calculated a speed command of 242 kt, the actually issued speed command would be 240 kt.

Further, a flip-flop protection ensures that the commanded speed does not swing between two values when close to the middle of two quantized values; and a look-ahead function prevents the system from commanding an acceleration shortly before a planned deceleration.

Speed commands in ASTAR apply immediately and according to MOPS-FIM a reaction is expected within 11 seconds after a command was issued ("7 seconds for Flight Crew delay [...], 3 seconds for aircraft response [...], and 1 second for latency")⁽⁹⁾.

2.3.2. Graphical User Interface (GUI)

The GUI design of ASTAR has also changed over from the early stages with FMDS, to the Interval Management Alternative Clearances (IMAC) ^(21,22) studies, and finally the ATD-1 flight test. The GUI design for the EFB and CGD used in the flight test are shown in Figures 2.9 and 2.10 respectively.

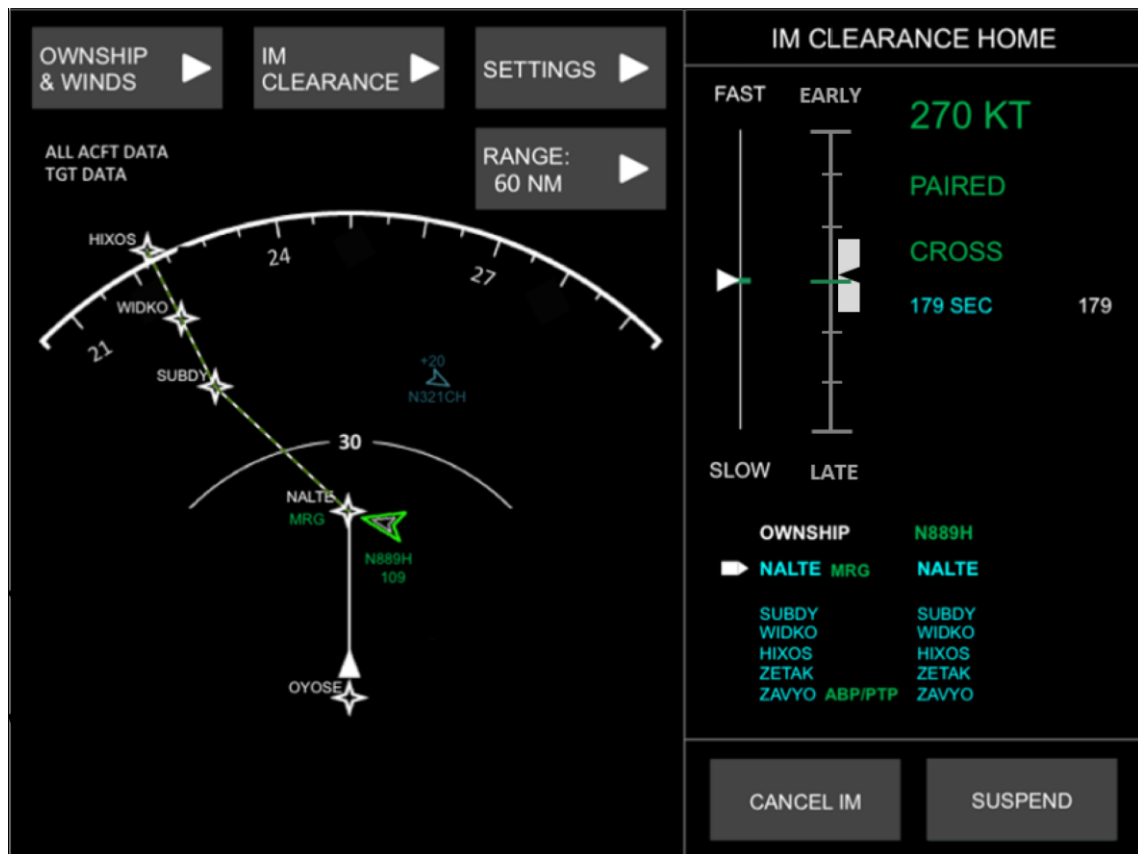


Figure 2.9 Overview of the ASTAR ATD-1 EFB page GUI ⁽¹⁷⁾



Figure 2.10 Overview of the ASTAR ATD-1 CGD page GUI ⁽¹⁷⁾

The EFB page contains of two sides, a navigation display mimicking part on the left and the IM clearance home, showing the IM situation, on the right. The navigation side shows the route of flight, including the waypoints en-route (star symbols), as well as the aircraft in the vicinity, with the TTF highlighted in green.

The IM clearance home shows the current commanded speed, (270 kt), the FIM status (Paired)

and FIM clearance type, i.e., mode, (Cross) in green. The 179 SEC in cyan displays the ASG, and the 179 in white the actual spacing time in seconds.

The Fast/Slow-Indicator (FSI) indicates the relation between the actual CAS and the instantaneous CAS expected by the system, and the Early/Late-Indicator (ELI) indicates the expected spacing situation at the ABP. Here both FSI and ELI are almost in their center position, indicating that the aircraft is flying at the expected speed and the spacing error is close to 0. Below is the waypoint list for the Ownship and TTF, here both approaching NALTE and ending at ZAVYO.

The CGD copies the upper right part of the IM situation, including the FSI, ELI, speed command, and FIM status. When the speed command changes, the new command is shown in reverse video, here black letters on a white background, for 10 seconds. If conformance monitoring is available, i.e., if the system has access to the speed set on the MCP, the speed command will start to flash after 10 seconds if the correct speed is not set.

The speed command value is set to display the target speed of a speed change, i.e., the speed at which the flight is to be continued once it is reached. Therefore, during a speed change the FSI becomes the primary conformance instrument to tell the crew if the actual deceleration rate must be adjusted, e.g. by managing thrust or drag (deploying speed brakes).

2.4. ATD-1 Flight Test

In cooperation with Boeing, Honeywell and United Airlines, NASA tested the above-mentioned technology and interfaces in a 19-day flight test trial in January and February 2017.

In this trial, three aircraft have participated of which one served as a target aircraft using ADS-B Out, and the other two were equipped with ADS-B In and FIM avionics. The target aircraft flew its approaches using different speed schedules and with changing initial errors and the following FIM aircraft tried to achieve their spacing goal, i.e., resolve any spacing error, accordingly.

Four different FIM clearance types: “Maintain”, “Capture”, “Cross-Merge”, and “Cross-FAF” have been tested during the trial.

Maintain and Capture are clearances for traffic on the same track (in-trail), hence both use the CTD control law. In Maintain operation FIM tries to keep the spacing situation, either in time or distance, that was present at the beginning of the operation, whereas Capture tries to establish a spacing situation, based on the ASG, first and then continues on Maintain.

Cross-Merge and Cross-FAF are used for traffic on merging routes, thus use the TBO law. Their goal is to achieve a spacing situation at the ABP. Cross-Merge switches into Maintain mode (using the CTD control law) once the aircraft have joined on the same track and the ASG was achieved. In contrast, Cross-FAF sets the aircraft up for landing on the Final Approach Fix (FAF).

Accordingly, in this thesis the latter two are of interest.

The spacing performance results for all trials are shown in Figures 2.11 and 2.12 and

Tables 2.1 and 2.2 below. FIM operation is deemed as in conformance (pass), if the spacing goal was reached within ± 10 seconds of the ASG. As a requirement 95% of all data is expected to be in conformance.

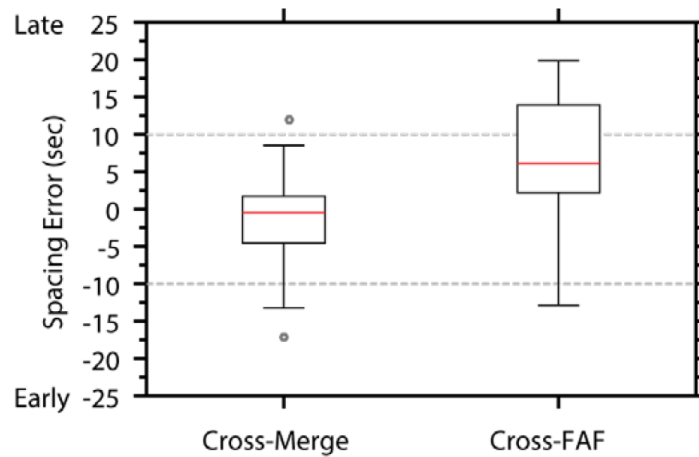


Figure 2.11 Boxplots of the Cross clearances spacing performance ⁽¹⁷⁾

Table 2.1 Spacing performance for the Cross clearance trials ⁽¹⁷⁾

Clearance Type	N	Mean [s]	SD [s]	Pass [%]
Cross-Merge	25	-1.65	6.24	84
Cross-FAF	41	6.24	8.28	59

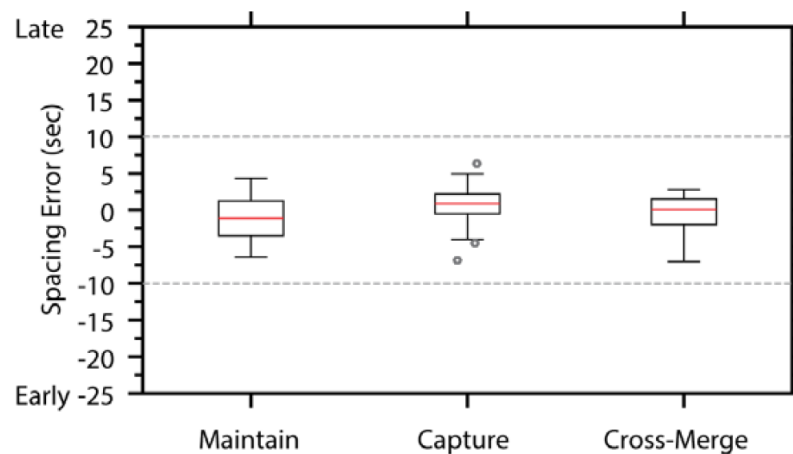


Figure 2.12 Boxplots of the Achieve stage spacing performance ⁽¹⁷⁾

Table 2.2 Spacing performance after the Achieve stage ⁽¹⁷⁾

Clearance Type	N	Mean [s]	SD [s]	Pass [%]
Maintain	18	-1.13	2.99	100
Capture	32	0.55	2.63	100
Cross-Merge	27	-0.47	2.45	100

The results show that for the Cross clearances (TBO), the required pass rate of 95 % is not achieved. However, for all Achieve stages, that is once the aircraft are in-trail and use the Maintain mode, the pass rate is at a perfect 100%. This has two implications:

First, even if the spacing goal is not achieved at the ABP during Cross-Merge operation, this can still be recovered during the in-trail stage, making FIM operation overall successful.

Second, future research efforts should be devoted to the TBO control law, rather than the CTD control law.

The other focus of the flight test was on the human factor, i.e., the pilots' acceptance of the FIM operation. Before the flight test, all participating pilots received computer-based and simulator training, so that they were familiar with the FIM avionics and associated procedures. Further, during the trials, a daily pre-briefing, explaining the approaches of the day, was conducted.

The crew was then surveyed after each run and at the end of the day, using a questionnaire that was divided into a quantitative and a qualitative section. The quantitative section asked the crew for their agreement on statements using a 7-point Likert scale (1 = "Completely Unacceptable", 7 = "Complete Acceptable"), whereas the qualitative section allowed for free comments.

Two questions from the quantitative section, showing the responses for the Cross-Merge operation, are listed in Table 2.3. In the test an a priori assumption was made that the crew will report the FIM operation as acceptable ('5' or better) ⁽¹⁷⁾.

Table 2.3 Survey responses for the Cross-Merge operation ⁽¹⁷⁾

Clearance Type	N	Mean [-]	SD [-]
Rate the Overall acceptability of the IM operation	137	5.9	1.0
Rate the Operational acceptability of the IM speed	137	5.6	1.2

From the results it can be seen that the a priori assumption was met, and FIM operation in general is acceptable. However, when looking at the pilots' comments to each question, some comments have been mentioned frequently. In detail:

- ✈ "Too many IM speed changes and/or excessive use of throttle/speed brake" ⁽¹⁷⁾
- ✈ "IM speed reversals are inefficient, and if flaps must be raised are operationally unacceptable" ⁽¹⁹⁾
- ✈ "Expected deceleration rate did not always appear to be accurate" ⁽¹⁷⁾

Consequently, it was determined that some of the above-mentioned aspects "would likely be unacceptable to line pilots during typical day-to-day operations" ⁽¹⁸⁾.

Further it was noted that “No foreknowledge of the next IM speed meant that the flight crew could only be reactive”⁽¹⁷⁾. In other words, the crew has no information about when the next speed command will be issued, and what that command will be.

In conclusion, pilots requested that “speed commands should be limited to one per minute”⁽¹⁹⁾, and NASA recommended to “explore alternative control law techniques to allow for tradeoffs between spacing error and IM speed change behavior to reduce the rate of speed changes and speed reversals”⁽¹⁸⁾, so that operational implementation can be achieved.

2.5. Other Concepts

2.5.1. Continuous Descent Operations (CDO)

Continuous Descent Operations (CDO), sometimes also referred to as Continuous Descent Approaches (CDA), are a fuel saving descent strategy. Historically, descents from cruise altitude until landing are done in steps, temporarily holding altitudes as instructed by ATC or published on an approach chart; CDOs however have the ideal that an aircraft will start its descent at cruise altitude but then continues to descent all the way until touchdown on the runway. The motivation for this type of operation is that the aircraft can stay at cruise altitude longer, where it usually performs more efficiently, i.e., has a better fuel burn. A comparison between the two descent strategies is shown in Figure 2.13:

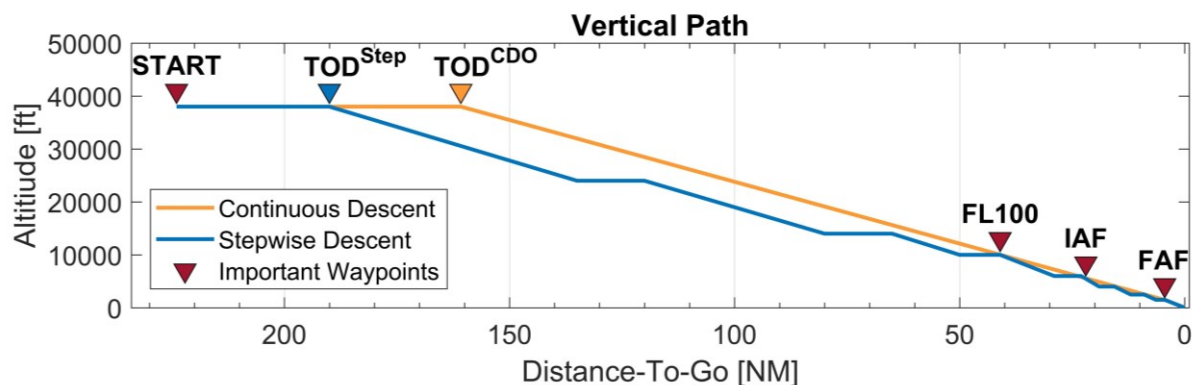


Figure 2.13 Comparison between continuous, here fixed FPA, and stepwise descents (TOD: Top of Descent, FL: Flight Level, IAF: Intermediate Approach Fix, FAF: Final Approach Fix)

In Japan, CDOs are currently employed at 3 airports (Kansai, Kagoshima, and Naha), however so far only during night time⁽⁴⁰⁾.

CDOs can be conducted in different ways, for example using idle thrust, so that the speed, i.e., deceleration rate, is controlled by the aircrafts pitch, and the descent rate will be what naturally sets in; or using a fixed Flight-Path Angle (FPA) in which the speed and thus the deceleration rate are managed by thrust and drag and the descent rate can be calculated from the FPA and the current speed.

Fixed FPAs have the benefit that the resulting flight path is easier to predict, however, since they can require drag as a mean to set an expected deceleration rate, and the A/P has no authority over the speed brakes in flight, they require the pilots to actively deploy speed brakes when needed, thus potentially increasing their workload.

The simulator experiments conducted in References (41) and (42) used widebody aircrafts to evaluate the feasibility of fixed FPA descents and concluded that, while the ideal FPA differs from aircraft to aircraft, an FPA of -2.5° is operationally feasible in terms of pilot workload and performance. In this thesis most approaches have been designed with an FPA of -2.2° , corresponding to vertical flight path shown in Figure 2.13, to allow for an additional buffer on the conservative side.

2.5.2. Base of Aircraft Data (BADA)

The Base of Aircraft Data (BADA) is a database administrated by Eurocontrol, that contains performance parameters and standard speeds for over 400 different aircraft types⁽⁴³⁾.

Besides the equations to calculate the lift, drag, thrust, and fuel flow, BADA also provides equations for speed envelope and atmospheric calculations and conversions. Some of these conversions, e.g., Calibrated Airspeed to True Airspeed (CAS to TAS) are shown in Appendix A.

The BADA Total Energy Model⁽⁴³⁾, which combines the aircraft's thrust (Thr), drag (D), mass (m), altitude (h), True Airspeed (V_{TAS}) and the earth's gravitation (g_0), as per

$$(Thr - D) V_{TAS} = mg_0 \frac{dh}{dt} + mV_{TAS} \frac{dV_{TAS}}{dt}, \quad (2.7)$$

was used to calculate when additional drag, i.e., speed brakes were required during descent and conversely how much thrust was available for accelerations. BADA also offer a simplification for the calculation of the Total Energy Model, called the Energy Share Factor, however this factor was not employed and complete calculations were made implementing the current circumstances.

For this thesis, a dedicated simulation environment, based on Java, was developed, that implements BADA in Version 3.12.⁽⁴³⁾ along the equations of MOPS-FIM. This environment was used for all simulations and experiments in Chapters 4-6.

3. FEASIBILITY STUDY TOWARD TOKYO INTERNATIONAL AIRPORT

The following chapter describes the feasibility studies of FIM operation on approaches in the Tokyo International Airport. Results were partially shown in “Evaluating Applied Flight-deck Interval Management using Monte Carlo Simulations on the K-Supercomputer”⁽⁴⁴⁾, published in the Transaction of the Japan Society of Aeronautical and Space Sciences, Vol. 62, No. 6 and “Preliminary Study on Interval Management for Improving Aircraft Speed Command Behavior”⁽⁴⁵⁾, presented at the 55. Aircraft Symposium of the Japan Society for Aeronautical and Space Sciences, in Matsue, Japan. Figures have been reprinted with permission.

The routings described in this chapter were current as of April 26th, 2018 as per Aeronautical Information Circular NR014/18, but have since been revised. In some paragraphs past tense is used to reflect the situation.

3.1. Introduction

The objective of this study was to gauge the performance of the ASTAR algorithm as a benchmark in preparation for the design of the new algorithm. Furthermore, it was mandatory to investigate the feasibility of FIM on the current common arrival routes toward RJTT, to ensure that the approach route design itself does not pose any obstacle to the successful operation of FIM.

For this purpose the Electronic Navigation Research Institute’s (ENRI) SPICA simulator⁽²⁵⁻²⁷⁾, was used and run on the RIKEN K computer, that allowed for exhaustive Monte Carlo simulations. New to previous studies on FIM operation toward RJTT, workload and efficiency related factors, such as the number of speed commands and reversals were investigated and furthermore, other aspects important to the speed control law behavior and ASTAR based FIM are highlighted.

3.2. Simulation Environment

3.2.1. SPICA

The SPICA (“SpacIng Time Intervals of Arrival Aircraft Conducting Aircraft Surveillance Applications System Interval Management”⁽²⁵⁾) simulator was developed by ENRI in collaboration with NASA^(25,26).

SPICA implements both the ASTAR trajectory generator and TBO speed control law. The latter was originally implemented in version 10 (ASTAR10) and as an integrated (A/THR connected) system⁽⁴⁵⁾. In later studies, SPICA was updated to ASTAR13 in a federated implementation, that issues speed commands in discrete steps of 5 kt or 0.01 Mach⁽⁴⁶⁾.

Further, five proprietary aircraft models, representing the Boeing 737, 747, 767, 777, and 787 are integrated in the simulator. However, these models lack a speed brake model, and consequently speed brakes are not used in SPICA.

Per run SPICA can simulate up to 20 aircraft, i.e., 5 groups of 4 aircraft, in which the last 3 can engage in FIM operation. The scenery, that is the route and weather information, and initial conditions, i.e., aircraft type, target spacing, etc., are defined through external files.

Technically, the simulator is realized as a C++ program, and a GUI, mimicking the radar screen of an ATCo, rounds up its features.

3.2.2. K Computer

The RIKEN K computer was a supercomputer manufactured by Fujitsu that commenced operation in June 2011. At the time, K was the fastest supercomputer in the world, and the first to reach a performance of over 10 petaflops⁽⁴⁷⁾. K used a node-network consisting of over 80,000 units, each employing an octa-core processor operating at 2.0 GHz.

In this thesis the node-network of K was used to run up to 120 nodes in parallel, therefore significantly decreasing the time required for the computation-intensive Monte Carlo simulations performed in this study from one year (for a single machine) to three days.

In August 2019 K was decommissioned and is scheduled to be replaced by the approximately 100 times faster “Fugaku” in 2021.

3.2.3. Arrival Scenarios to Tokyo International Airport

The simulations in this study were separated into two major scenarios:

The first is an en-route scenario, that has its initial waypoints located approximately 200 NM away from the airport and terminates at a given Standard Terminal Arrival Route (STAR) entry waypoint, approximately 30-50 NM out. STARs are published flight procedures that guide aircraft toward a runway in the terminal area; Accordingly, their entry waypoint is a typical location at which aircraft will merge, or already have merged.

The second scenario is an approach scenario, which begins at multiple STAR terminal entries that continue to the same runway threshold. Here the merging point can be as late as the FAF.

A third, night time, scenario that lies in between the two scenarios was also investigated.

Aircraft to RJTT usually enter the terminal area from either the North (formerly via STONE) or the South (via ADDUM). Figures 3.1 and 3.2 show typical arrival routes toward the respective entries that were in use at the time this research was conducted.

Arrivals using STONE normally composed of domestic traffic from northern Japan (here simulated from ZAHAN on), and international traffic from Europe (starting en-route airway Y301, merging at LANAI), and North America (starting at ESCAL, merging at DAIGO). The approximate route length is 140 NM.

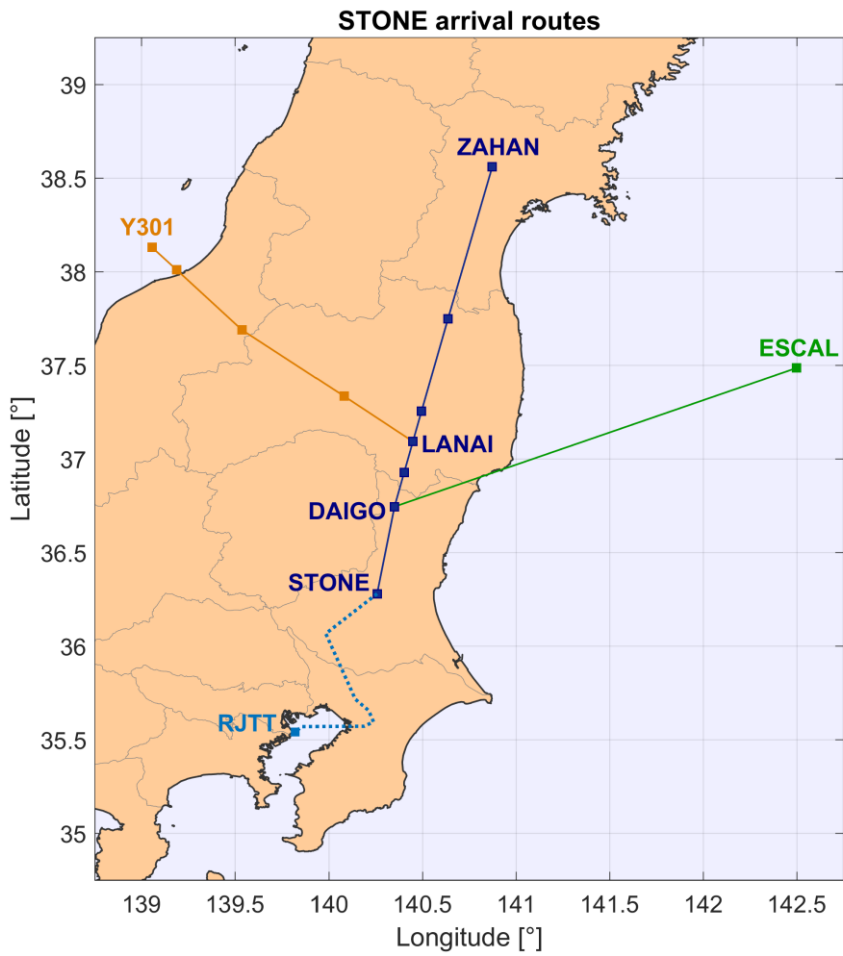


Figure 3.1 Routing for the en-route scenario with Terminal Entry STONE ⁽⁴⁴⁾

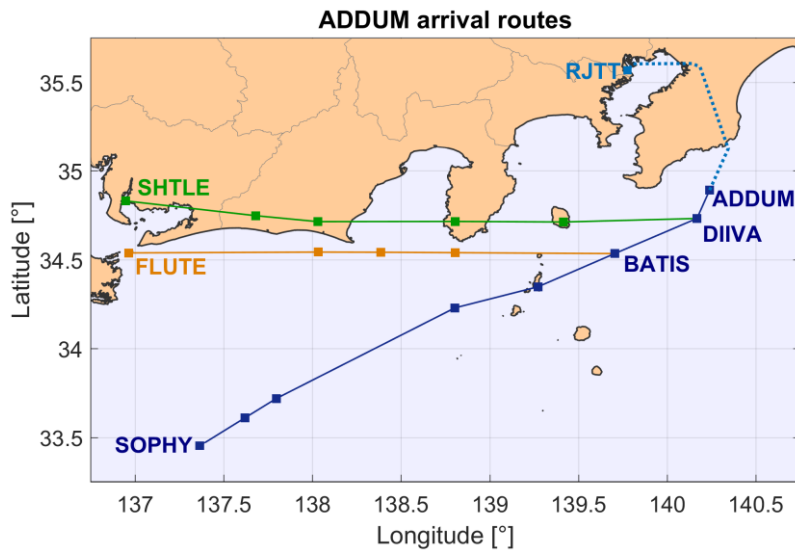


Figure 3.2 Routing for the en-route scenario with Terminal Entry ADDUM ⁽⁴⁴⁾

Arrivals via ADDUM consisted of domestic traffic from western Japan and Okinawa, and international traffic from South-East Asia, here represented by routes originating from SOPHY, FLUTE (merging at BATIS), and SHTLE (merging at DIIVA). The average route length is 170 NM.

The characteristic difference between the two scenarios is the course of all routes in relation to each other. For example, in the ADDUM scenario the aircraft are on parallel or acute courses, whereas in the STONE scenario the two international arrivals are almost on opposing courses.

By contrast, during night time flights from either direction are guided along the sea shore to abate the noise emission over land and inhabited areas. The corresponding routing is shown in Figure 3.3. Here, traffic is guided to UTIBO first, and then continues over the Tokyo Bay inlet to waypoint KAIHO, resulting in an average route length of 172 NM. Different to the previous two entries, KAIHO is significantly closer to the airport and situated at a lower altitude.

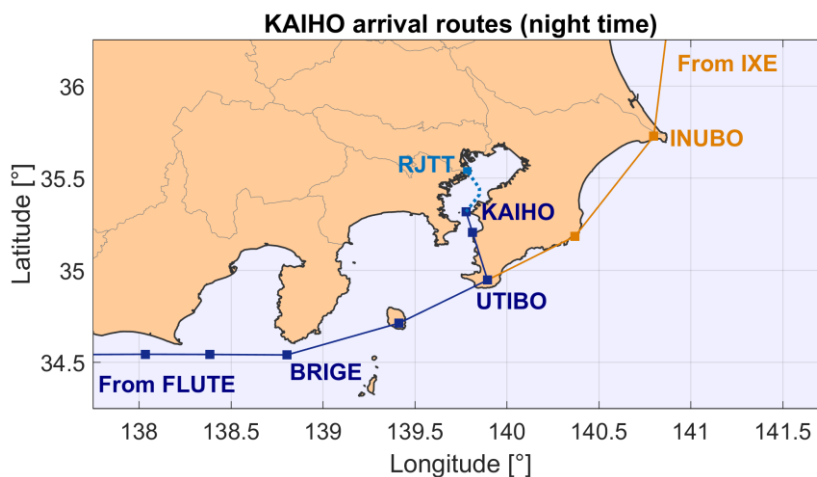


Figure 3.3 Routing for the night scenario with termination point KAIHO ⁽⁴⁴⁾

In regular day operations, two out of four runways (RWY) at RJTT are designated for landings. For example, RWY 34L and 34R during northerly winds, and RWY 22 and 23 during southerly winds. Which of the two is used, is normally determined by the terminal entry point of the flight (ADDUM = RWY 34L / RWY 22, STONE = RWY 34R / RWY 23) as illustrated in Figure 3.4.

However, for shorter taxi times on the ground, or if one runway becomes unavailable, e.g., due to a technical delay, aircraft are guided to the other runway as well (indicated by dash-dot lines). This kind of operation was simulated in the approach scenarios. The approximate route length is 45 NM (RWY 34L / 34R) and 60 NM (RWY 22 / 23) respectively.

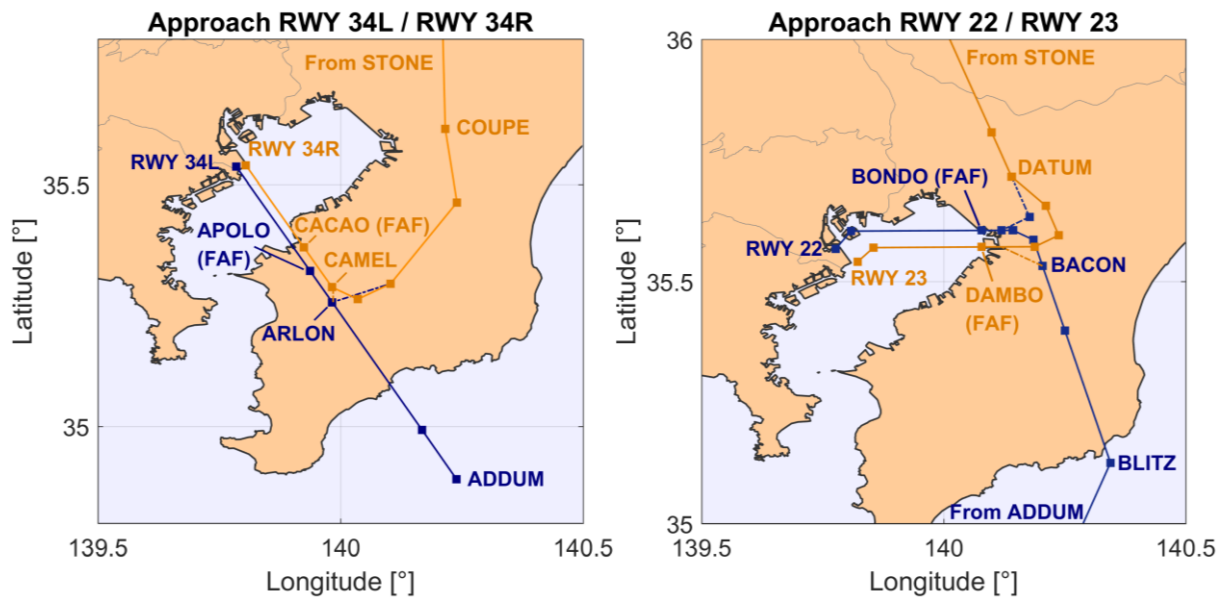


Figure 3.4 Routing for the approach scenarios depending on the runway in use ⁽⁴⁴⁾

Vertically, all traffic was simulated as fixed FPA CDO approaches as described in Subsection 2.5.1, meaning an FPA of -2.2° is assumed from the TOD until the aircraft is established on the glideslope.

3.2.4. Wind Conditions

Two wind datasets, one representing winter conditions (observed on February 14, 2017, 12:00 UTC) and the other representing summer conditions (August 8, 2017, 18:00 UTC) were utilized in this study. From early fall until late spring strong westerly winds, reaching top speeds well over 100 kt at FL300 (30,000 ft) and above, blow over the main island of Japan. During the summer months these winds move northwards, resulting in more benign wind conditions over central Japan. Both conditions are reflected in the datasets.

3.2.5. Aircraft

Aircraft were always simulated in four groups of four aircraft each, so that the last three aircraft engage in FIM, giving a total of twelve FIM aircraft per simulation. Their sequence, i.e., the starting waypoint for each aircraft, was predetermined, but each group had a different order to ensure all possible pairings were tested.

The aircraft type was selected randomly, based on the distribution of actual arrival traffic to RJTT, surveyed in Ref. (46). Aircraft models that were not represented in SPICA were assigned the most comparable model, e.g., an Airbus A320 would be added to the probability of the Boeing 737.

3.2.6. Initial Conditions

In the en-route scenarios, all aircraft started with the same speed (Mach 0.83) and at the same flight level (FL380 = 38,000 ft); The final speed and altitude for the en-route scenario, given by the respective waypoint constraint, was also the initial setting for the approach scenarios (i.e., ADDUM: 10,000 ft @ 230 kt, STONE: 11,000 ft @ 250 kt, and KAIHO: 4,000 ft @ 230 kt).

The simulation start times were arranged in such a way that flight time differences caused by different route lengths and conditions were eliminated.

Nevertheless, each flight started with a randomly chosen spacing error within ± 15 s, so that the maximum initial spacing error between two aircraft could be ± 30 s.

3.2.7. Evaluated Data and Number of Simulations

Evaluated parameters included the final spacing error, that is the remaining spacing error at the runway threshold, the number of speed commands and their frequency, and the number of reversals. FIM operation was deemed successful as per ATD-1 conformance definition (i.e., arrival within ± 10 s of the ASG).

Each scenario was simulated 10,000 times, so that with 12 FIM aircraft each, a total of 120,000 datasets were taken.

3.3. Results

The following subsections show the spacing performance for each scenario as a histogram and boxplot graph combination. For both graphs, the x-axis represents the spacing error. Bars in the histogram have a width corresponding to 1 s and are shown for the area from 0 to 20,000 occurrences for the en-route and night scenarios, and up to 55,000 occurrences for the approach scenarios. In all scenarios the initial spacing error distribution is shown in silver-gray. For the en-route scenarios the winter data is shown in navy and the summer data in yellow, whereas in the approach scenarios navy and yellow represent the individual runways.

The boxplots are shown below the histogram in corresponding colors, and are drawn according to the Tukey convention, i.e., the box contains 50% of all data and the whiskers have a maximum length of 1.5 times the interquartile range (the length of the box). Results outside of the whiskers are considered as “outliers”. Here however, outliers are omitted for better readability.

3.3.1. En-route Scenario

Figure 3.5 and Table 3.1 show the results for the en-route scenarios to ADDUM and STONE.

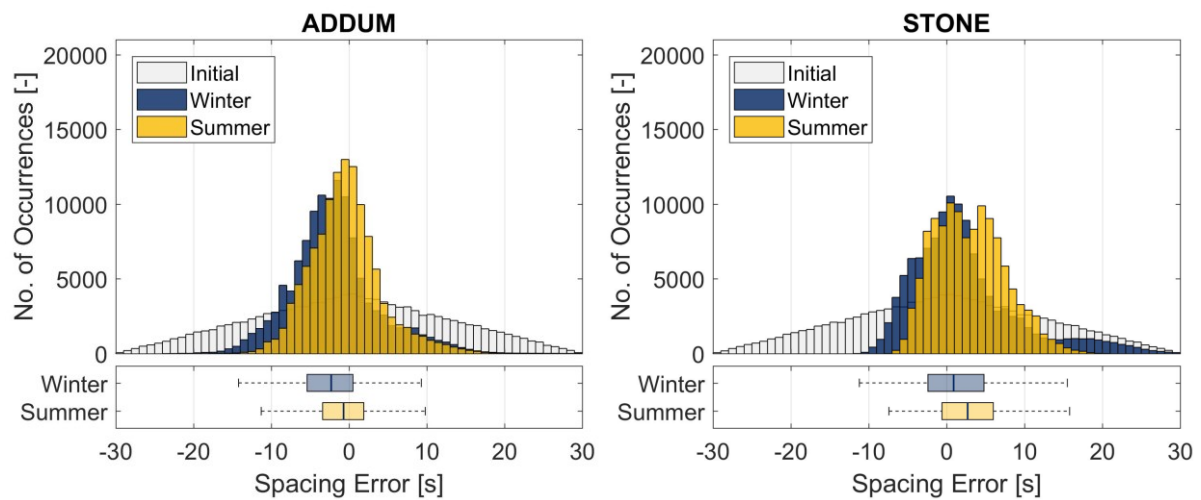


Figure 3.5 Spacing performance for the en-route scenarios

Table 3.1 Results for the en-route scenarios

Parameter	ADDUM	ADDUM	STONE	STONE
	Winter	Summer	Winter	Summer
Success rate [%]	89.6	95.6	87.6	92.3
Median spacing error [s]	-2.30	-0.70	0.90	2.70
Mean spacing error [s]	-1.96	-0.46	2.26	2.95
Standard deviation [s]	5.80	4.73	6.95	4.53
Interquartile range [s]	5.90	5.30	7.20	6.60
Mean number of speed commands [-]	23.7	17.4	25.5	28.3
Commands issued within less than 60s [-]	18.9	12.8	22.2	24.0
Mean reversals [-]	2.0	1.1	1.0	1.0

As seen in the histograms, an overall improvement of the spacing error, compared to the initial conditions, is observed. Only the STONE – Winter scenario shows a distinctive tail towards the positive spacing error side, which is further discussed in Subsection 3.4.1.

Mean final spacing errors range from -1.96 s (ADDUM – Winter) to $+2.95$ s (STONE – Summer). However, the desired success rate of 95% is only achieved for the ADDUM – Summer scenario (95.6%); the lowest success rate was observed for the STONE – Winter scenario (87.6%). Furthermore, the winter scenarios showed SDs higher than the 5 s anticipated in Subsection 2.1.1. By contrast, the summer scenario, with more benign wind conditions, shows overall better results.

The high number of speed commands is owing to the fact that the ASTAR logic used here did not incorporate an end speed logic; Operationally realistic numbers and a further discussion are given in Subsection 3.3.4. Finally, for all scenarios on average at least one reversal was observed.

3.3.2. Night Scenario

Results for the night scenario toward KAIHO are shown in Figure 3.6 and Table 3.2.

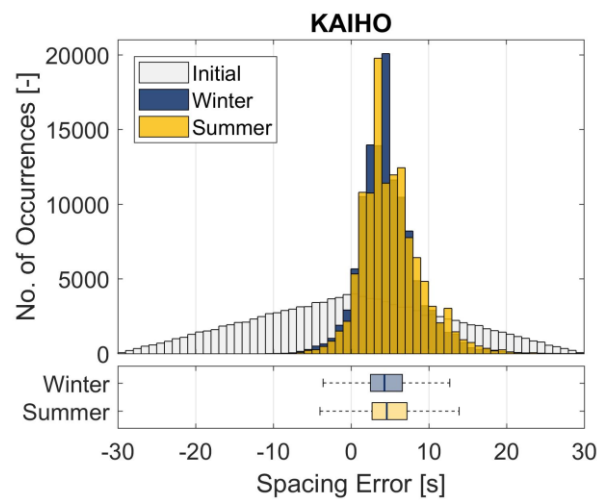


Figure 3.6 Spacing performance for the night time scenario

Table 3.2 Results for the night scenario

Parameter	KAIHO Winter	KAIHO Summer
Success rate [%]	91.6	89.2
Median spacing error [s]	4.30	4.60
Mean spacing error [s]	4.72	5.22
Standard deviation [s]	3.69	3.87
Interquartile range [s]	4.10	4.50
Mean number of speed commands [-]	22.9	22.6
Commands issued within less than 60s [-]	17.8	16.7
Mean reversals [-]	1.8	1.9

Compared to the previous en-route scenarios, a more evident peak for the final spacing error can be observed in the histogram. Nevertheless, the overall success rate was just 91.6% (Winter) and 89.2% (Summer) respectively, because most aircraft arrived with a delay, indicated by the mean spacing error of +4.72 s and +5.22 s respectively. In contrast, an improvement in the SD was observed, showing satisfactory results at 3.69 s and 3.87 s.

However, if, in an operational environment, a systematic offset, as observed here, is detected by ATC, the overall success rate could easily be improved by intentionally reducing the ASG.

The total number of speed commands did slightly improve compared to the en-route scenarios; however, the mean number of reversals was high for both scenarios, at 1.8 at 1.9 respectively.

3.3.3. Approach Scenario

Figure 3.7 and Table 3.3 show the results for the approach scenarios.

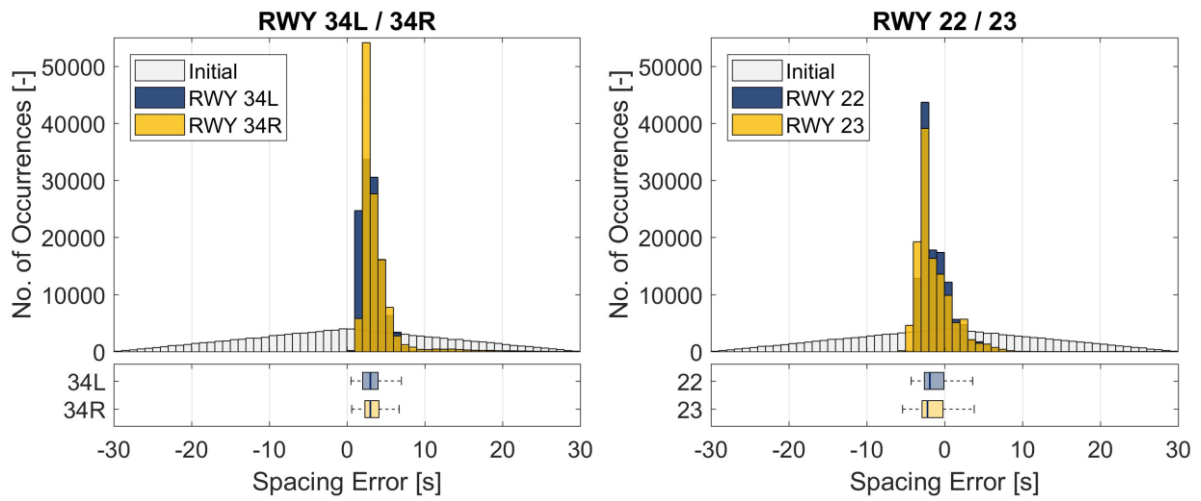


Figure 3.7 Spacing performance for the approach scenarios, divided by active runway

Table 3.3 Results for the approach scenarios

Parameter	RWY 34L	RWY 34R	RWY 22	RWY 23
Success rate [%]	97.0	97.1	100	99.8
Median spacing error [s]	3.00	3.00	-1.90	-2.20
Mean spacing error [s]	3.52	3.65	-1.18	-1.36
Standard deviation [s]	2.66	2.50	2.00	2.41
Interquartile range [s]	2.00	1.80	2.50	2.70
Mean number of speed commands [-]	13.6	13.6	20.0	20.0
Commands issued within less than 60s [-]	10.9	10.7	16.4	16.4
Mean reversals [-]	1.5	1.3	1.6	1.4

The approach scenarios showed the overall best results; to the extent that the y-axis scale had to be extended to 55,000. The success rate is satisfactory for all scenarios, accentuating for RWY 22 at 100% (only 4 of the 120,000 FIM operations were unsuccessful).

Conversely, the SD was also satisfactory for all runways, with results between 2.00 s (RWY 22) to 2.66 s (RWY 34L).

The mean spacing errors show a slightly delayed arrival for RWY 34L and RWY 34R and a marginally early arrival on RWY 22 and RWY 23.

In line with the shortest route length, the overall fewest commands were also observed for RWY 34L and RWY 34R.

Despite the overall good performance, reversals are still present for all scenarios, ranging from 1.3 (RWY 34R) to 1.6 (RWY 22).

3.3.4. End Speed Logic

The results in Subsections 3.3.1 - 3.3.3 showed the data for ASTAR13 without a so called end speed logic (ESL), meaning the commanded speed is the direct output of the speed control law, discretized in 5 kt steps. During planned deceleration segments this causes continuously changing commands as the ASTAR algorithm follows the nominal speed profile (depicted by the orange line in Figure 3.8). Naturally, this is not desirable as the pilots would have to constantly set a new speed on the MCP. Therefore, NASA implemented a secondary speed command, called the end speed command ⁽¹⁴⁾, that displays the final speed of the deceleration segment including any FIM commanded offset (dashed green line) to the pilots. This logic was added to the SPICA simulator, but albeit having a positive impact on the number of speed commands, had a negative impact on the spacing performance. For comparison the final spacing error, standard deviation, number of speed commands, and those issued within 60s are shown in Tables 3.4 – 3.7 respectively.

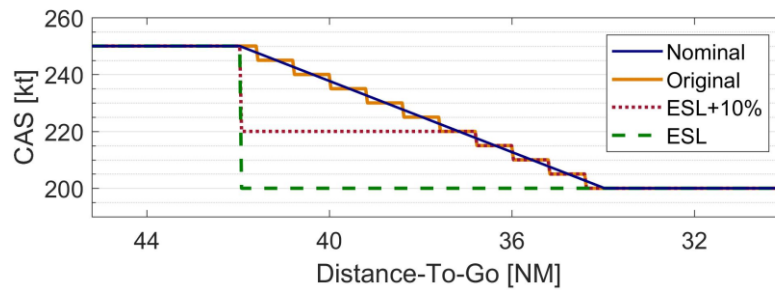


Figure 3.8 Speed command behavior for different ESL tolerances ⁽⁴⁴⁾

Looking further into the issue, previous studies with the SPICA simulator ^(45,46) indicated that the achieved deceleration rate differed significantly from the expected deceleration rate, usually showing a much higher deceleration rate. Accordingly, when the end speed was set at the beginning of a deceleration, the actual target speed was achieved much earlier than estimated by the algorithm. This furthered a delayed arrival, which impacted the performance with the ESL.

Table 3.4 Mean Final spacing error with and without an ESL for each scenario

Logic	ADDUM Winter	ADDUM Summer	STONE Winter	STONE Summer	KAIHO Winter	KAIHO Summer	RWY 34L	RWY 34R	RWY 22	RWY 23
Orig.	-1.96	-0.46	2.26	2.95	4.72	5.22	3.52	3.65	-1.18	-1.36
ESL	3.07	5.65	7.16	8.01	11.51	12.93	12.19	12.64	16.61	18.03

Table 3.5 SD of the final spacing error with and without an ESL for each scenario

Logic	ADDUM Winter	ADDUM Summer	STONE Winter	STONE Summer	KAIHO Winter	KAIHO Summer	RWY 34L	RWY 34R	RWY 22	RWY 23
Orig.	5.80	4.73	6.95	4.53	3.69	3.87	2.66	2.50	2.00	2.41
ESL	11.23	10.67	11.32	6.68	15.13	17.05	7.35	7.30	19.69	22.30

Table 3.6 Total number of speed commands issued with and without an ESL for each scenario

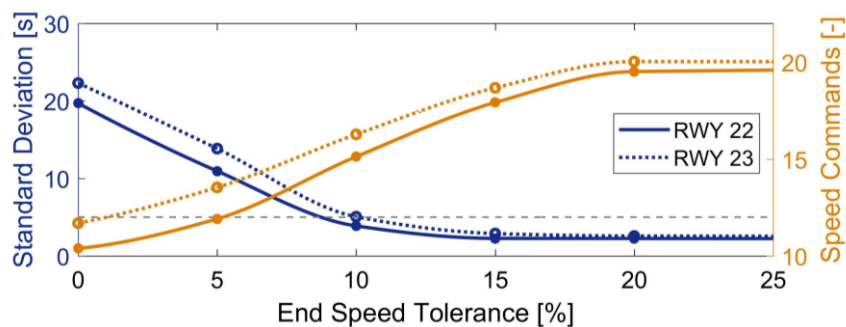
Logic	ADDUM Winter	ADDUM Summer	STONE Winter	STONE Summer	KAIHO Winter	KAIHO Summer	RWY 34L	RWY 34R	RWY 22	RWY 23
Orig.	23.7	17.4	25.5	28.3	22.9	22.6	13.6	13.6	20.0	20.0
ESL	13.8	6.7	13.0	15.8	12.3	11.8	6.9	7.1	10.4	11.7

Table 3.7 Speed commands issued within less than 60s with and without an ESL for each scenario

Logic	ADDUM Winter	ADDUM Summer	STONE Winter	STONE Summer	KAIHO Winter	KAIHO Summer	RWY 34L	RWY 34R	RWY 22	RWY 23
Orig.	18.9	12.8	22.2	24.9	17.8	16.7	10.9	10.7	16.4	16.4
ESL	8.7	2.2	9.8	11.5	7.6	6.7	4.0	3.9	7.1	8.2

Therefore, if the profile was to follow the nominal profile, i.e., the instantaneous FIM speed, as close as possible, so that the effect of the mismatching deceleration rate was the smallest, the ESL may not be used. As a trade-off, it was experimented to use the ESL, but with a tolerance, so that first an intermediate speed, like the end speed but higher, is set and then the re-adjustment is continued as needed (shown for a tolerance of +10% by the red dotted line in Figure 3.8). Tolerances that were explored are 0%, 5%, 10%, 15%, and 20%.

Figure 3.9 shows the effect of the tolerance on the number of speed commands (orange) and the resulting standard deviation (blue) by the example of the approach scenarios to RWY 22 (solid line) and RWY 23 (dotted line). The axes are drawn in a relative scale, as to include the minimum and maximum values. Intermediate values have been interpolated by cubic spline interpolation.


Figure 3.9 Progression of SD and commands depending on the end speed tolerance ⁽⁴⁴⁾

It can be seen the SD of the final spacing error is the highest for a tolerance of 0%, where in contrast the number of speed commands is the lowest. The SD reaches its minimum at approximately 15%, whereas the speed commands reach their maximum at 20%.

A visual trade-off point, i.e., the lowest SD and number of commands is found at approximately 7%; however, with respect to the SD goal of 5 s (Subsection 2.1.1), all tolerances lower 10% do not qualify as their SD is higher. Therefore, for the best trade-off that still renders acceptable results a tolerance between 10% and 15% is suggested.

3.3.5. Chained Operation

An earlier simulation using ASTAR10, presented in Ref. (45), examined the stability of chained operation, also referred to as the “string stability”.

The simulation used the same runway configurations and weather conditions as in Subsection 3.3.3, however in a different initial error setup. For example, instead of starting aircraft with their nominal spacing plus a random initial error, a fixed initial error was applied to each aircraft in one group, so that their errors cumulated. For example, if all aircraft started with the same relative error of -10 s, the first aircraft has to delay its arrival by 10 s, and consequently the second aircraft has to delay its arrival by $10+10 = 20$ s and so on.

The initial fixed errors were -20 s, -10 s, 0 s, and $+10$ s. With respect to the initial error, the random spacing error was reduced to ± 10 s, so that the extreme conditions could result in a relative error of -40 s or $+30$ s and with accumulated effects -80 s or $+50$ s.

The results showed that the third aircraft in the chain of aircraft with -20 s, i.e., the aircraft that potentially needs to delay its arrival by 80 s, was the most critical. An example is shown in Figure 3.10. Therefore, in this case a pilot or controller intervention is indicated, and additional delay would need to be generated by alternative means, e.g., S-turns.

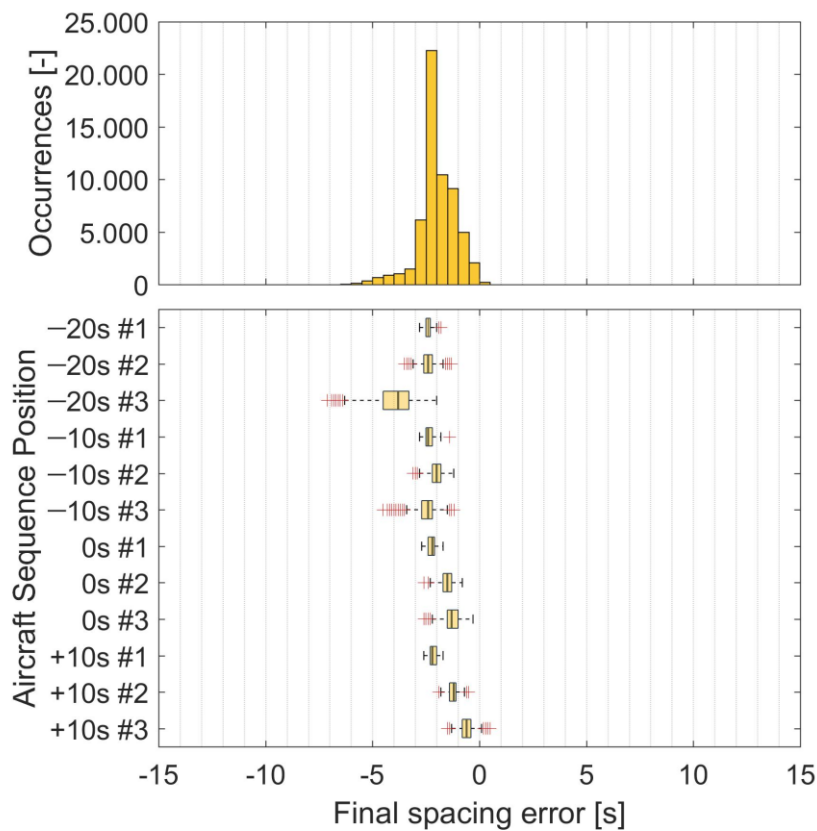


Figure 3.10 Spacing performance for chained FIM operations, by example of RWY 23 ⁽⁴⁵⁾

3.4. Discussion

3.4.1. Wind Effects

Further investigation of the winter data of the STONE scenario showed that the distinctive tail seen in the data histogram was caused almost exclusive by traffic originating from waypoint ESCAL. The corresponding waypoint-by-waypoint comparison is displayed in Figure 3.11.

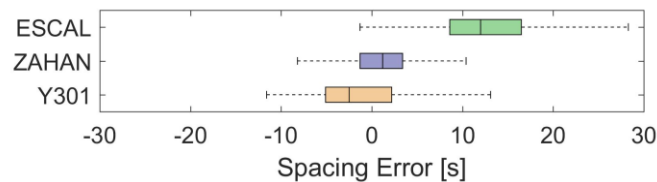


Figure 3.11 Spacing performance for the STONE winter scenario, divided by start point ⁽⁴⁴⁾

Examining the wind direction (W_D), velocity (W_V) and course (CRS) of each routing, a significant difference for the initial tailwind component ($W_{||}$), i.e., the wind parallel to the aircraft's course and the resulting ground speed (GS) was observed, as shown in Table 4.10 for the conditions at FL400.

Table 3.8 Wind conditions and GS at the initial waypoint for the STONE - Winter scenario ⁽¹⁷⁾

Initial WP	CRS [°]	W_D [°]	W_V [kt]	Wind description	$W_{ }$ [kt]	GS [kt]
ESCAL	247.2	269.5	89.9	Headwind	-83.2	391.7
ZAHAN	193.0	273.3	68.5	Crosswind	-11.5	459.7
Y301	140.0	278.8	75.3	Quartering Tailwind	+56.7	530.1

While the initial wind conditions have been considered in the scenario design, any deviation from the nominal profile, e.g., by a FIM command or a different than expected deceleration rate, also changed the amount of impact the wind had on the arrival time.

In this scenario the most notable example is the arrival from ESCAL, that experiences a tailwind component of -83.2 kt (headwind), causing a tendency for a later arrival. In comparison, traffic from Y301 experiences a tailwind component of +56.7 kt and a tendency for an earlier arrival.

Therefore, here a combination of a lead aircraft originating from Y301 and a trailing aircraft from ESCAL would cause the most unfavorable FIM conditions.

The example of the two routes highlights that certain combinations have a higher likelihood for FIM to fail, i.e., not achieve the required spacing performance. Accordingly, consideration should be given to which routes and combination thereof are favorable for FIM operation.

Furthermore, in this example the combined GS difference was 138.3 kt, considerably higher than what the 15% CAS tolerance for ASTAR could compensate. Therefore, the GS difference might also be used as an indicator for the complexity of FIM operation.

Support by ATC in selecting appropriate pairings could significantly improve this situation.

3.4.2. Effect of Runway Proximity on the Spacing Performance

From the en-route scenario to the approach scenarios a constant improvement in the standard deviation of the spacing performance and more prominent peaks in the histograms were observed.

The improved performance with proximity to the runway is partially related to the lower altitude of the aircraft. For example, at lower altitude winds are usually weaker than at higher altitudes. Further, the air is denser, causing for a smaller spread between the CAS and TAS, and accordingly a lower GS. Finally, the speed on approach is generally slower than during cruise, thus speed changes with the same step size have a higher impact at lower speeds than at higher.

Notably, even with the same initial error distributions for all scenarios, the approach scenarios were able to achieve their performance. It is therefore hypothesized that applying the results of the en-route as input to the approach scenarios, would render further improved results.

3.4.3. Reasons for High Numbers in Speed Commands and Reversals

Concentrating on an operationally realistic environment, i.e., excluding the SPICA peculiar phenomenon of increased speed commands when not using an ESL, two contributing factors for the number of speed commands and reversals were identified, depicted in Figure 3.12:

First, the ASTAR algorithm's design to calculate speed commands in relation to the current nominal speed. By example, when a FIM command is issued (DTG 77 NM in Figure 3.12) the aircraft either accelerates or decelerates according to the spacing error's sign. Once the error is resolved, ASTAR would then command to return, i.e., decelerate or accelerate, back to the nominal speed (65 NM). Thus, even when successful, two commands are issued for one counteraction.

Second, it was observed that ASTAR sometimes issues commands in relatively close proximity to planned decelerations. While a look ahead function was implemented in ASTAR13 that inhibits an acceleration if the nominal speed profile showed an upcoming deceleration⁽¹⁴⁾, still some commands with rather low efficiency were observed. By example, if a speed command of +10 kt is issued 45 s before a planned deceleration, and the assumed acceleration and deceleration rate is 0.5 kt/s, then the new speed would be effectively kept for only 5 s.

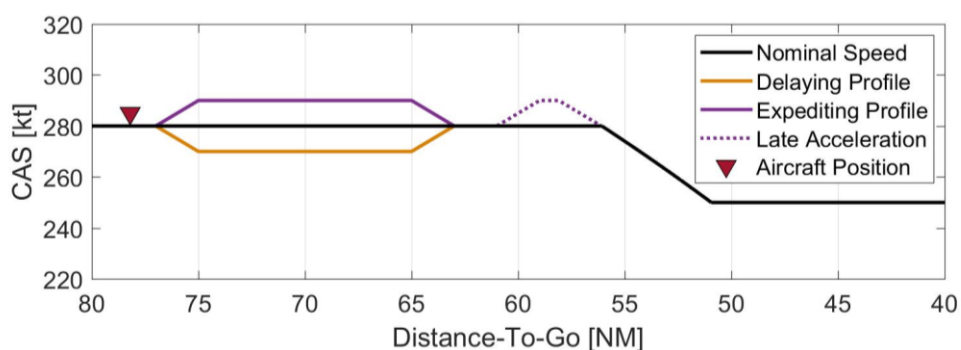


Figure 3.12 Characteristics of the ASTAR algorithm that increase speed commands⁽⁴⁵⁾

3.5. Conclusion of Chapter 3

Overall, the results shown in Subsections 3.3.1 - 3.3.3 demonstrated a good FIM performance, yet, for the en-route and night scenarios not always satisfactory in regard to the 95% criteria. Nevertheless, it was shown that initial spacing errors of ± 30 s can significantly be reduced, by using FIM. Notably, the success rate and standard deviation of all scenarios improved with proximity to the runway, indicating a satisfactory performance at the runway threshold.

Furthermore, a chained operation study showed that strings of two FIM aircraft generally do not pose a problem, however in adverse conditions of cumulating negative error, the risk for FIM to fail increases from the third aircraft on.

The wind conditions in the STONE – Winter scenario have shown that attention must be given to the choice of suitable FIM aircraft pairings, and that the relative GS difference might be an indicator of the likelihood of FIM to succeed. Here, the oversight of ATC can tremendously contribute to the success of FIM by assigning pairings with favorable conditions.

Other than the above, no circumstances were identified that would prohibit or obstruct the application of FIM on routes toward Tokyo International Airport.

Finally, factors that contribute to an increased number of speed commands issued by ASTAR have been identified and were considered during the design of the new algorithm described in Chapter 4.

4. INTERVAL MANAGEMENT – SPEED PLANNING

The following Chapter describes the design and performance of the proposed control logic. Results were partially shown in Ref. (48), “Reducing Speed Commands in Interval Management using Speed Planning”, published in *The Aeronautical Journal*, and Ref. (49), “Evaluating Control Logics for Flight-deck Interval Management”, presented at the 6th ENRI International Workshop on ATM/CNS, in Tokyo, Japan. Figures have been reprinted with permission.

4.1. Introduction

Recognizing the findings of the ATD-1 flight test (Section 2.4), the proposed control logic was designed with the motivation to alleviate the reported increase in pilot workload by minimizing the need for additional speed commands and giving the crew a better comprehensibility, i.e., foreknowledge, of the system’s intentions. The system therefore uses a different control concept than ASTAR, in that it examines the entire remaining speed profile and available speed envelope to modify primarily the planned speed changes.

The logic was hence given the name “Interval Management – Speed Planning” (IM-SP).

The following subsections give an overview of the concepts and terminology of IM-SP, explain its algorithm, and present two benchmark studies comparing the performance of IM-SP to ASTAR.

4.2. Speed Plan Definitions

4.2.1. Time Required Map

To analyze the aircraft’s speed envelope, estimate profile modification effects, and reduce computation time, a time required map is generated from the aircraft’s planned route, vertical profile and (forecast) winds.

Essentially, the map is a representation of the aircraft’s speed envelope, i.e., maximum and minimum speed, over the remaining flight distance, meaning from calculation of the map to the ABP (or beyond), further divided into quadrants of uniform distances (d_{Step} , here = 0.02 NM) and speed steps (CAS_{Step} , here = 1 kt).

For each attainable airspeed, i.e., quadrant within the envelope, the required flight time (t_{Req}) for d_{Step} is calculated from the aircraft’s GS, as a function of the CAS, corrected for atmospheric conditions, i.e., the TAS, and wind. The respective values are stored within the map, which then serves as a look-up table for the calculation of alternative speed plans.

The speed envelope borders itself, i.e. minimum and maximum speed, are defined from a

combination of aircraft specific limitations, waypoint or legal constraints (e.g. 250 kt below 10,000 ft) and assumed acceleration rates.

Figure 4.1 shows an example of the speed envelope, nominal speed profile and time required map for a Boeing 787-8 on approach to RJTT. The time required for each distance step is indicated by the background color (blue = faster speed / shorter time, yellow = slower speed / longer time).

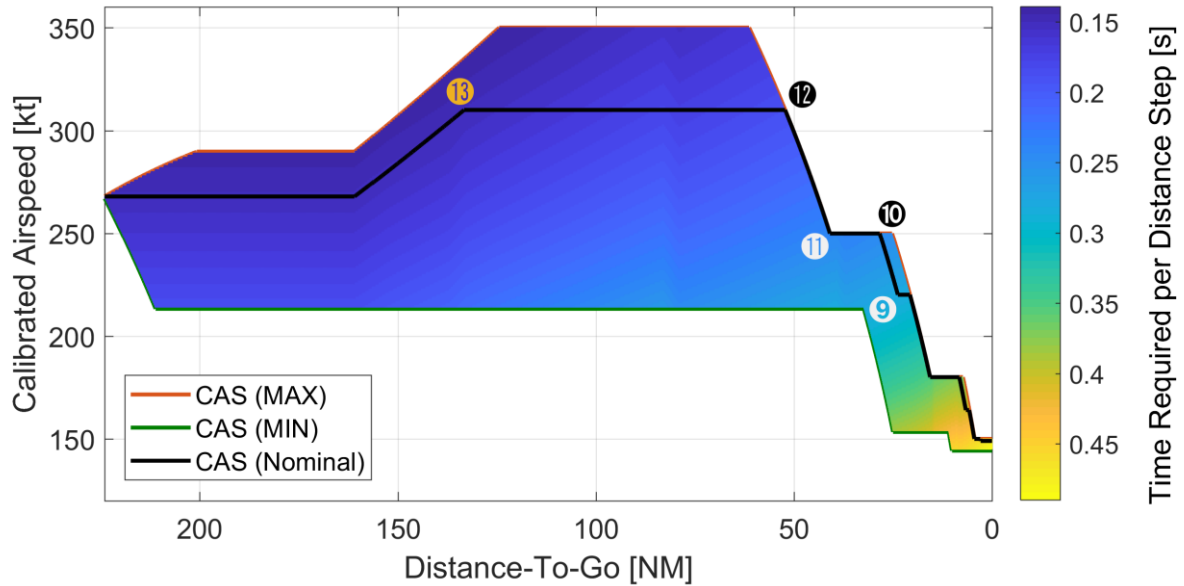


Figure 4.1 Speed envelope and nominal speed for a Boeing 787-8⁽⁴⁸⁾
(Reference speeds per BADA, $d_{\text{step}} = 0.02$ NM)

Table 4.1 Action Points list for the nominal profile⁽⁴⁸⁾

AP	DTG [NM]	CAS [kt]	CAS _{TGT} [kt]	Type
14	223.96	M0.84	M0.84	Initial
13	133.32	M0.84	310	Transition
12	52.26	310	250	Deceleration
11	40.94	250	250	Constant CAS
10	28.40	250	220	Deceleration
9	23.78	220	220	Constant CAS
8	20.74	220	180	Deceleration
7	15.64	180	180	Constant CAS
6	8.28	180	164	Deceleration
5	6.62	164	164	Constant CAS
4	5.78	164	150	Deceleration
3	4.48	150	150	Constant CAS
2	3.00	150	149	Deceleration
1	2.90	149	149	Constant CAS
0	0	149	149	Final

4.2.2. Action Point Concept

The Action Point (AP) concept is used to concisely describe the aircraft's speed plan. Every event significant to the speed profile, e.g., the initial and terminal point of the profile, the beginning and end of a speed change, or conversely, the end or beginning of a Constant CAS Segment (CCS), and the Mach/CAS transition are referred to as an AP.

These APs are further described by their position (DTG), initial CAS and target CAS (CAS_{TGT}), and type. A comprehensive list for the speed profile in Figure 4.1 is shown in Table 4.1 and selected APs are marked within the figure.

A speed plan modification can then be denoted by addressing the respective AP by superscript, e.g., AP^8 represents the eighth AP, and indicating the change by subscript, e.g., AP_{CAS-10} indicates a CAS_{TGT} change of -10 kt; Combined: AP_{CAS-10}^8 .

4.3. Speed Plan Modifications

4.3.1. Planned Speed Changes

Figure 4.2 shows the two modification types (CAS_{TGT} or DTG) applicable to planned speed changes or existing APs.

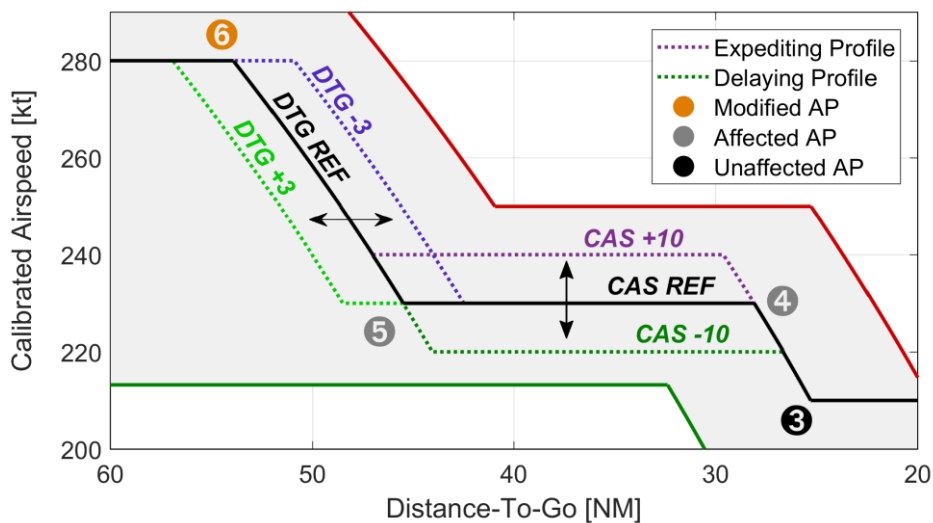


Figure 4.2 Principle for modifications made to planned speed changes ⁽⁴⁸⁾

CAS_{TGT} modifications alter the target speed, i.e., the speed that is to be achieved at the end of the speed change, and conversely the speed of the next CCS, and leave the DTG of the AP, that is the position where the speed change is initiated, unchanged.

However, a CAS_{TGT} modification has an effect on the subsequent two APs. In the example of Figure 4.2, the CAS_{TGT} of AP^6 is modified and accordingly the CAS and DTG values of AP^5 and AP^4 are affected.

CAS_{TGT} changes are calculated in the interval i_{CAS} (here 1 kt, equal to CAS_{Step}) within the range of r_{CAS} (20 kt), but can neither assume values outside the speed envelope, nor values higher or lower than the previous or next CCS respectively. For example, if the CAS_{TGT} is 230 kt and minimum speed is 213.4 kt (as seen for AP⁶ in Figure 4.2), the lowest value that CAS_{TGT} is examined for is 214 kt.

DTG modifications alter the position where the speed change is initiated, but do not change the CAS_{TGT} . Accordingly, in the example in Figure 4.2 a DTG change to AP⁶ also changes the DTG of AP⁵, but not its CAS, and leaves AP⁴ entirely unaffected.

Modifications of the DTG are calculated in the interval i_{DTG} (0.5 NM) and in the range of r_{DTG} (5 NM). If the full range cannot be used, e.g., because a speed constraint, or the next planned speed change requires a deceleration to begin, the last possible position is also evaluated. E.g., if the speed change cannot be shifted farther than -0.8 NM, both -0.5 NM and -0.8 NM are considered.

In general, all upcoming planned speed changes are considered for modification. However, if the next planned deceleration is too close to ensure sufficient crew reaction time (Subsection 4.5.3.3) to implement the change as intended, all but the segment directly ahead will be considered for modification.

4.3.2. Additional Speed Changes

When a modification to an existing speed change is not possible or advisable, an additional (unplanned) speed change, i.e., new AP, can be added to the CCS the aircraft is currently on (or if the aircraft is currently executing a speed change, to the next CCS), as shown in Figure 4.3.

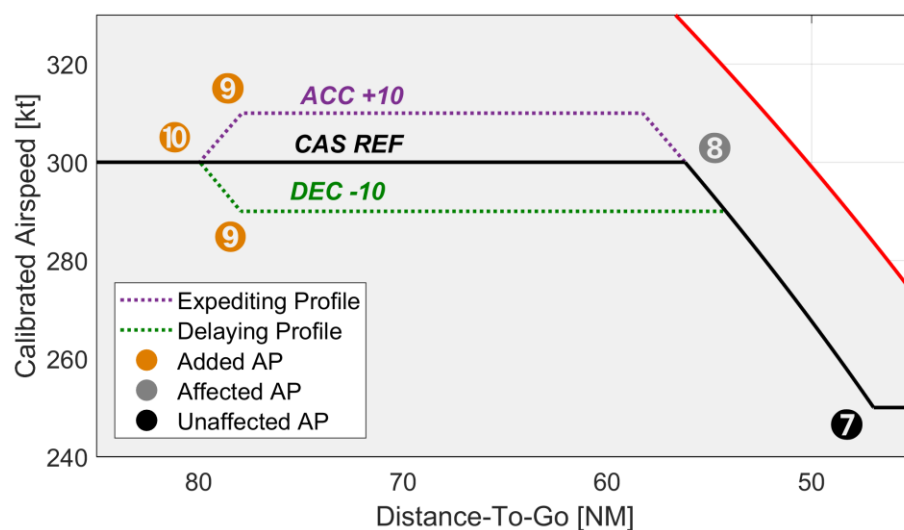


Figure 4.3 Principle for the addition of unplanned speed changes ⁽⁴⁸⁾

Naturally, the direction of the change, i.e., acceleration or deceleration, is dependent on the sign of the spacing error, that determines if the arrival must be expedited (positive error) or delayed (negative error). Either way, the new speed is kept until the next planned speed change, or the speed envelope requires the speed to be left.

New APs (AP¹⁰ and consequently AP⁹ in Figure 4.3) can be inserted anywhere on the CCS between the earliest possible moment, i.e., 11 s after annunciation, as in ASTAR, and the latest possible position that allows the new speed to be maintained for 5 NM (approximately 60 s) to comply with MOPS-FIM and the request made in Ref. (19).

Accelerations are limited to +10% of the current CAS, whereas decelerations are limited to -20 kt, identical to a CAS_{TGT} change.

4.4. Algorithm Considerations

As the speed plan modification examples have shown, multiple methods exist to change the speed plan in response to the spacing error. In fact, when analyzing the entire speed profile many solutions may be available to resolve a given problem, as shown in Figure 4.4 for the example of a spacing error of -5 s.

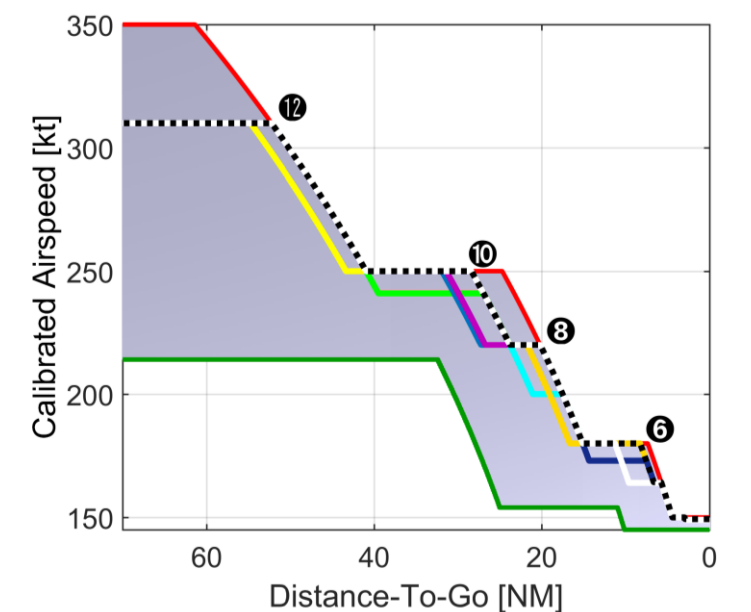


Figure 4.4 Solutions to mitigate a spacing error of 5 s to within ± 0.5 s ⁽⁴⁸⁾

Each colored profile represents a solution that reduces the spacing error to within ± 0.5 s. Henceforth, to determine which of the available modifications is the most appropriate, other attributes than just the remaining spacing error must be taken into consideration, thus giving the need for a multi-input selection algorithm.

4.5. Proposed Algorithm

IM-SP uses a two-staged rule-based selection process: The first stage is a time gate to reduce the available modifications to those which resolve the spacing error. The second stage employs an attribute-based cost-function to determine the finally selected modification. The flow of the selection stages is depicted in Figure 4.5 and a detailed pseudo-code given below:

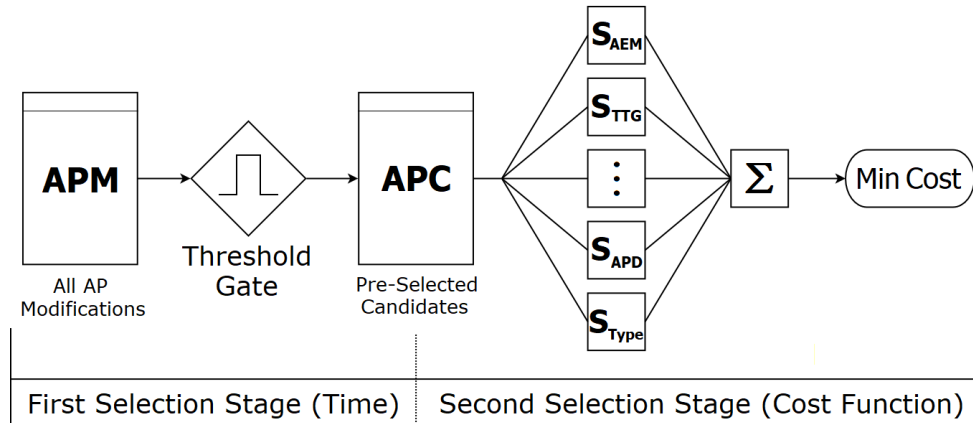


Figure 4.5 Flow of the IM-SP selection algorithm ⁽⁴⁸⁾

IM-SP pseudo-code ⁽⁴⁸⁾

*/*on first time initiation*/*

1) Analyze remaining speed schedule and save every speed segment change as AP

*/*inspect planned speed changes*/*

2) **for each** AP

1) Find achievable AP modifications AP_{Chg}^i // $i = (0,1,\dots,n)$ order in speed schedule
// 0: latest AP, n: AP directly ahead

2) Calculate remaining spacing error RSE for AP_{Chg}^i

3) Store AP_{Chg}^i and RSE in AP modification set APM

end for

*/*inspect unplanned speed changes*/*

3) Find achievable modifications on current segment AP_{Chg}^{n+1}

4) Calculate RSE for AP_{Chg}^{n+1}

5) Store AP_{Chg}^{n+1} and RSE in APM

/ first stage selection */*

6) **for each** AP_{Chg}^j in APM // $j = (0,1,\dots,n,n+1)$

if (RSE of $AP_{Chg}^j \leq$ Error Threshold) // Threshold Gate

Copy AP_{Chg}^j to preselection set APC

end if

end for

/ second stage selection */*

7) **for each** AP_{Chg}^j in APC

Calculate total cost $S = \text{SUM}(s_k \cdot q_k)$ for AP_{Chg}^j

end for

8) Substitute AP_{Chg}^j with lowest cost, for AP^j in speed schedule

4.5.1. First Stage – Time-based Preselection

The first stage examines each profile modification AP_{chg}^j (Subsection 4.2.2), that is achievable at the time of calculation (t) for its resulting ETA. Succeeding, the individual remaining spacing error (RSE, $e()$ *) is then calculated similar to Equation 2.6:

$$e(AP_{chg}^j, t)^* = ETA(AP_{chg}^j, t) - RTA(t) \quad (4.1)$$

All modifications and their corresponding RSE are then stored in the AP modification dataset APM (Figure 4.5). Modifications with an RSE within a pre-defined error threshold (e_{Thres} , here 0.5 s) are then copied to a second dataset, called the AP candidate dataset APC :

$$APC = \{AP \in APM \mid |e(AP_{chg}^j, t)^*| \leq e_{Thres}\} \quad (4.2)$$

In the event that APC has no elements, i.e. no modification has an RSE within e_{Thres} , the dataset is extended, so that the modification with the lowest absolute RSE (AP_{min}, t) is included, and all other modification within e_{Thres} of AP_{min} are also considered:

$$APC = \{AP \in APM \mid |[e(AP_{chg}^j, t)^* - e(AP_{min}, t)^*]| \leq e_{Thres}\} \quad (4.3)$$

For example, if the best achievable RSE is 0.7 s, then all modification with an RSE of up to 1.2 s will be copied to APC .

All modifications within APC are then passed on to the cost function for further examination.

4.5.2. Second Stage – Cost Function

The cost function contains a total of five elements, which are divided into two base and three penalty attributes. The final cost of a profile modification $S(AP_{chg}^j)$ is determined by the sum of the individual attribute costs (s_k), multiplied by their corresponding weight factor (q_k):

$$S(AP_{chg}^j) = \sum_{k=0}^n s_k \cdot q_k \quad (4.4)$$

or described in vectoral terms, using the individual cost vector \vec{s} and weight vector \vec{q} :

$$S(AP_{chg}^j) = \vec{s}(AP_{chg}^j) \cdot \vec{q}. \quad (4.5)$$

The weight factors are introduced to allow for user-defined prioritization of the cost function attributes. All individual costs are normalized, i.e., have a value between 0 and 1, where 0 expresses the lowest (best) cost and 1 the highest. The base attributes' weight factors are interdependent ($q_1 + q_2 = 1$, Subection 4.5.3.6), so that their combined cost ($s_1 + s_2$) cannot be greater than 1; however, the penalty attributes are independent, so that the final cost S can assume a value greater 1.

Finally, from all modifications within APC the candidate with the lowest cost, $\min(S(AP_{Chg}^j))$, is selected, and its modification is applied to the speed plan.

4.5.3. Attributes

4.5.3.1. Arrival Expedition Margin (s_{AEM})

The Arrival Expedition Margin (AEM) is the first base attribute and is introduced as an indicator how much further (positive) error the system is able to compensate, i.e., how much the arrival of the aircraft can still be expedited, after the respective modification was made.

From another perspective, the AEM indicates how close the aircraft is already flying to its maximum speed profile. Flying close to the maximum speed profile implies a risk that unexpected events or other sources of error can cause the aircraft to exceed, i.e., fail to meet, the assigned spacing goal. Accordingly, a high AEM is generally desirable.

The absolute value of the AEM is calculated by subtracting the TTG of the modified speed profile from the fastest available profile at the point where the modification becomes effective:

$$AEM_{ABS}(AP_{Chg}^j) = TTG_{Fastest}(AP_{Chg}^j) - TTG(AP_{Chg}^j). \quad (4.6)$$

Accordingly, an AEM of 0 indicates that the aircraft is already on the fastest profile and a positively increasing error can no longer be compensated; Otherwise AEM_{ABS} will indicate a negative value.

To avoid a bias toward earlier changes, which naturally have a higher AEM, the AEM can be put into relation to the DTG:

$$AEM_{DTG}(AP_{Chg}^j) = \frac{AEM_{ABS}(AP_{Chg}^j)}{DTG(AP_{Chg}^j)}. \quad (4.7)$$

The cost for the AEM (s_{AEM}) is then expressed by normalizing AEM_{DTG} over all candidates within APC :

$$s_{AEM}(AP_{Chg}^j) = \frac{AEM_{DTG}(AP_{Chg}^j) - AEM_{DTG,\min}}{AEM_{DTG,\max} - AEM_{DTG,\min}}, \quad (4.8)$$

so that the modification with the best AEM_{DTG} will have an AEM cost s_{AEM} of 0.

4.5.3.2. Time-To-Go (s_{TTG})

The TTG is the second base parameter and used to indicate when, i.e., where on the speed plan, an AP modification becomes effective in relation to a desired, target timing (TTG_{TGT}). Naturally, during early stages of FIM operation, that is at high DTG and TTG values, higher uncertainties in the spacing error are expected. At this stage, immediate actions could turn out to be counterproductive, e.g., when the actions of the TTF cancel out an initial error, and now additional action is needed to revert the Ownships's first action.

Accordingly, it is advisable to suppress premature system reactions. In ASTAR this was realized with the DTG-dependent gain parameter $g1$; in IM-SP this is realized by employing a TTG_{TGT} . The TTG_{TGT} expresses a target TTG to the ABP, and modifications close to it are linearly rewarded, i.e., a modification at TTG_{TGT} receives the lowest cost (0) and conversely, very early or very late modifications have a higher cost (up to 1).

Here TTG_{TGT} is set to 60 s to promote speed plan changes with a high lead time, so that changes are revertible, and further to prevent that the last command occurs close to the ABP, so that the crew has sufficient time between the last command and a FIM mode change or termination.

The cost (s_{TTG}) is calculated depending on if the modification occurs before or after TTG_{TGT} , according to:

$$s_{TTG}(AP_{Chg}^j) = \begin{cases} \frac{TTG(AP_{Chg}^j) - TTG_{TGT}}{TTG(\text{Current Position})}, & TTG(AP_{Chg}^j) \geq TTG_{TGT} \\ \frac{TTG_{TGT} - TTG(AP_{Chg}^j)}{TTG_{TGT}}, & \text{else} \end{cases} \quad (4.9)$$

4.5.3.3. Time-To-React (s_{TTR}).

The Time-To-React (TTR) is the first penalty attribute and it is used to inhibit modifications that require immediate or short-noticed crew reaction. This penalty is introduced to reduce the probability that the crew is interrupted by a speed command and to overcome the lack of "foreknowledge" as mentioned in Ref. (17).

In IM-SP the desired crew notification time (TTR_{TGT}) is at least 60 s in advance. In contrast, the crew reaction time of 7 s (or 11 s total delay, including engine delay and latency), as described in MOPS-FIM and used in ASTAR, is used only as the lowest acceptable time for a speed change.

Therefore, excluding the 1 s latency, modifications with a notification time less than TTR_{TGT} receive a linear penalty as follows:

$$s_{TTR}(AP_{Chg}^j) = \begin{cases} \frac{TTR_{TGT} - TTR(AP_{Chg}^j)}{TTR_{TGT} - 10s}, & 10s < TTR(AP_{Chg}^j) < TTR_{TGT} \\ 0, & TTR(AP_{Chg}^j) \geq TTR_{TGT} \end{cases} \quad (4.10)$$

Accordingly, modifications requiring an immediate crew reaction receive a penalty cost (s_{TTR}) of 1, and conversely those with a TTR of more than 60 s receive a cost of 0, i.e., no penalty.

4.5.3.4. AP Distance (s_{APD})

To prevent that a modification moves two speed changes too close together, i.e., causing speed commands to become “too frequent” ⁽¹⁹⁾, the AP distance (APD) is also introduced as a penalty attribute. Here, speed changes receive a penalty when moved closer together than the distance threshold d_{Thres} of 5 NM. Conversely, if no other AP is within d_{Thres} , then no penalty is applied.

The cost (s_{APD}) increases with proximity and is defined by the closest AP, i.e., the previous or next, as per:

$$s_{APD}(AP_{Chg}^j) = \frac{d_{APThres} - \min(d_{NextAP}(AP_{Chg}^j), d_{PrevAP}(AP_{Chg}^j))}{d_{APThres}} \quad (4.11)$$

4.5.3.5. AP Type (s_{Type})

Last, the modification type is used as a penalty attribute, to promote modifications made to existing speed changes, as opposed to adding additional commands or APs. The cost (s_{Type}) is a fixed value and set to 0.5 for additional decelerations and 1 for additional accelerations.

In contrast, modifications made to existing speed changes, including those added by previous modifications, receive no penalty, i.e., a cost of 0.

4.5.3.6. Weight Factor Settings

The weight factor settings for this first iteration of IM-SP have been determined on experience and with the aim to equally balance each factor.

As mentioned in Subsection 4.5.2, the scoring attributes are interdependent, i.e., $q_{AEM} + q_{TTG} = 1$, so that the base attribute cost is between 0 and 1. Furthermore, with respect to the opposing nature of s_{AEM} (benefiting modifications with a high AEM to DTG ratio, usually found during earlier phases of flight) and s_{TTG} (favoring late modifications with high lead times), this interdependence ensures that the system’s behavior, i.e., its priority, can be directly derived from the weight settings.

Using equal balancing, i.e., $q_{AEM} = q_{TTG}$, the constraint $q_{AEM} + q_{TTG} = 1$ leads to a value of 0.5 for both. q_{TTR} and q_{APD} have also been set to 0.5 respectively, only q_{Type} was set to a lower value of 0.3, to prevent a strong bias because of its fixed value. A summary of all weights is shown in Table 4.2.

Table 4.2 Attributes and weight factors used in the IM-SP cost function ⁽⁴⁸⁾

Category	Base		Penalty		
	AEM	TTG	TTR	APD	Type
Value (q)	0.5	0.5	0.5	0.5	0.3

4.5.4. Speed Plan Optimization

After each modification the speed plan is analyzed for possible optimization. If for example two consecutive APs, one marking the end of a deceleration, and the other the beginning of a deceleration, have identical CAS and DTG values, the two deceleration segments are combined into one long segment. Similar, if two changes are very close by to each other, i.e., the time between deceleration end and start is less than 5 s, then the system tries to find a single deceleration that replaces the two decelerations, based on the condition that the combination does not alter the error by more than 0.5 s.

4.5.5. System Initiation and Continuous Operation

Upon system activation, the time required map, APs and corresponding TTG values for the current speed profile are generated as shown in Figure 4.6. From there on, the system enters the continuous operation mode as shown in Figure 4.7.

In this mode, certain conditions are monitored that need to be fulfilled before a speed plan modification is initiated. First, the validity of the time required map is checked. If for example a wind forecast update was received, the map is recalculated as described before.

Next, the spacing error is calculated. If its absolute value is greater than the modification threshold e_{Modify} (1 s) and further its value has changed more than 1 s since the error was last handled, then the modification process is initiated and the speed profile is re-planned. The latter condition was implemented to avoid permanent system activation in case the spacing error has risen above e_{Modify} , but can no longer be reduced below the threshold.

A speed plan modification is expected to reduce the absolute error below 0.5 s, identical to the threshold gate for APC. If, however, this cannot be achieved with a single modification, meaning e_{Thresh} for APC needed to be extended, the speed plan modification process is invoked one more time within the same cycle, including the previous modification.

Finally, the modified speed plan is displayed to the flight crew.

The continuous operation mode cycle is evoked at least once per second, to reflect the rate at which ADS-B messages are transmitted and accordingly the TTF's ETA is updated.

Based on a JAVA simulation environment on an Intel Core i7-6700HQ at 2.6 GHz with 16 GB of RAM and using one core only, the IM-SP initiation process takes between 0.5 and 1 s, whereas a single modification cycle takes between 0.1 to 0.2 s.

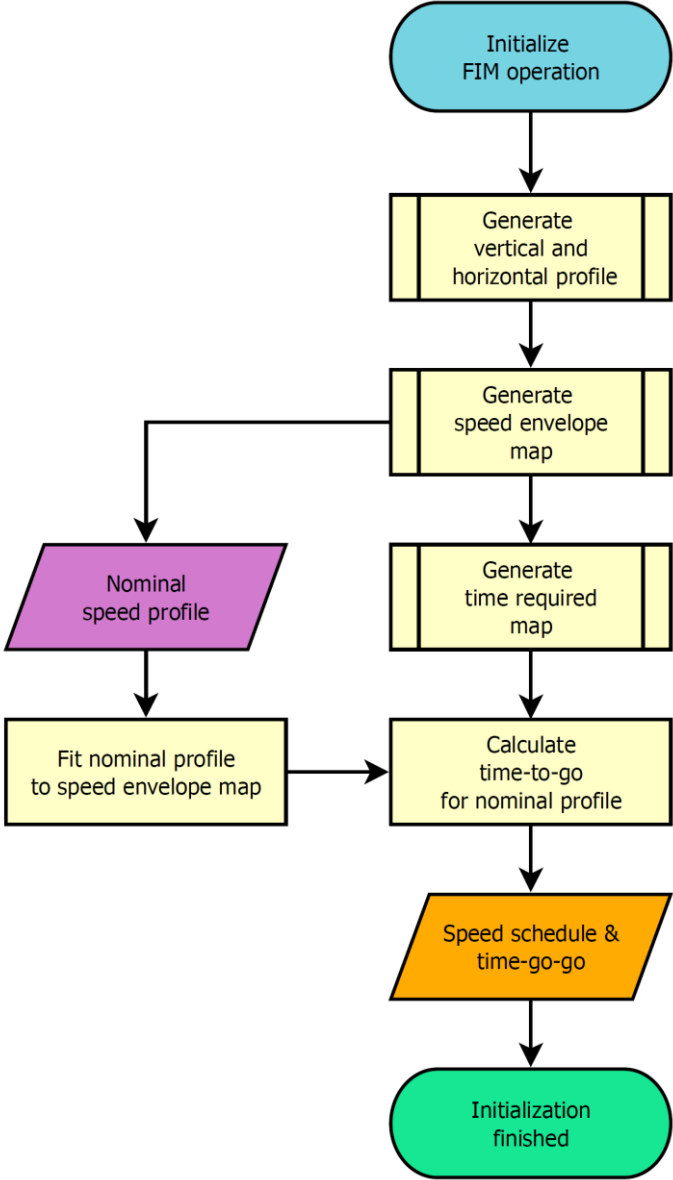


Figure 4.6 Flowchart for the IM-SP system initiation process⁽⁴⁸⁾

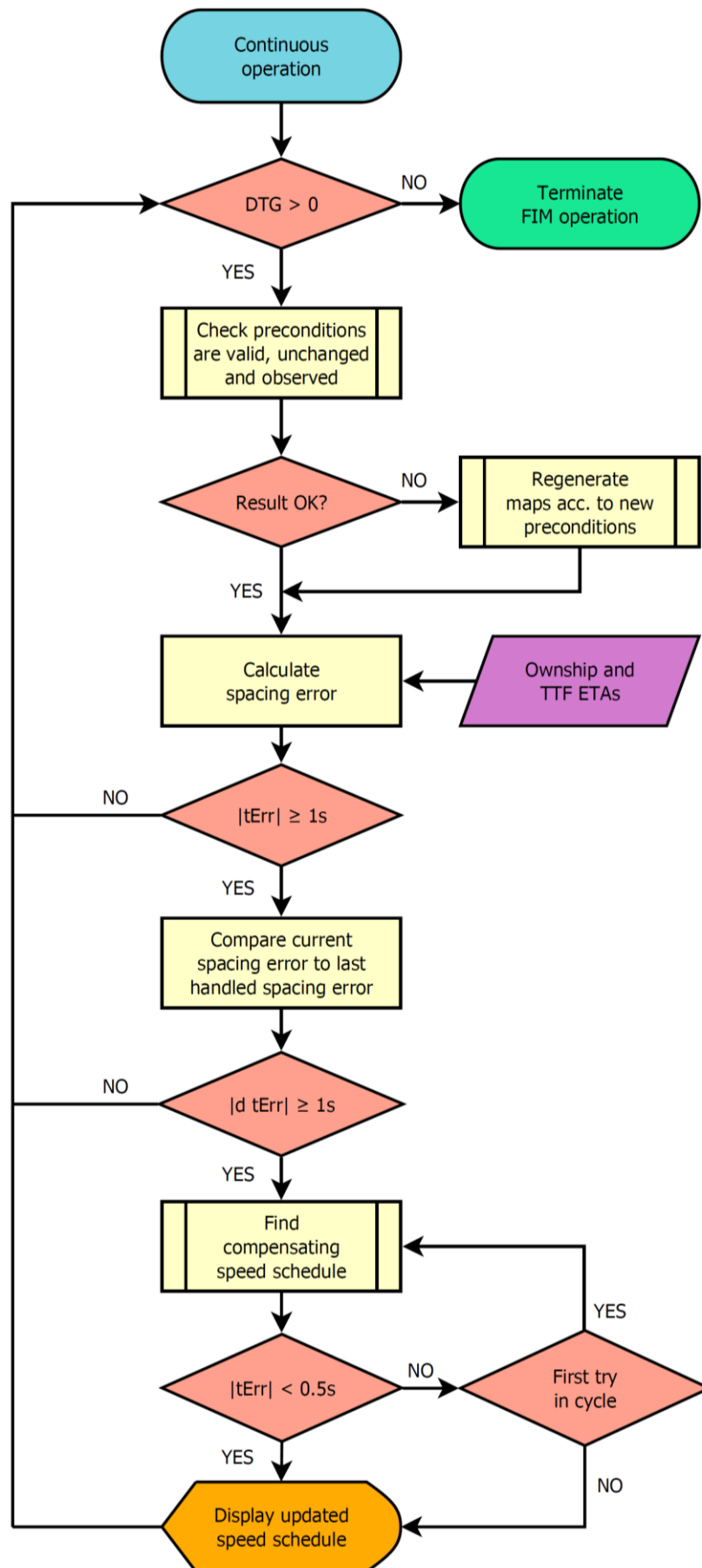


Figure 4.7 Flowchart for the IM-SP continuous operation mode ⁽⁴⁸⁾

4.6. Simulation Scenario I

Two major benchmark studies, comparing IM-SP to ASTAR, were conducted under different environmental conditions. The first one, IM-SP's initial study, from here on referred to as "Scenario I", simulated a Boeing 787-8 approaching RJTT from the east (here, approximately 200 NM away from the airport) to its Runway 34 L. The setup and results are shown in this section. The second study, referred to as "Scenario II", was done in preparation for the flight simulator evaluation (Chapter 6), and simulated an Airbus A320-200 on a shortened scenario (approximately 50 NM away from the airport). Its details are shown in Section 4.7.

4.6.1. Routing

The simulation starts at waypoint SMOLT and continues via SUNNS, SHOES, PQD, UMUKI, and KAIHO to the Instrument Landing System (ILS) X approach for RWY 34 L (Ref. (50), Appendix C), as depicted in Figure 4.8. The total flight distance is approximately 224 NM. This route would for example be used by traffic originating from Hawaii.

The vertical flight path is generated from assuming a standard 3° glide slope from the runway threshold to the Final Approach Fix (FAF) AZURE, and from there on a 2.2° fixed-FPA descent (as described in Subsection 2.5.1) until the Top of Descent (TOD) at an altitude of 38,000 ft (FL380). Published crossing altitudes were adapted to accommodate the vertical flight path, as depicted in Figure 4.9.

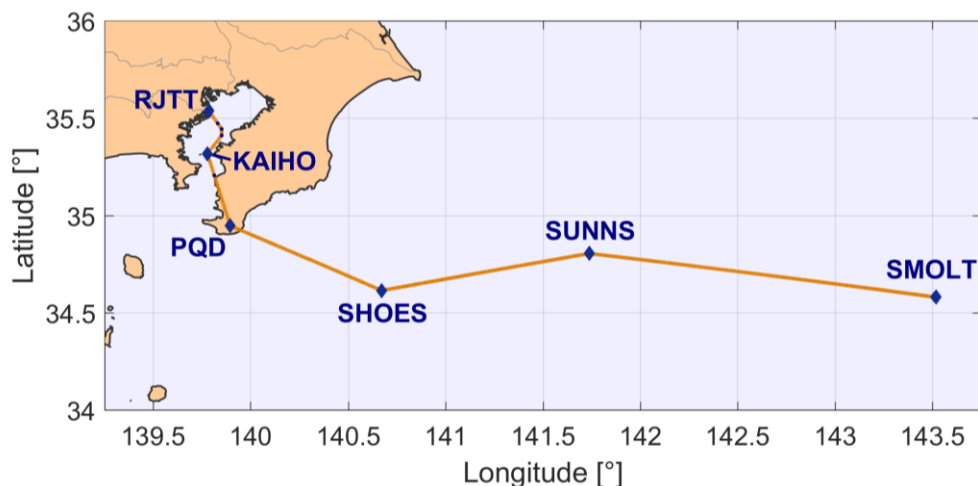


Figure 4.8 Lateral flight path for Scenario I ⁽⁴⁸⁾

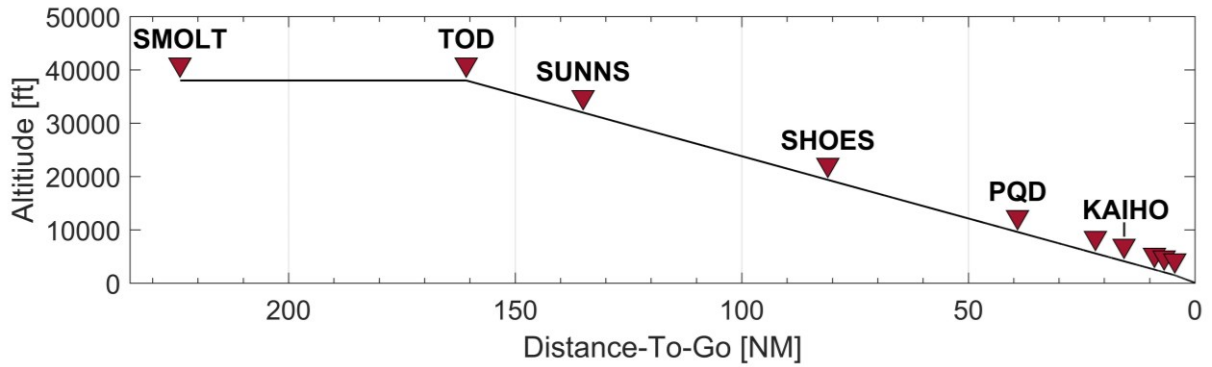


Figure 4.9 Vertical flight path for Scenario I ⁽⁴⁸⁾

4.6.2. FIM Operation

In this scenario FIM operation commences at a DTG of 130 NM and ends 3 NM before the runway threshold, from where on the final approach speed is assumed. The (final) spacing error is measured at the runway threshold.

The reference speed profile for the Ownship, limited to area of FIM operation, is shown in Figure 4.10. The speed profile for the entire simulation is identical to the one shown in Figure 4.1.

Speed constraints are established at FL100 (250 kt), KAIHO (180 kt), and AZURE (150 kt).

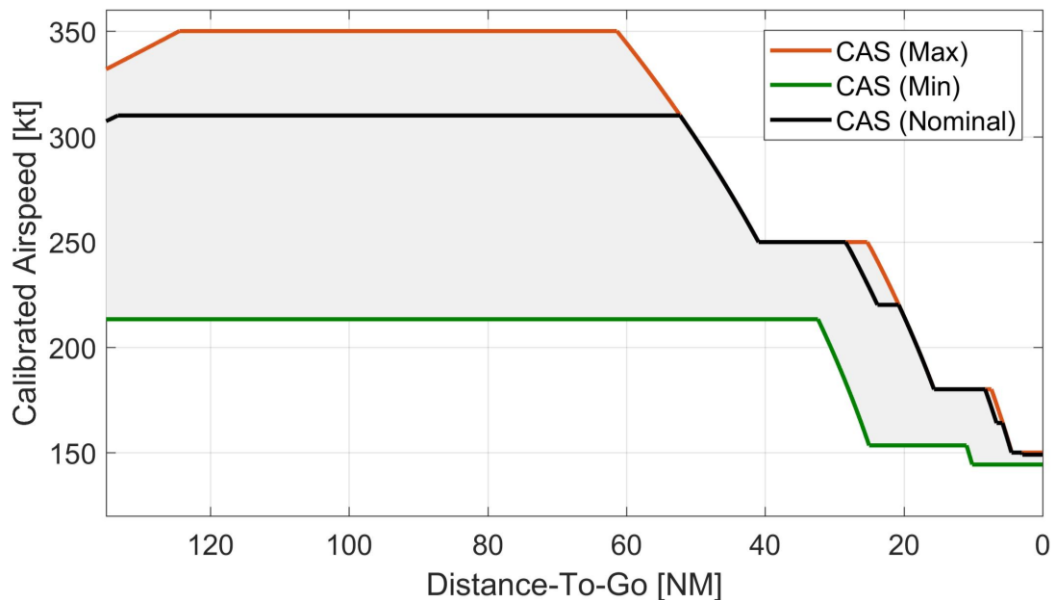


Figure 4.10 Reference speed profile for Scenario I

The TTF was also modeled as a Boeing 787-8. The spacing error between the TTF and Ownship was realized through different error patterns, that apply a flight time dependent error to the TTF's TTG (and ETA), so that in response, the Ownship has to react to the error, i.e., change its speed or speed profile depending on the respective FIM logic. All error patterns are listed in Appendix B.

4.6.3. Number of Simulations

In this scenario a total of 147 individual simulations were made. These were composed of 7 initial base errors (-30, -20, -10, 0, +10, +20, +30) [s], plus 5 error patterns (A-E), with 2 different amplifications (Low & High), 2 directions (+ & -), and the 7 initial offsets. ($7 + 5 \cdot 2 \cdot 2 \cdot 7 = 147$.)

4.6.4. Nominal Values

Using the actual winds reported on September 15, 2013 at 12:00 UTC and assuming international standard atmospheric (ISA) conditions, Table 4.3 shows the nominal values for the Ownship flying its BADA nominal speed profile, adapted for the waypoint and altitude speed-constricted speed envelope.

Table 4.3 Nominal values for Scenario I

Parameter	Value Unit
Ownship Aircraft Type	Boeing 787-8 -
Flight Distance (DTG)	223.96 NM
Flight Time (TTG)	2146.8 s
Speed Changes	6 -
Fuel Burn	1600.4 kg
Speed Brake Use Time	393.3 s
Target Aircraft Type	Boeing 787-8 -
Nominal Spacing (Distance)	4 NM
Nominal Spacing (Time)	100 s
FIM Initiation	130.00 NM
FIM Termination	3.00 NM

Here, the reference flight time is calculated at 35 min 46.8 s (2146.8 s) which must then be shortened or extended, according to the spacing situation.

For the given aircraft wake vortex category pairing (Heavy follows Heavy), the nominal spacing is 4 NM⁽³²⁾. Assuming a final approach speed of 150 kt, this translates to a nominal spacing time of 96 s, here rounded to 100 s.

Different to the previously used FIM conformance definition (95% of all trials have to be within ± 10 s of the ASG, Section 2.4), here, the target has been tightened to ± 5 s to acknowledge the simulation environment.

Metrics, other than the final spacing error and partially included in Table 4.3, that have been used to evaluate each respective logic for its performance are as follows:

4.6.4.1. Number of Speed Commands and Accelerations

As before, the number of speed commands, i.e., speed changes, is used as a direct indicator of the required pilot interaction or expected workload. Ideally, the number of speed changes remains unchanged in regard to the nominal profile (here 6).

Closely related to the number of commands is the number of accelerations. While in case of excessive spacing an acceleration might be inevitable in order to achieve the spacing target, an acceleration following a deceleration would indicate a reversal, which is neither desirable nor economic. Accordingly, the nominal and ideal number of accelerations is 0.

4.6.4.2. Fuel Burn

The fuel burn is the primary economy and ecology indicator, representing operating cost and CO₂ emission. Naturally, a low fuel burn is desirable. However, in order to achieve the IM spacing goal, i.e., adjust the arrival time, FIM needs to depart from the nominal profile and thus, on average, a higher than reference (1600.4 kg) fuel burn must be expected. Nevertheless, FIM logics should achieve the IM goal with the least necessary effort, i.e., the lowest possible additional fuel burn, as fuel economy has an impact on the acceptance of FIM, especially from an operator's perspective.

4.6.4.3. Speed Brake Use Time

The purpose of the speed brakes is to generate additional drag, either to increase the rate of descent or the deceleration rate. Here speed brakes are solely used for the purpose of speed control. The demand for speed brakes was calculated via the Total Energy Model (Equation 2.7).

Whenever the required deceleration rate could not be achieved with idle thrust alone, the use of the speed brakes for the minimum time required was assumed.

Here the nominal use time is 6 min 33.3 s (393.3 s). It should be noted though, that in CDO, especially with a fixed FPA, and even more for modern high-efficiency wing aircraft, speed brakes are required more often and their use time is considerably longer than with stepwise descents.

Yet, the use of speed brakes is not always appreciated by pilots, as for example company procedures might require them to have their hand on the speed brake lever for the duration of deployment, thus binding mental resources. Therefore, in general, short use times are desired.

4.6.4.4. Reference Profile Deviation

The Reference Profile Deviation (RPD) is a new metric, introduced to indicate how much the final speed profile has deviated from the reference profile. While no immediate conclusion from the RPD to, for example, the fuel burn can be made, a smaller RPD indicates overall less changes. The RPD is calculated by multiplying the CAS deviation, i.e., the difference between the nominal and

commanded CAS, by the distance it was flown. In other words, it describes the area between the actual and nominal speed curve on the CAS/DTG graph. Accordingly, the RPD's unit is kt*NM.

4.6.5. Results

For a better understanding of the working mechanisms and the resulting speed profiles generated by each logic, a detailed case example is given before the overall results are shown. As a reminder the elemental differences of both logics are again highlighted in Table 4.4.

Table 4.4 Design differences of ASTAR and IM-SP (as used in this simulation)

Parameter	ASTAR	IM-SP
Correcting Variable	Current speed	Speed profile
Control Method	Feed-forward	Rule-based
Speed Incrementation	5 kt	1 kt
Maximum Deviation from Nominal CAS	±15%	±20 kt or 10%
Waypoint Speed Constraints	Lifted (15%)	Enforced
Command Notification Time	7 s (11 s)	≥ 7 s (11 s)

The color coding (ASTAR = blue, IM-SP = red), is kept throughout this chapter.

Since ASTAR requires waypoint speed constraints to be lifted by 15% to work as intended, while IM-SP does not, a second version of ASTAR, but here with speed constraints enforced, was also calculated for comparison purposes and is shown for the overall results (colored in green).

Effects on the reference flight time, owing to the different design characteristics of each logic (e.g., speed incrementation) were accounted for at the beginning of the simulation.

4.6.5.1. Case Example

The following subsection gives a detailed analysis of the results for error pattern E, "SPICA", with a low amplification factor and in positive direction, in short referred to as "SPICA Low+".

Table 4.5 shows the final results, measured at the runway threshold.

Table 4.5 Results for the "SPICA Low+" simulation ⁽⁴⁸⁾

Parameter	ASTAR	IM-SP
Final error [s]	1.4	1.1
Commands [-]	14	7
Accelerations [-]	4	1
Fuel burn [kg]	1641.6	1666.2
Speed brake use [s]	430.0	389.0
RPD [kt*NM]	432.9	974.9

Both logics achieve the spacing target with similar performance, showing a final spacing error of 1.4 s (ASTAR) and 1.1 s (IM-SP). However, over the entire scenario ASTAR commanded 14 speed changes, 4 of them being accelerations, of which two qualify as reversals. In comparison, IM-SP commands only half as much speed changes, i.e., 7, with 1 acceleration and 0 reversals.

Figure 4.11 further depicts the resulting speed profiles, error progression, actual spacing distance, fuel flow, and speed brake deployment status. The x-axis represents the DTG, limited to the area of FIM operation, and is aligned for all graphs.

The remaining error over distance graph shows the spacing error as calculated by each logic at the respective DTG. Further, the uncompensated spacing error (orange line), that is the progression of the spacing error that would set in if no IM action was taken, is shown. The progression of the curves for IM-SP and ASTAR highlights one of their design differences:

The sudden drop of the remaining spacing error for the IM-SP algorithm at FIM initiation (DTG 130 NM) indicates that the speed schedule re-planning process was evoked and the initial error was eliminated. Here this was realized by a 13 kt acceleration, commencing at a DTG of 118.5 NM (approximately 90 s after FIM initiation), that is kept until the next planned deceleration, here to 250 kt. This speed profile then becomes the basis for further modification. A history of all modifications is shown in Table 4.6.

In comparison, with ASTAR the spacing error reduces gradually as the commanded speed takes effect. ASTAR's reaction to the initial error is an immediate acceleration of 5 kt, which is later reverted when the TTF starts to decelerate (reduction of the uncompensated spacing error) at a DTG of 90 NM. Further, it can be seen that the ASTAR profile leaves the speed envelope during the later phases of flight, indicating the need for the 15% constraint tolerance to perform properly.

The actual spacing distance graph shows that the IM-SP aircraft closes in faster on the TTF than the ASTAR aircraft, which can be explained with the higher top speed of the IM-SP aircraft and its later reaction to the deceleration of the TTF at 90 NM. Nevertheless, at no point is the minimum separation of 4 NM jeopardized and both aircraft arrive at the runway threshold with sufficient, but not excessive, spacing of 4.4 NM (ASTAR) and 4.3 NM (IM-SP) respectively.

In terms of fuel economy, the ASTAR generated profile caused a fuel burn of 1641.6 kg, whereas the IM-SP profile shows a notably higher fuel burn at 1666.4 kg. Further examining the fuel flow graph, it can be seen that despite ASTAR commanding more accelerations, seen as spikes in the fuel flow graph, the continued high-speed segment of IM-SP, that requires more continuously applied thrust as a result of increased drag, caused for the higher overall fuel burn.

Last, the speed brakes were commanded fewer times, shorter in total, and more continuously with IM-SP (389.0 s) than with ASTAR (430.0 s). The increased time with ASTAR in this scenario can be accredited to the increased number of deceleration segments, as a result of the reversals.

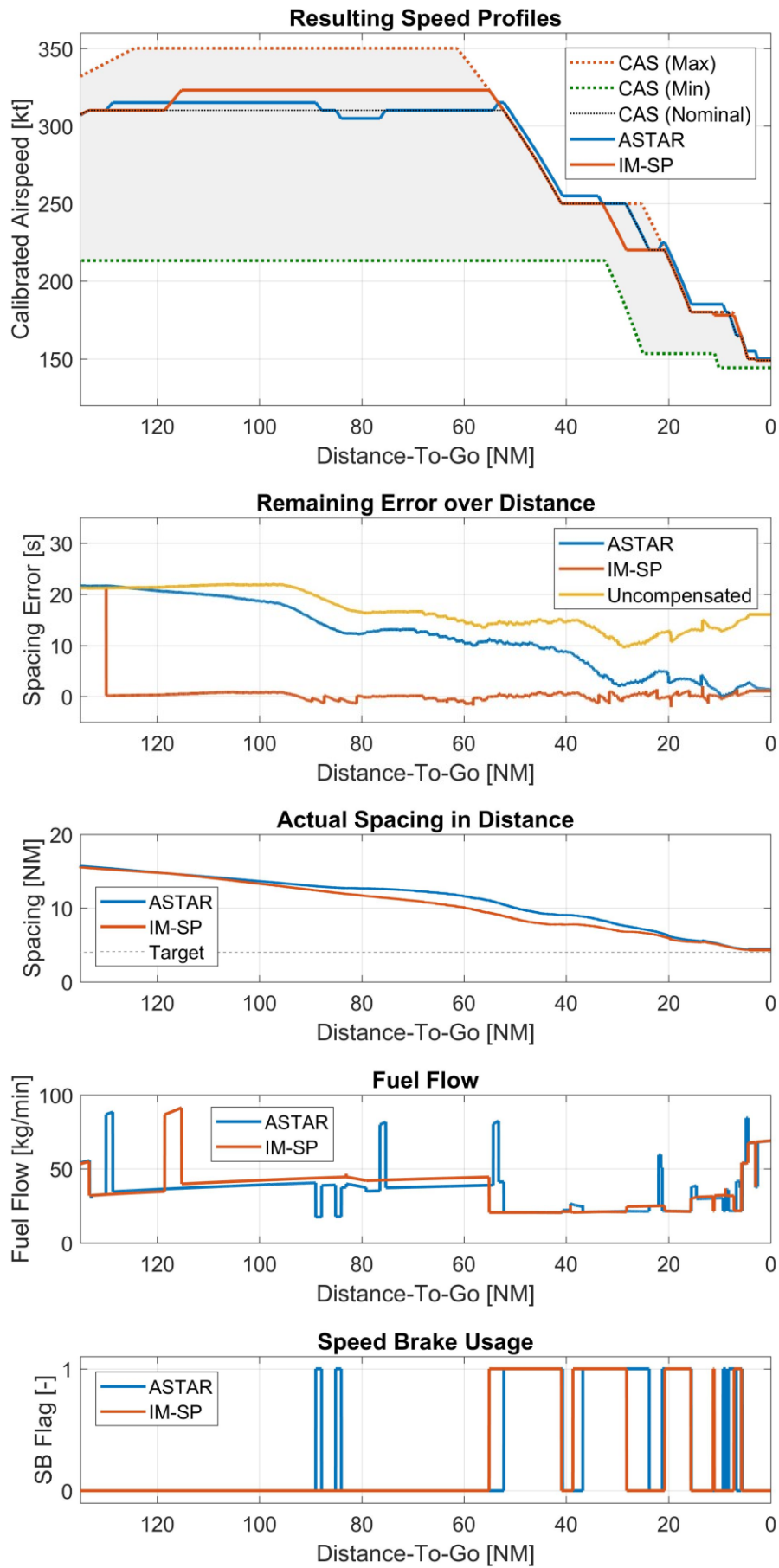


Figure 4.11 Detailed comparison of the “SPICA Low+” simulation with +20 s initial error⁽⁴⁸⁾

Table 4.6 shows the speed plan modifications history of IM-SP. The table lists the DTG at which the modification was decided, the affected AP, the change type, effect on the TTG, and TTR.

The total 19 modifications consisted of 12 DTG changes, 6 CAS_{TGT} changes and 1 acceleration. The shortest TTR was observed for the last speed change with 31 s, the second shortest was 34 s, all other changes were announced at least one minute in advance.

Modifications 17-19 also highlight the capability of IM-SP to revert its modifications in case the spacing error diminishes on its own. In detail, the CAS_{TGT} of AP² was first reduced by -4 kt, but then returned in two steps (+3 kt, +1 kt) to its original state.

Table 4.6 Speed plan modification history of IM-SP⁽⁴⁸⁾

No	DTG [NM]	AP	Change	Δ TTG [s]	TTR [s]
1	129.98	14	ACC + 13	- 21.1	85
2	89.66	10	DTG + 0.5	0.8	584
3	87.30	10	DTG + 1.0	1.5	552
4	84.32	10	DTG + 0.5	0.8	521
5	80.94	10	DTG + 1.0	1.5	480
6	63.30	10	DTG + 0.5	0.8	323
7	58.18	10	DTG + 1.0	1.5	266
8	33.64	6	DTG + 1.0	1.7	365
9	31.58	6	DTG + 1.0	1.7	322
10	29.00	6	DTG + 0.5	0.9	279
11	24.38	6	DTG - 0.5	- 0.9	225
12	22.26	6	CAS + 6	- 2.0	195
13	19.50	6	DTG + 2.0	2.1	119
14	18.26	6	DTG - 1.0	- 1.0	118
15	15.94	6	CAS + 3	- 1.2	80
16	13.36	6	CAS + 5	- 2.0	34
17	12.26	2	CAS - 4	1.7	180
18	6.60	2	CAS + 3	- 1.3	74
19	4.54	2	CAS + 1	- 0.4	31

4.6.5.2. Overall Results

Figures 4.12 and 4.13, and Tables 4.7 - 4.9 show the results for all 147 simulations grouped by logic. Here, these are ASTAR with waypoint speed constraints lifted by 15%, as shown before, (A13, blue), ASTAR limited to speed constraints (LTD, green) and IM-SP (SP, red) enforcing constraints by design.

The boxplots are drawn according to the Tukey-convention (as described in Section 3.3), with outliers marked by a “+”, and the mean value marked by an “x”. Where applicable, reference values (as shown in Table 4.3) or target boundaries are indicated by gray dashed lines.

The overall best spacing performance, indicated by the final error, was achieved with ASTAR with limits lifted, at a mean -0.59 ± 1.12 s. Notably all samples are within the target range of ± 5 s. IM-SP delivers comparable performance at 0.66 ± 1.87 s, indicating a neglectable difference in the absolute mean value, but an increased standard deviation.

Even though the median value for IM-SP (0.20 s) is better than for ASTAR (-0.51 s), few samples have failed to meet the target range. Figure 4.13, showing the results for each error pattern, amplification, and direction respectively, indicates that the outliers were specifically caused by the “Linear High-” setup. The difficulty of this particular setup is discussed in Subsection 4.8.1.

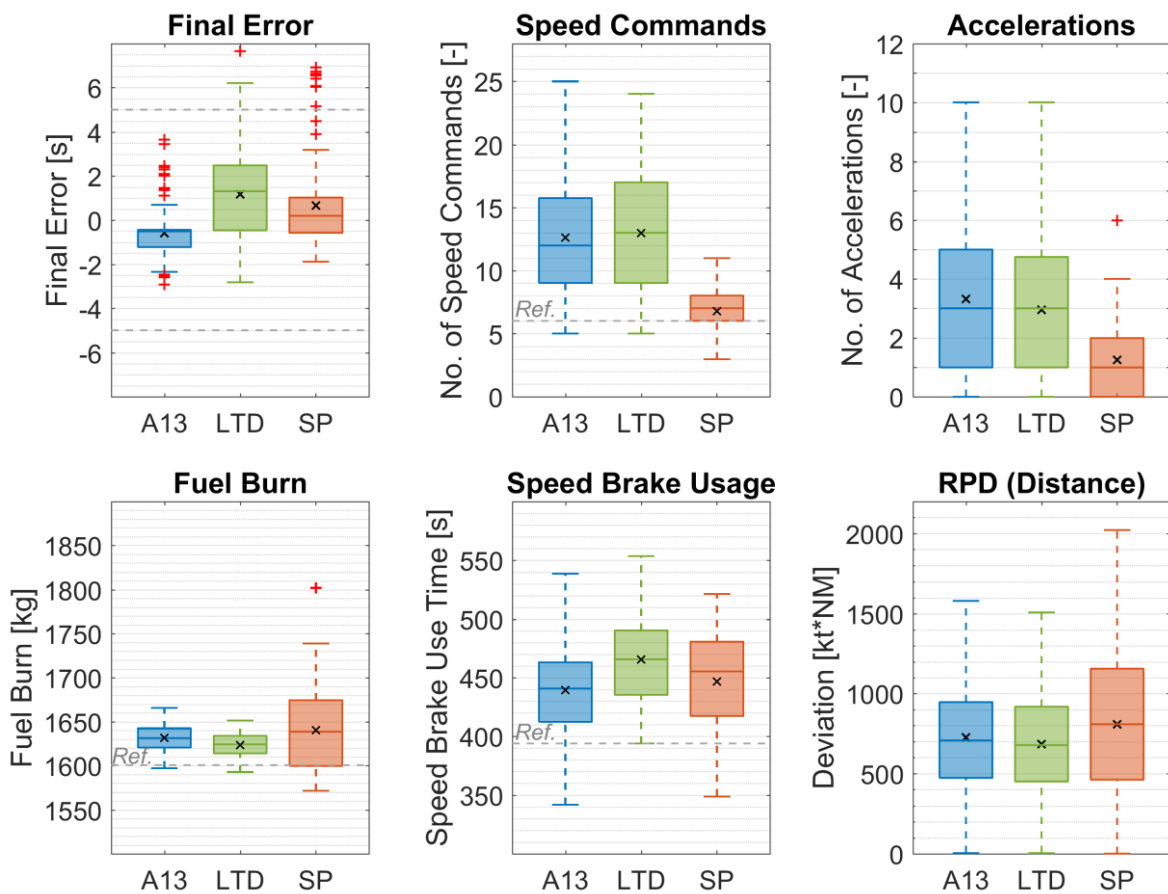


Figure 4.12 Boxplot for all simulations of Scenario I ⁽⁴⁸⁾

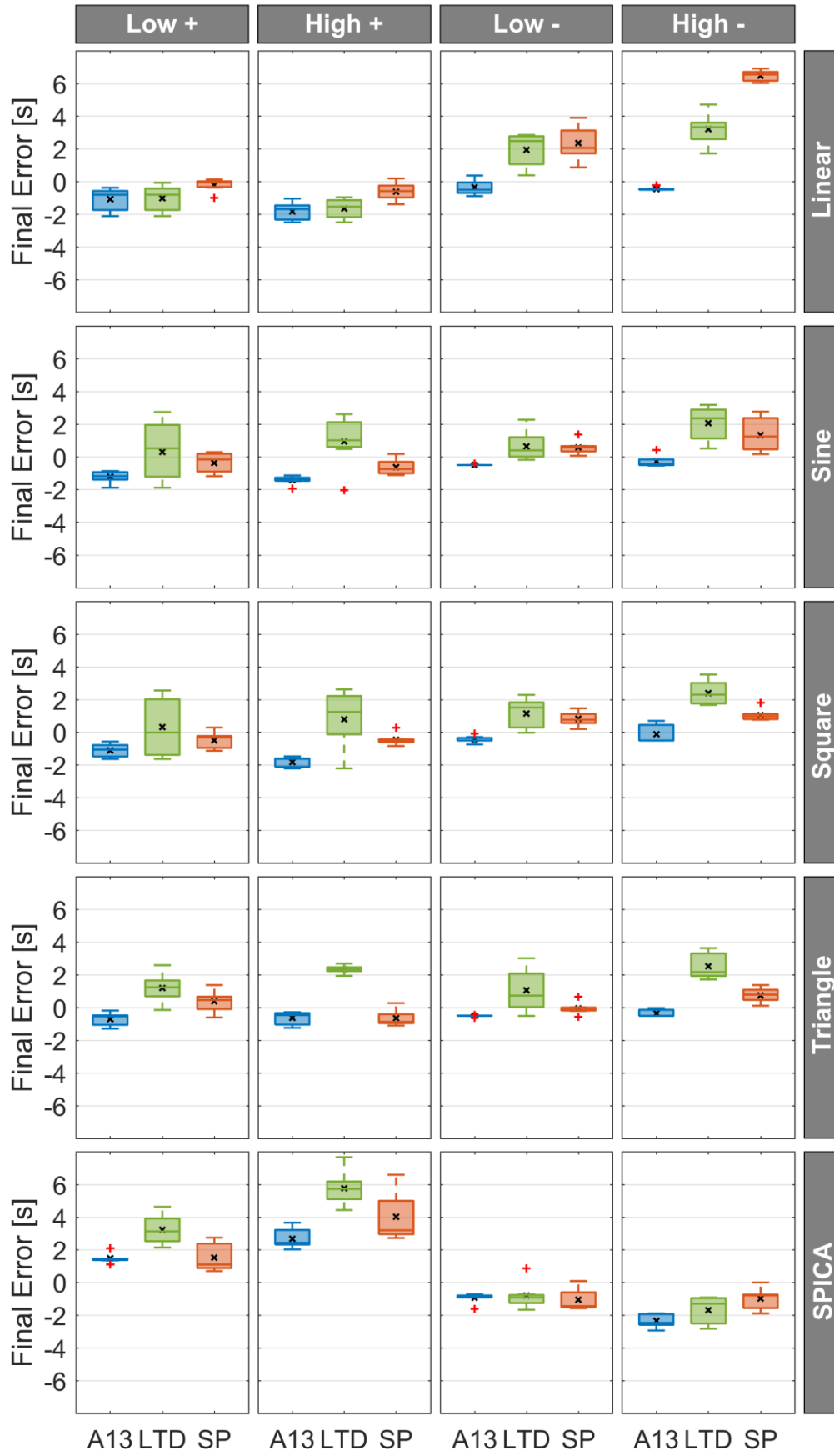


Figure 4.13 Boxplot for all simulations, grouped by pattern, direction, and amplification ⁽⁴⁸⁾

Table 4.7 Overall results for ASTAR (A13) ⁽⁴⁸⁾

Parameter	Median	Mean	SD
Final error [s]	-0.51	-0.59	1.12
Speed commands [-]	12	12.6	4.6
Accelerations [-]	3	3.3	2.3
Fuel burn [kg]	1631.3	1631.8	15.5
Speed brake use [s]	440.8	439.5	39.7
RPD [kt*NM]	707.4	726.7	339.8

Table 4.8 Overall results for ASTAR Limited (LTD) ⁽⁴⁸⁾

Parameter	Median	Mean	SD
Final error [s]	1.31	1.18	2.02
Speed commands [-]	13	13.0	4.5
Accelerations [-]	3	2.9	2.1
Fuel burn [kg]	1624.3	1623.5	13.2
Speed brake use [s]	465.7	465.6	39.7
RPD [kt*NM]	678.5	684.7	328.4

Table 4.9 Overall results for IM-SP (SP) ⁽⁴⁸⁾

Parameter	Median	Mean	SD
Final error [s]	0.20	0.66	1.87
Speed commands [-]	7	6.8	1.5
Accelerations [-]	1	1.3	1.2
Fuel burn [kg]	1638.6	1640.2	44.8
Speed brake use [s]	455.5	446.9	41.8
RPD [kt*NM]	809.3	808.8	433.2

Limited ASTAR delivers the highest final error, i.e., lowest spacing performance at 1.31 ± 2.02 s, with a median of 1.31 s, and also renders the highest outlier of all logics.

The reduction of speed commands, the primary focus of IM-SP, was successfully achieved, requiring only 6.8 ± 1.5 (median 7) commands, compared to 12.6 ± 4.6 (12) for ASTAR and 13.0 ± 4.5 (13) for its limited variant. In other words, IM-SP reduces speed commands by up to 46% compared to ASTAR in its intended implementation, and, on average, requires only one additional command compared to the nominal speed profile, to provide sufficient spacing performance.

Likewise, the number of accelerations was also reduced to 1.3 ± 1.2 (1) with IM-SP, compared to 3.3 ± 2.3 (3) with ASTAR, and 2.9 ± 2.1 (3) with its limited variant; A reduction by 60%.

Figure 4.14 shows the difference for the median number of commands, grouped by error pattern, amplification, and direction, as a bar chart. The bars indicating the accelerations are overlaid, e.g., the median command difference for the “Triangle Low+” simulation is 6, of which 2 are accelerations.

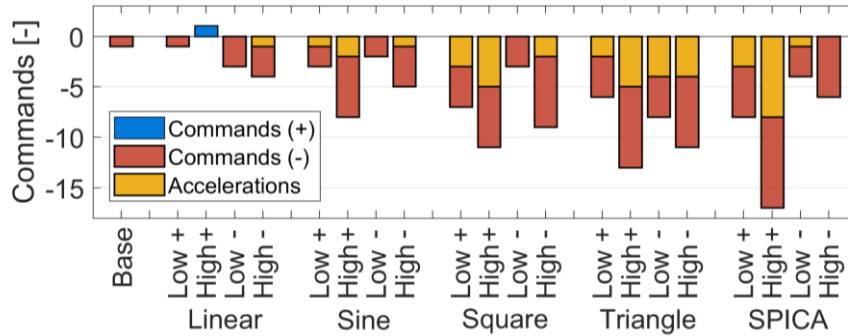


Figure 4.14 Median difference in commands and accelerations by error pattern ⁽⁴⁸⁾

The fuel burn is very consistent for both implementations of ASTAR, owing to its design to operate close to and return to the nominal speed profile once the spacing error is mitigated. Results show the fuel burn at 1631.8 ± 15.5 kg (A13) and 1623.5 ± 13.2 kg (LTD) respectively.

The lower fuel burn for LTD can be accredited to the fact that once on the maximum speed profile, accelerations are inhibited, thus naturally limiting the maximum fuel burn.

IM-SP showed a marginally higher fuel burn compared to A13 (+0.5%), but a significantly higher standard deviation, resulting in a mean 1640.2 ± 44.8 kg. While this implies that IM-SP can generate speed profiles with lower fuel burn than ASTAR, its overall fuel burn is less consistent.

The speed brake use time was comparable for all logics, with the highest value observed for LTD. As the limited implementation cannot compensate the spacing error as quickly as the unlimited implementation, it must remain on its maximum speed profile longer, thus requiring prolonged use of the speed brakes.

Last, the RPD also highlights the design characteristic of ASTAR to operate close to the reference profile or deviate for shorter distances, as opposed to IM-SP, that maintains a new speed until the next speed change, as seen in the example given previously. Further, since IM-SP can shift speed changes in distance, it can accumulate a higher RPD more easily.

4.7. Simulation Scenario II

Scenario II is a condensed version of Scenario I, adapted for the flight simulator evaluation in Chapter 6. In particular, only the last 15 min of the approach were simulated, to account for the limited time available during the simulator trials, but also to include the approach phases with the highest workload. Further, the aircraft type was changed to an Airbus A320-200 to match the flight simulator model.

4.7.1. Routing

The lateral path is identical to Scenario I, however, here the simulation is started between SHOES and PQD at the inserted waypoint START, as depicted in Figure 4.15. The remaining DTG is 62.3 NM.

START is set at FL150 on the 2.2° descent flight path as shown in Figure 4.16.

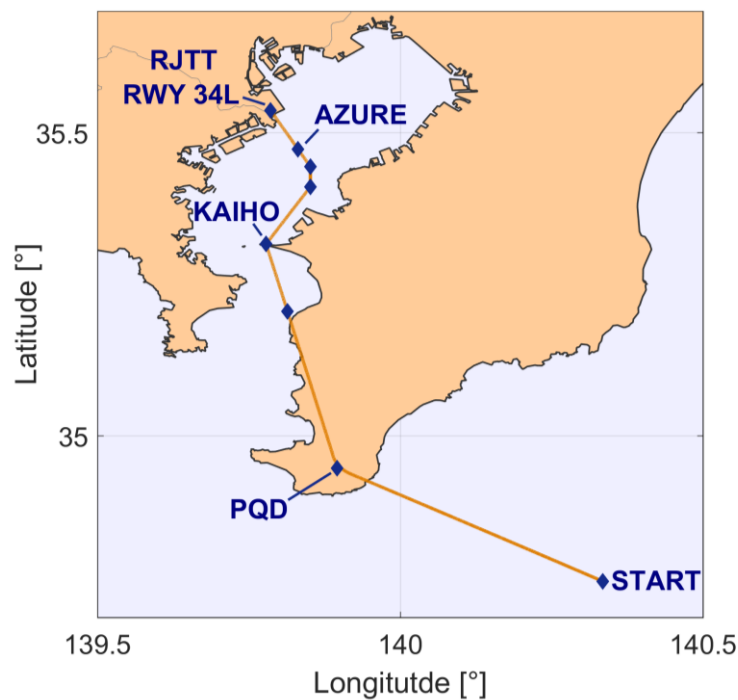


Figure 4.15 Lateral flight path for Scenario II ⁽⁴⁹⁾

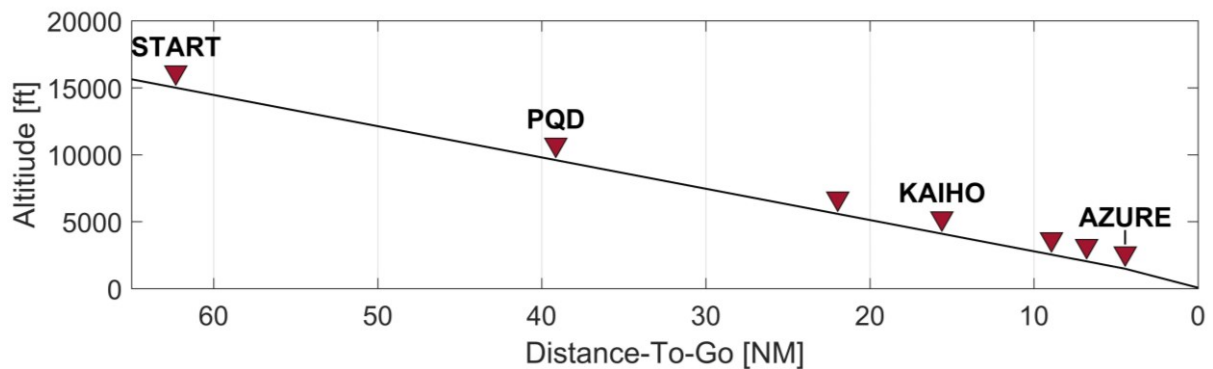


Figure 4.16 Vertical flight path for Scenario II ⁽⁴⁹⁾

4.7.2. FIM Operation

FIM operation commences at a DTG of 60 NM, and is continued until a DTG of 3 NM as in Scenario I. Speed constraints have been slightly modified, with AZURE at 160 kt and an added stability criterion for the landing (LND) with 142 kt. The resulting nominal speed profile is shown in Figure 4.17.

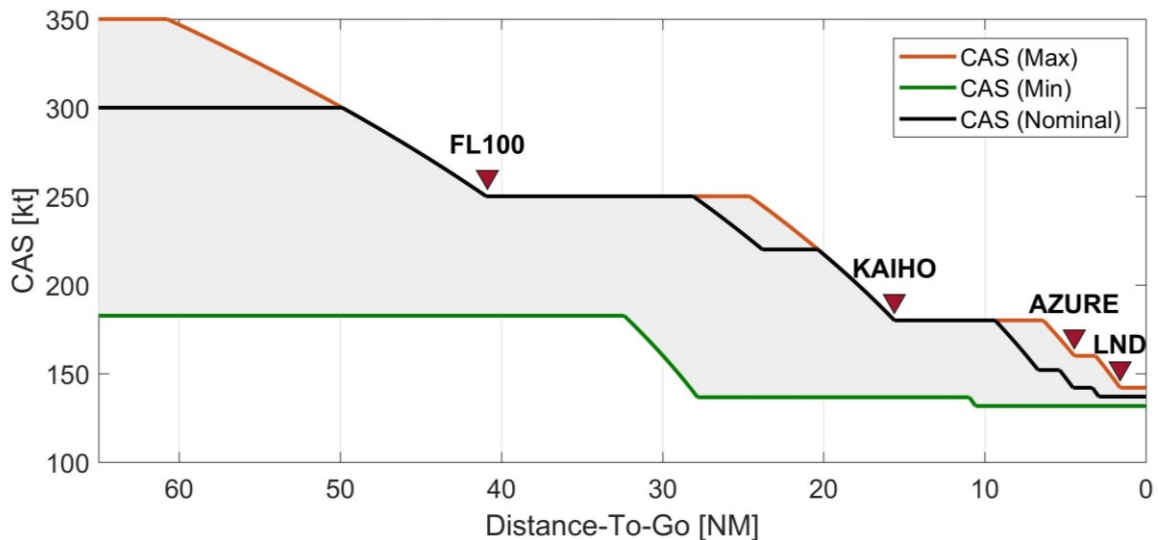


Figure 4.17 Reference speed profile for Scenario II ⁽⁴⁹⁾

4.7.3. Number of Simulations

Scenario II was simulated with a total of 225 individual setups. Acknowledging the shorter flight distance, i.e., assuming previous IM action, the outmost initial errors were decreased, but therefore simulated in smaller intervals, giving 9 initial base errors (-20, -15, -10, -5, 0, +5, +10, +15, +20) [s]. Further one more error pattern (F, "SHTLE") was introduced, giving a total of 6 patterns, each again using both amplifications, directions and all initial offsets. ($9 + 6 \cdot 2 \cdot 2 \cdot 9 = 225$.)

4.7.4. Nominal Values

To allow for an easier adaptation to the flight simulator, zero-wind and ISA conditions at mean sea level (MSL) have been assumed for Scenario II, giving the nominal values as shown in Table 4.10.

Here the wake vortex category pairing (Medium follows Heavy) requires 5 NM of distance spacing ⁽³²⁾, represented by 120 s in time.

Table 4.10 Nominal values for Scenario II ⁽⁴⁹⁾

Parameter	Value	Unit
Ownship Aircraft Type	Airbus A320-200	-
Flight Distance (DTG)	62.30	NM
Flight Time (TTG)	922	s
Speed Changes	6	-
Fuel Burn	298.7	kg
Speed Brake Use Time	307.4	s
Target Aircraft Type	Boeing 787-8	-
Nominal Spacing (Distance)	5	NM
Nominal Spacing (Time)	120	s
FIM Initiation	60.00	NM
FIM Termination	3.00	NM

4.7.5. Results

The results are shown in Figure 4.18 and Tables 4.11 and 4.12, in the same manner as for Scenario I. However, here IM-SP was only compared to the intended, i.e., constraint-lifted, implementation of ASTAR.

As before, ASTAR delivered consistent results with all arrivals situated within a range of -2.8 and $+1.0$ s. However, in this scenario IM-SP performs better on average than ASTAR with a mean $+0.30$ s vs. -0.98 s and a median $+0.06$ s vs. -0.93 s.

Nevertheless, anew, some samples of the “Linear High–” setup failed to meet the target range. Interestingly, the standard deviation for each logic has been almost identical to those found in Scenario I, i.e., 1.09 s vs. 1.12 s for ASTAR, and 1.80 s vs. 1.87 s for IM-SP.

Speed commands were again reduced with IM-SP, this time by 44%. In detail, ASTAR needed 9.3 ± 2.1 (median 9) commands, whereas IM-SP commanded 5.2 ± 1.1 (6) speed changes. Notably, the mean number of speed commands with IM-SP is lower than the reference profile, indicating that in some cases the ability of IM-SP to combine speed changes was used.

Even more apparent is the number of accelerations, or the lack thereof, as IM-SP virtually eliminates the need for accelerations with an average 0.1 ± 0.3 (0), compared to the 1.3 ± 1.1 (1) of ASTAR.

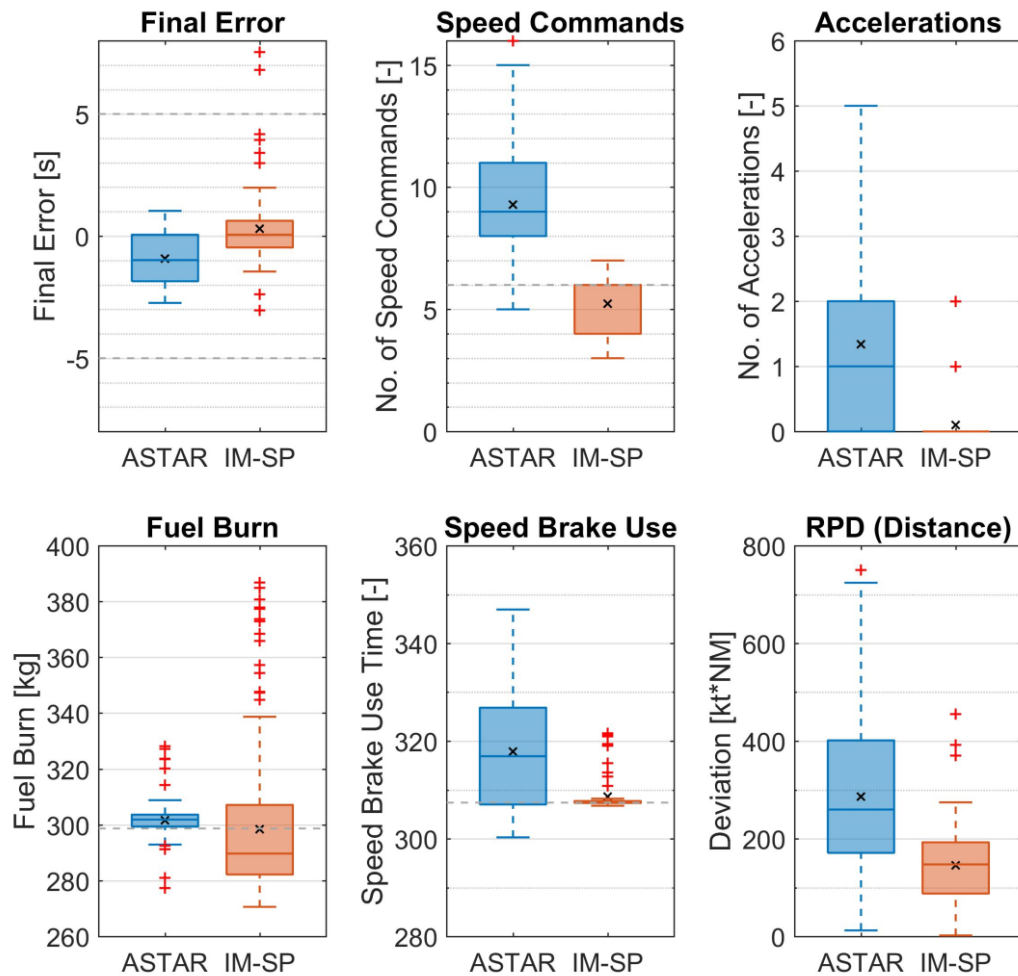


Figure 4.18 Boxplot for all simulations of Scenario II ⁽⁴⁹⁾

Notably, in Scenario II the overall fuel burn with IM-SP is lower than with ASTAR, however, again, the fuel burn is much more consistent with ASTAR than with IM-SP, rendering standard deviations of 5.5 kg and 23.5 kg respectively.

In contrast to Scenario I, the speed brake use time was lower and more consistent with both logics but especially IM-SP. Two factors contributed to this: The first, applying to both logics, is the aircraft type. As the Boeing 787 was developed roughly two decades after the A320, it has an increased aerodynamic performance, i.e., a higher lift to drag ratio, and therefore requires more drag, generated by the speed brakes, to achieve the prescribed deceleration rate. Further as the reference profile operates close to the maximum speed profile throughout the scenario and IM-SP rarely uses accelerations, the speed brake use time for IM-SP is relatively predetermined.

The operation close to the maximum speed profile also has a strong influence on the RPD, which this time is significantly lower with IM-SP, as it simply has less room to deviate, compared to ASTAR.

Table 4.11 Overall results for ASTAR ⁽⁴⁸⁾

Parameter	Median	Mean	SD
Final error [s]	-0.93	-0.98	1.09
Speed commands [-]	9	9.3	2.1
Accelerations [-]	1	1.3	1.1
Fuel burn [kg]	301.9	301.6	5.5
Speed brake use [s]	316.9	317.9	9.6
RPD [kt*NM]	259.9	286.6	152.5

Table 4.12 Overall results for IM-SP ⁽⁴⁸⁾

Parameter	Median	Mean	SD
Final error [s]	0.06	0.30	1.80
Speed commands [-]	6	5.2	1.1
Accelerations [-]	0	0.1	0.3
Fuel burn [kg]	289.7	298.5	23.5
Speed brake use [s]	307.5	308.7	3.7
RPD [kt*NM]	147.5	145.4	71.3

4.8. Discussion

4.8.1. Spacing Performance or the Linear Error Pattern

For most cases, IM-SP delivers sufficient spacing performance, however it struggles with the “Linear High–” setup in particular. In this scenario the spacing error is constantly increasing, i.e., the TTF is flying consistently faster than expected. Accordingly, the Ownship must also fly faster to expedite its arrival.

In the case of Scenario I, the maximum time the arrival can still be expedited for the reference profile after its initial deceleration is approximately 8 s (AEM = -8 s). In other words, after this point an additional error of 8 s causes the speed profile to become the maximum speed profile, as depicted in Figure 4.19, and any further excess will cause the aircraft to arrive later than required.

Assuming that part of this 8 s buffer was already used to expedite the arrival, as it is likely the case in the “Linear High–” setup, the results become even worse. While this is not a common case, the phenomenon and implied risk described here apply to all situations with a high initial error that further increases during the later phases of flight.

As, in its current design, IM-SP does not extend the speed envelope, potential countermeasures need to be proactive, i.e., must become effective before the AEM becomes saturated (0). One option would be to apply an artificial spacing error during the earlier phases of flight (generating an additional buffer), or in a similar fashion, a detection and optimization mechanism, that, while still possible, advances correcting actions to restore some AEM toward the end of the flight.

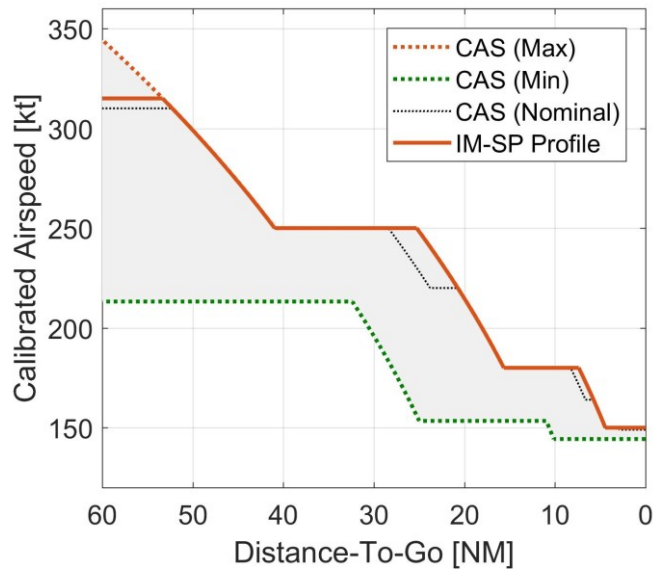


Figure 4.19 Saturated speed profile (AEM = 0) ⁽⁴⁸⁾

4.8.2. Application of Speed Constraints

As seen in Scenario I, ASTAR generates the best and most consistent results, provided that speed constraints are lifted. However, for operations in a high-density arrival environment, speed constraints are necessary, as they allow for some predictability and control of the traffic flow and therefore will remain in use for the foreseeable future. Further, individual national airspace systems might impose speed restrictions that cannot be waived by the ATCo (e.g., max. 250 kt below 10,000 ft MSL), and would require regulatory action first to exempt FIM aircraft.

Therefore, to make IM-SP's performance independent of the individual NAS, remove any uncertainty of the traffic situation allowing for the constraints to be lifted, and foremost, mitigate potential concerns and hesitations by the ATCo or Air Navigation Service Provider (ANSP) to clear FIM aircraft from constraints, IM-SP was designed to fit into current, constrained airspace systems.

In this environment, IM-SP demonstrated improvements over ASTAR. However, with respect to the problem of the profile running out of AEM, as described before, it could be hypothesized that extending IM-SP's planning area by 15% also, could be conducive to its performance.

4.8.3. Fuel Burn

The biggest drawback with IM-SP is its fuel burn, especially its variability. While the fuel burn was not a concern in the initial design of IM-SP, as compared to the number of speed commands, an increased fuel burn (as seen in Scenario I) is generally undesirable and would decrease the algorithm's acceptability with operators. Therefore, further algorithm optimization efforts should also take the fuel burn into account. One attempt is presented in Chapter 5.

4.9. Conclusion of Chapter 4

This chapter introduced the proposed control logic IM-SP, explained the motivation and design of its underlying functionalities, and showed two example scenarios to compare its performance to the benchmark logic ASTAR.

Results demonstrated that IM-SP successfully responded to the call to “explore alternative control law techniques to allow for tradeoffs between spacing error and IM speed change behavior to reduce the rate of speed changes and speed reversals”⁽¹⁸⁾, reducing speed commands by more than 40%, while delivering sufficient spacing performance, and without requiring the lifting of current speed constraints.

Limitations and weakness of the proposed logic have been highlighted, and are further addressed in the optimization study shown in the next chapter.

5. OPTIMIZATION OF IM-SP

The following chapter describes the analysis and optimization process of the cost function of IM-SP. Results were partially shown in Ref. (51), “Optimization of Interval Management – Speed Planning using SMPSO”, submitted to The Aeronautical Journal, currently under review. Figures submitted are used with permission.

5.1. Introduction

Naturally, when introducing a new or alternative technology, there are many objectives that need to be considered and a benefit must be perceptible to all parties involved in the implementation and operation of said technology. In case of FIM, the obvious primary objectives are the spacing performance, i.e., safety, and the operational feasibility, i.e. the pilot workload, previously expressed by the number of speed commands. Secondary objectives, not limited to FIM, but applicable to aircraft operation in general, include the operation costs, here expressed by the fuel burn. Accordingly, if a FIM logic was to be optimized, then It must be under all of the above-mentioned aspects.

In the case of IM-SP, an immediate way to tune the system’s response, i.e., optimize its behavior, is given by its cost function, in particular by altering the individual weight factors, as introduced in Subsection 4.5.3.

Therefore, a potential optimization strategy must be able to cope with multi-input, multi-objective optimization problems. Further, as the progression for each objective function is unknown, i.e. no derivative information is available, here, the choice is limited to non-derivate strategies.

From the recognized optimization algorithms capable to fulfil these requirements, this study explored “Particle Swarm Optimization” (PSO)⁽⁵²⁾, here in the variant of “Speed-constrained Multi-objective Particle Swarm Optimization” (SMPSO)⁽⁵³⁾ to optimize the system.

Both algorithms have been used in the aerospace domain for various optimization tasks; in case of SMPSO, for example to optimize the structure of airline hubs⁽⁵⁴⁾.

An explanation of the working principles of PSO and SMPSO, an analysis of the weight factors’ impact on the system performance, and the results of the optimization are shown in this chapter.

5.2. Particle Swarm Optimization (PSO)

5.2.1. Overview

Introduced in 1995, Particle Swarm Optimization (PSO) is a nature-inspired metaheuristic, belonging to the field of evolutionary algorithms, that simulates swarm or social behavior, comparable to the behavior of birds flocking or fish schooling⁽⁵²⁾.

Here, the swarm represents a group whose members, the particles, investigate a search space in pursuit of a common goal, i.e., the global minimum. During the search, particles are influenced by their own search experience (individual force) and by the group's experience (social force).

In detail, at first all particles are assigned an initial position (\vec{p}_0), and a random initial velocity (\vec{v}_0). The particle with the best initial position becomes the "leader" and shares its position, the global best (\vec{g}_{Best}), with the swarm. Further, each particle can memorize one more position, i.e., its individual best (\vec{p}_{Best}), which, in the first round, is identical to its initial position.

Once the particles start to move, they also experience inertia (ω), so that the velocity for the next round (\vec{v}_{n+1}) is determined by the following equation^(54,55):

$$\vec{v}_{n+1} = \omega \cdot \vec{v}_n + c_p \cdot r_1 \cdot (\vec{p}_{Best} - \vec{p}_n) + c_g \cdot r_2 \cdot (\vec{g}_{Best} - \vec{p}_n), \quad (5.1)$$

where c is a magnification factor, defined by the user, and r a random value, re-generated in each round. The next position for each particle is then determined by adding the velocity to its current position:

$$\vec{p}_{n+1} = \vec{p}_n + \vec{v}_{n+1}. \quad (5.2)$$

The particles then compare their new position to their memorized \vec{p}_{Best} , and if a better position was found, the new value is memorized and the old value is overwritten. Further, if the new value is better than \vec{g}_{Best} , the corresponding particle becomes the leader and the new global minimum is communicated to all other particles.

The search is ended after a fixed number of iterations or if another abort criterion is met.

5.2.2. Speed-constrained Multi-objective Particle Swarm Optimization (SMPSO)

SMPSO was introduced in 2009 as a further development of PSO and OMOPSO⁽⁵⁶⁾, an optimized multi-objective derivative of PSO presented in 2005. The mechanisms introduced with SMPSO allow the algorithm to achieve a faster and more uniform exploration of the pareto front⁽⁵³⁾.

The speed-constraint, giving SMPSO its name, was added as a countermeasure to a phenomenon called "swarm explosion"⁽⁵⁷⁾, in which particles would gain such a high velocity that they would pass over unexplored areas and get caught up at the boundaries of the search area.

In particular, SMPSO adds the magnification factors c of Equation 5.1, here randomly chosen for each round and particle and limited to the range $[1.5, 2.5]$ ⁽⁵⁸⁾, to obtain the variable

$$\varphi = c_p + c_g, \quad (5.3)$$

that is used to define a velocity constriction coefficient (χ). The idea for the coefficient was originally proposed in Ref. (57) and is presented here in the shortened form of:

$$\chi = \begin{cases} \frac{2}{2-\varphi-\sqrt{\varphi^2-4\varphi}}, & \varphi > 4 \\ 1, & \varphi \leq 4 \end{cases}. \quad (5.4)$$

This coefficient is then applied, i.e., multiplied, to the velocity of the PSO algorithm (Equation 5.1) and the resulting speed is further limited in each dimension j , to the range $[-\delta_j, \delta_j]$, defined by:

$$\delta_j = \frac{(\text{upper_limit}_j - \text{lower_limit}_j)}{2}, \quad (5.5)$$

effectively limiting the speed in each dimension (v_j) to half the dimension's span.

Further, SMPSO implements a mutation concept, acquired from OMOPSO that randomly adds movement to the particles to achieve a better exploration of the search space, and to prevent lock-ups in local minima.

Technically, the SMPSO algorithm was realized as part of the Multi-objective Evolutionary Algorithm (MOEA) Framework 2.12 by Dave Hadka ⁽⁵⁸⁾. The MOEA framework is a free and open-source framework for Java and was implemented into the existing simulation environment used throughout this thesis.

5.3. Optimization Problem

5.3.1. Decision Variable

The system response of IM-SP, i.e., which speed plan the algorithm ultimately chooses, if multiple solutions to a given spacing error exist (Subsection 4.5.2), can be manipulated by the weight factor vector \vec{q} (Subsection 4.5.3.6), which governs the impact of the individual costs (s_k) on the overall cost S . Accordingly, \vec{q} is used as the decision variable.

Originally, \vec{q} contains five elements $[q_{AEM}, q_{TTG}, q_{TTR}, q_{APD}, q_{Type}]$, however, because of the dependability $q_{AEM} + q_{TTG} = 1 \Leftrightarrow q_{TTG} = 1 - q_{AEM}$, \vec{q} can be reduced to four elements, giving:

$$\vec{q} = \begin{pmatrix} q_1 \\ q_2 \\ q_3 \\ q_4 \end{pmatrix} = \begin{pmatrix} q_{\text{AEM}} \\ q_{\text{TTR}} \\ q_{\text{APD}} \\ q_{\text{Type}} \end{pmatrix}. \quad (5.6)$$

5.3.2. Objective Function

The areas of concern for (IM-SP based) FIM, that are addressed in this optimization study, can be grouped into the three categories: performance, economy, and usability, represented by the final error, fuel burn, and number of commands respectively.

For the latter an additional distinction has been made, explained later, so that in total four objectives apply to the optimization problem, giving the following general equation for the objective function f :

$$\begin{aligned} \text{Minimize } f(\vec{q}) &= (f_1(\vec{q}), f_2(\vec{q}), f_3(\vec{q}), f_4(\vec{q})). \\ \text{Subject to } 0 &\leq q_i \leq 1 \text{ with } i = 1..4 \end{aligned} \quad (5.7)$$

The four respective objective functions, partially adapted to enable minimization, are:

- 1) The spacing error, i.e., the absolute value of the final error:

$$f_1(\vec{q}) = |e(t)|. \quad (5.8)$$

- 2) The fuel burn:

$$f_2(\vec{q}) = \text{Fuel Burn}. \quad (5.9)$$

- 3) The number of speed commands (n), put in relation to the number of commands of the reference profile (n_{Ref}):

$$f_3(\vec{q}) = |n - n_{\text{Ref}}|, \quad (5.10)$$

as to have neither more commands, i.e., more interaction, nor less. Too few commands should also be avoided, because they imply a risk that too many speed changes are combined, resulting in too large speed-change magnitudes; another undesired behavior found in the ATD-1 flight test⁽¹⁷⁾.

- 4) The number of the so called “critical” commands (n_{Crit}):

$$f_4(\vec{q}) = n_{\text{Crit}}. \quad (5.11)$$

Critical commands are defined as commands with very short lead times (here $TTR \leq 15$ s), i.e., commands that are likely to either interrupt the crew in other tasks, or in contrast, are more likely to be slipped or not executed as intended. In other words, this objective coincided with the design criterion of IM-SP to give the crew more foreknowledge of the systems intention and to avoid the above-mention situations. Conversely, the ideal number of critical commands is 0.

5.3.3. Block Diagram

Figure 5.1 shows the block diagram of the IM-SP logic and the situation of the four objective functions. The diagram originates at the Ownship's trajectory block on the left, from where the current speed plan and speed envelope are directly passed to the IM-SP core, highlighted in the center. The Ownship's TTG is compared to the nominal TTG to obtain the spacing error (as per Equation 2.2) and then passed to IM-SP. Including the current wind forecast and environmental conditions, IM-SP subsequently calculates a new speed plan, which is looped back to the Ownship's trajectory and passed on to the flight dynamics which allow for an estimation of the new TTG. Finally, the updated TTG is looped back to the Ownship's trajectory block, closing the cycle.

The number of total and critical commands can be obtained from the change history of IM-SP, and the total fuel burn is obtained from integrating the fuel flow from the flight dynamics block.

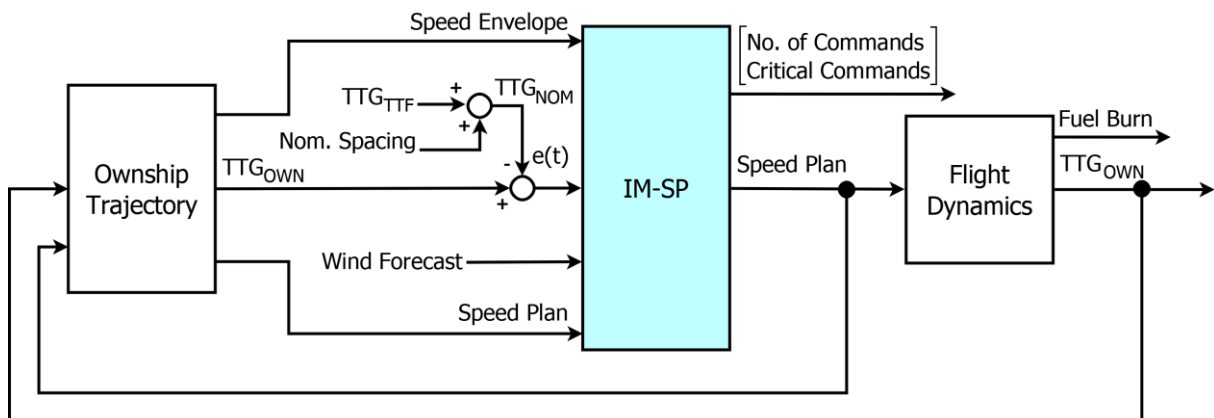


Figure 5.1 Block diagram of the IM-SP algorithm ⁽⁵¹⁾

5.3.4. SMP SO Settings

For computation time considerations the optimization with SMP SO was done in two steps: first, the actual optimization with a reduced data set and afterwards a benchmark test with the full dataset, testing the emerged candidates.

The reduced dataset contained all error patterns (A-F) in both directions, however limited to the high amplification and without an initial offset, plus the 6 base errors, giving a total of 18 setups ($6 + 6 \cdot 2 = 18$). For the individual objective functions the mean value of the 18 setups was used.

The settings used for the SMPSO algorithm are shown in Table 5.1:

Table 5.1 SMPSO Settings

Setting	Value
Number of Particles	81
Evaluations per Particle	50
Simulations per Evaluation	18
Mutation Probability	1 in 6

In the original paper of SMPSO⁽⁵³⁾ and in the MOEA Framework⁽⁵⁸⁾ PSOs are run with 100 particles. Here 81 particles were chosen as the closest number to 100 representing a uniform search space distribution in all dimensions, i.e., three particles for each of the four decision variables ($3^4 = 81$).

With respect to the computation time, the number of evaluations per particle was set to 50, (compared to the default value of 100 used in the MOEA Framework).

The probability for mutation is originally set to 15% in Ref. (53), however the MOEA Framework uses a probability of 1 in 6 ($\approx 16.67\%$), which was adopted here. All other settings were also retained from the default settings of the MOEA Framework.

In result, the computation of all 4050 evaluations, run on a machine with similar performance to the one described in Subsection 4.5.5, took approximately three and a half days.

5.4. Weight Factor Vector Analysis

In preparation for the optimization, an analysis of the individual elements of \vec{q} was conducted to obtain a better understanding of their effect on the four objective functions.

In addition, four non-objective parameters have also been examined, that are: the number of accelerations, the speed brake use time, the RPD (as used before in Chapter 4), and the maximum reference CAS deviation.

The last metric indicates the highest difference between the reference CAS and commanded CAS recorded throughout the flight, and is another mean to indicate the final speed profile's shape and potential acceptability.

In the following each element has been simulated in the range of 0 (not applied) to 1 (fully applied), in 0.01 unit intervals, while the other three elements were retained from the original setting (Table 4.2). The simulation setup was the same as in Scenario I, but also included the error pattern "SHTLE" (F), giving a total of 175 simulations ($7 + 6 \cdot 2 \cdot 2 \cdot 7 = 175$) per setting. The figures presented in this section show the weight factor's value on the x-Axis and the progression of the mean value (blue) and SD (orange) of all simulations for the respective setting on the y-Axis.

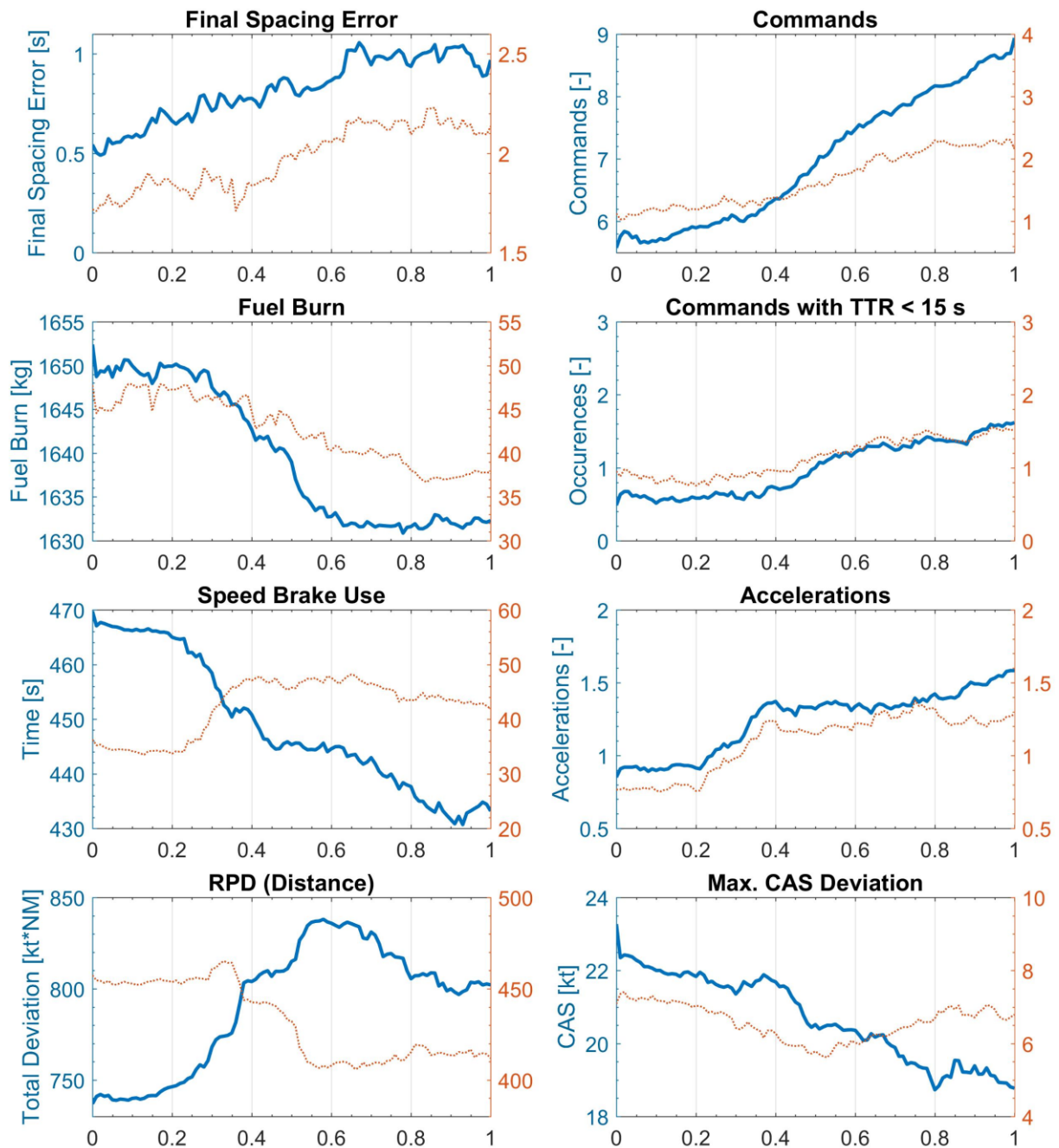


Figure 5.2 Overall results depending on q_{AEM} (equivalent to $1 - q_{TTG}$)⁽⁵¹⁾

5.4.1. Arrival Expedition Margin vs. Time-To-Go

As seen in Figure 5.2, the two scoring attributes have a strong impact on all parameters.

Distinctively, low values for q_{AEM} (high q_{TTG}) cause the lowest final spacing error, the least total commands, critical commands, accelerations, and the lowest RPD, but also the highest fuel burn, the longest speed brake use, and the highest CAS deviation. For high q_{AEM} values, the opposite is the fact, with all parameters, except the RPD, showing a more or less steady increase, or decrease respectively, over the full range. In contrast, the RPD shows a distinct peak, located away from the vicinity of the boundary settings, at 0.58.

Notably, for q_{AEM} values up to 0.25, less commands than with the reference profile (6) are observed, and other parameters like the fuel burn and the speed brake use time remain relatively stable. However, from there on a faster change of all parameters, especially the RPD, can be observed, indicating a change of the system's behavior.

Therefore, if the system was optimized solely for its spacing performance and commands, i.e., disregarding the fuel burn, it seems persuasive to choose a q_{AEM} in the previous mentioned range, or even 0. However, upon inspection of the profiles generated for this range, an operationally undesired behavior, hereafter referred to as “backloading” was observed. An example profile, suffering from the phenomenon is shown in Figure 5.3.

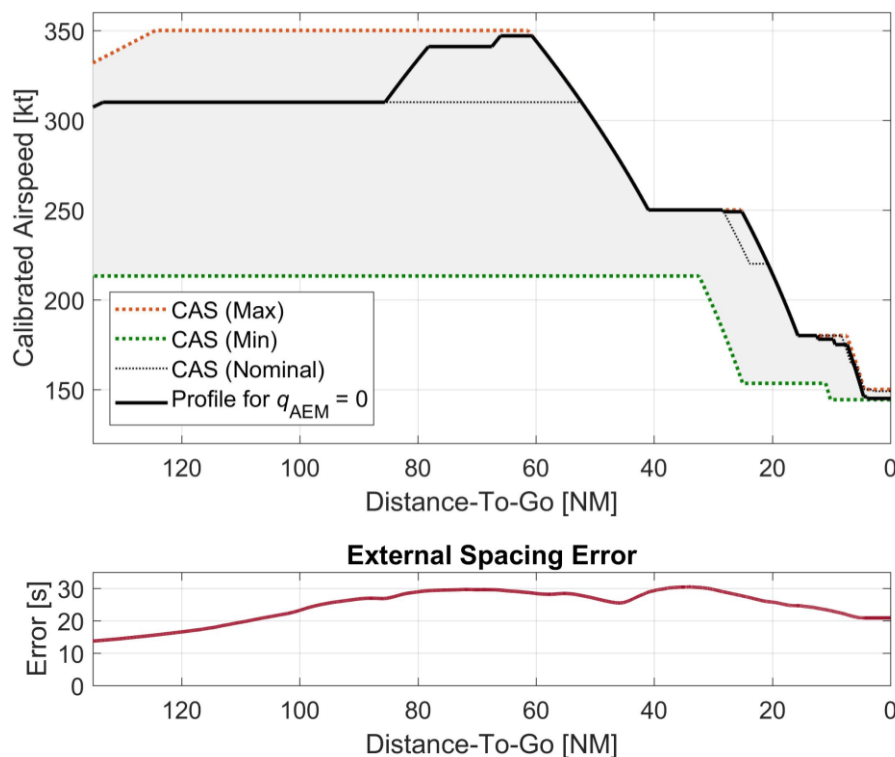


Figure 5.3 Backloading phenomenon observed with low q_{AEM} values⁽⁵¹⁾

In this example the aircraft is exposed to a positive initial error, that continues to increase to a top value of +30 s. Owing to the particular progression (SHTLE), and the characteristics of S_{TTG} to summarize modifications to the later phases of flight (as described in Subsection 4.5.3.2), the system tries to delay the counteraction as long as possible, but ultimately has to react, provoking short high-magnitude accelerations. In this particular example, in two steps, first from 310 kt to 340 kt, and then again to 347 kt, with the latter only to be held for the minimum distance of 5 NM.

Furthermore, this behavior is also conducive to the problem of running out of AEM (as described in Subsection 4.8.1) during early stages of flight.

The backloading phenomenon was observed for q_{AEM} values up to 0.3, corresponding to the sudden rise in RPD. Accordingly, q_{AEM} values lower 0.3 were not considered in the optimization.

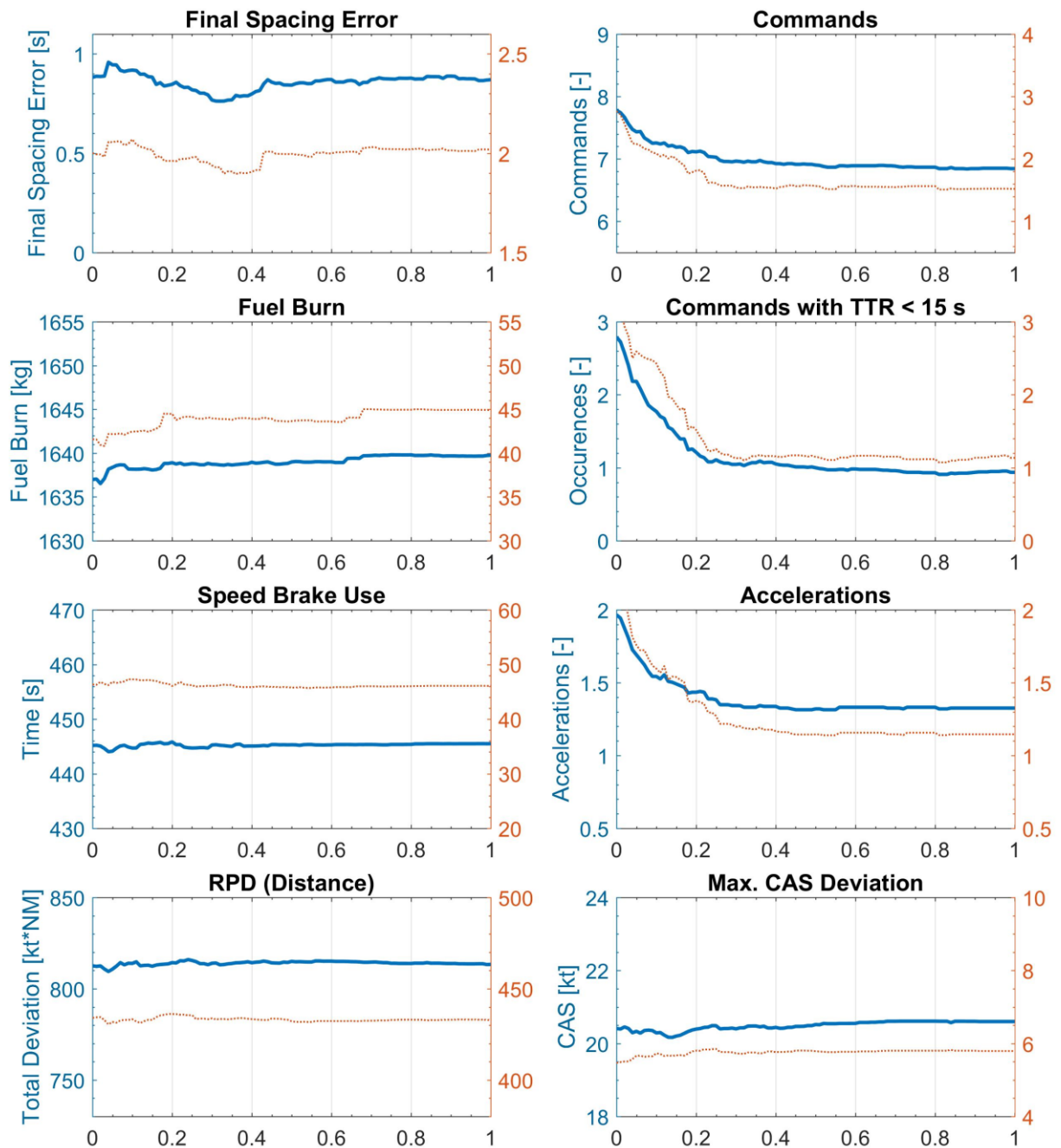


Figure 5.4 Overall results depending on $q_{TTR}^{(51)}$

5.4.2. Time-To-React

As seen in Figure 5.4, the TTR penalty effectively reduces the number of critical commands from 2.8 to 1, additional to an overall improvement in commands and accelerations. The minimum spacing error is observed at $q_{TTR} = 0.33$, approximately the value at which the number of commands also starts to stabilize. The final spacing error itself stabilizes for a $q_{TTR} \geq 0.45$.

All other parameters remain virtually unaffected.

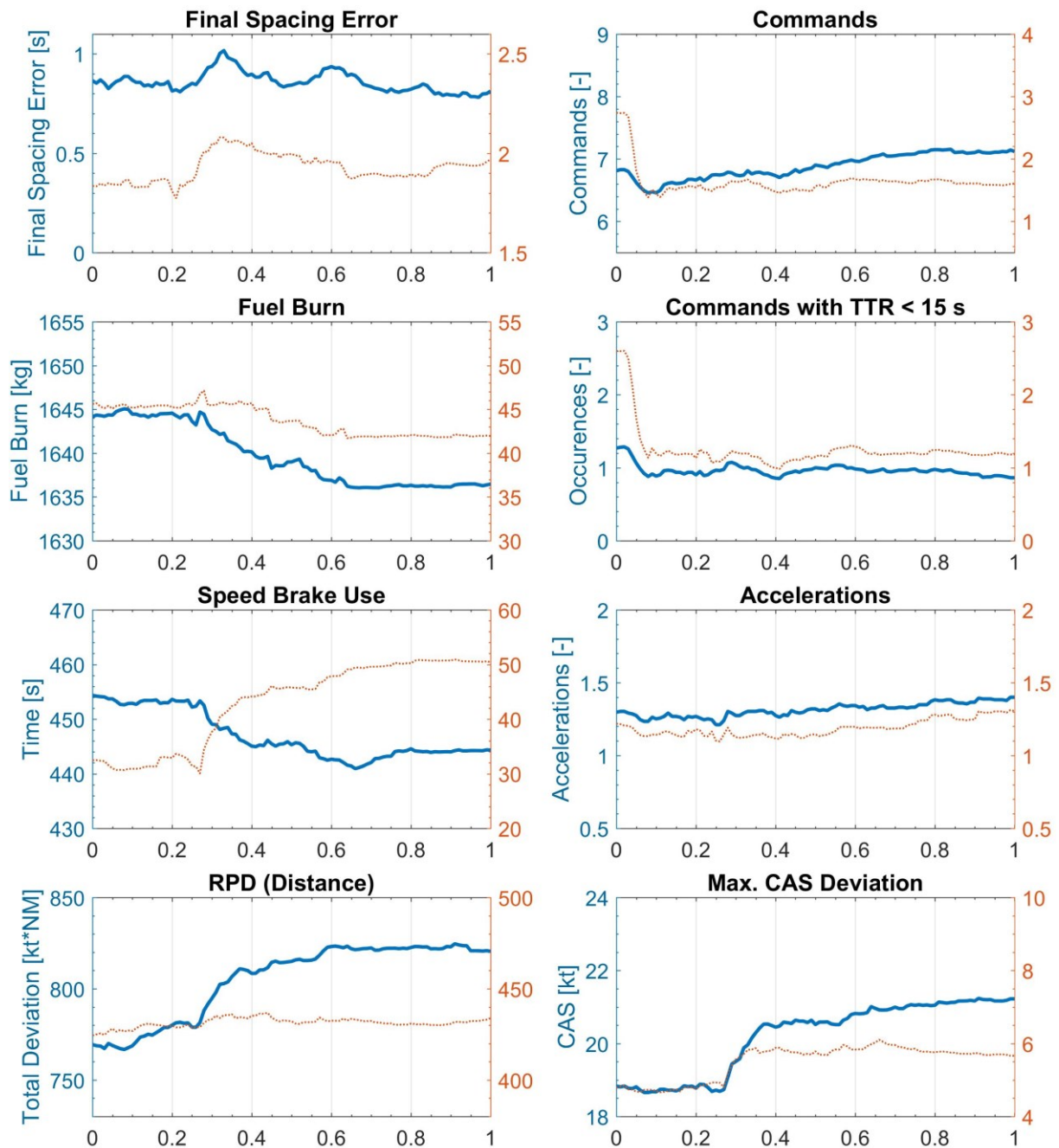


Figure 5.5 Overall results depending on q_{APD} ⁽⁵¹⁾

5.4.3. Action Point Distance

While the APD penalty does not consult any of the parameters shown in Figure 5.5 directly, its intention to avoid close-sequenced speed changes, by furthering fewer but higher magnitude speed changes, is partially reflected by the synchronous rise of the RPD and max. CAS deviation for a $q_{APD} \geq 0.25$. At the same time, a reduction of the fuel burn and speed brake time can be observed. Other distinctive marks include an initial drop of the total and critical commands when q_{APD} is applied initially, and the constant minor increase of the total commands with q_{APD} .

The final spacing error peaks at a q_{APD} of 0.34, but remains relatively unaffected otherwise.

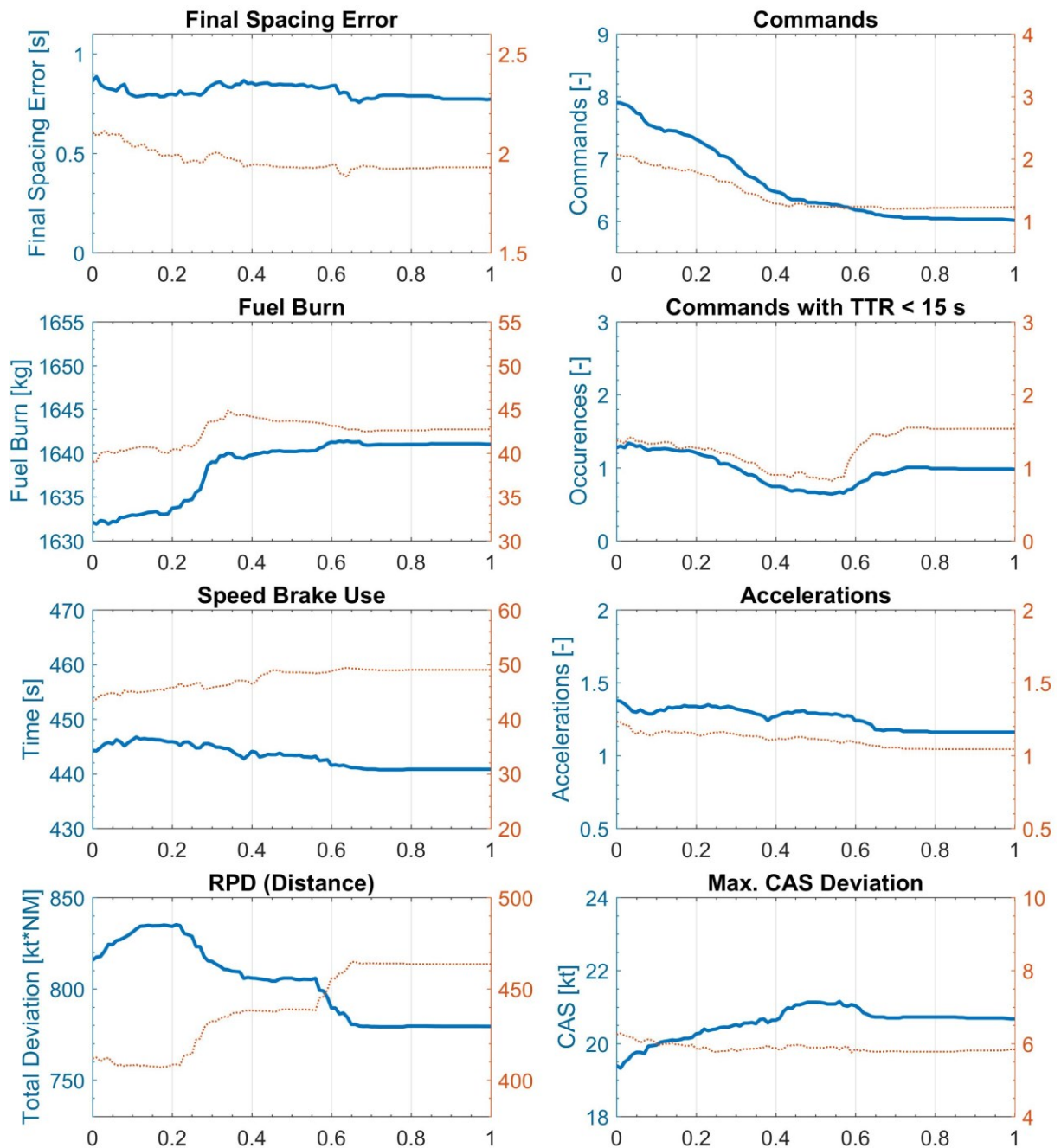


Figure 5.6 Overall results depending on $q_{\text{Type}}^{(51)}$

5.4.4. Action Point Type

The purpose of the type penalty is to favor changes to the planned speed changes instead of adding new ones. As seen in Figure 5.6, this is successfully achieved, reducing speed commands from 7.9 (when not applied) to the reference value of 6 (fully applied).

Furthermore, The RPD is reduced in two steps, from a q_{Type} of 0.25 to 0.32 and from 0.56 to 0.65, where after all values stabilize. However, the first drop in the RPD is accompanied by a sudden rise in the fuel burn. The final spacing error remains widely unaffected, with a neglectable increase for values between 0.27 and 0.66.

5.4.5. Analysis Summary

Though it must be noted that the single parameter analysis does not reflect potential correlations of any of the parameters, two conclusions can be made:

First, the penalty attributes (s_{TTR} , s_{APD} , s_{Type}) work as intended, i.e., they suppress undesired profiles characteristics, but have only neglectable effect on the overall spacing performance.

Second, an improvement in spacing performance or commands usually comes at the expense of a higher fuel burn, or vice-versa. Therefore, a simultaneous improvement of both objectives is not feasible and a trade-off solution must be sought.

5.5. Multi-objective Optimization

5.5.1. SMPSO Optimization Results

In total, SMPSO found 87 individual solutions for the optimization problem. Accounting for the trade-off situation between the fuel burn and all other objective functions, results are shown as three scatter plots (Figures 5.7-5.9). The plots show the fuel burn on the x-axis and the final error, command difference and critical commands on the y-axis respectively, with axis limits chosen to include all solutions. The pareto fronts are indicated and have been drawn by linear interpolation and extrapolation.

From all solutions, two distinctive solutions have emerged that are located on two of the three pareto fronts and did neither have a mean final error higher than 1 s nor increase the number of commands by more than one. According to their distinguished traits, the solutions are referred to as the “time optimal” (T+) and “fuel improved” (F+) solution.

The “time optimal” solution (T+, with $\vec{q}_{T+} = [0.32, (0.68), 1.00, 0.32, 0.55]$) is the overall best solution in regard to the final spacing error (0.33) and command difference (0). Further, in comparison to the original setting, it reduces the number of critical commands, but shows a higher fuel burn.

The “fuel improved” solution (F+, with $\vec{q}_{F+} = [0.76, (0.24), 0.98, 0.97, 0.81]$) is an overall trade-off, that, relative to the original settings, improves the fuel burn, total commands, and critical commands, at similar spacing performance.

The results and weight factor settings for each solution are shown in Tables 5.2 and 5.3. The results of the original setting are given for comparison and represent the full data set.

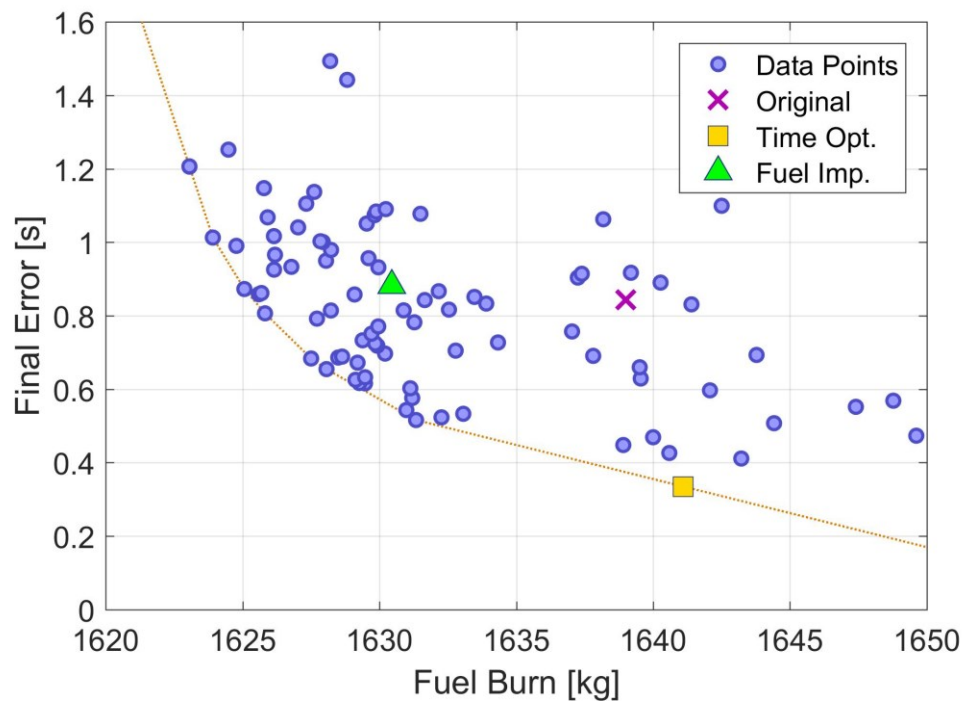
In Figures 5.7-5.9, T+ is indicated by an orange square, F+ is indicated by a green triangle, and the original setting is indicated by a violet x-mark. The color coding is kept throughout all figures and tables in this chapter.

Table 5.2 Weight factor settings by profile ⁽⁵¹⁾

Weight Factor	(Original)	Time Opt.	Fuel Imp.
Arrival Expedition Margin (q_{AEM})	0.50	0.32	0.76
Time-To-Go (q_{TTG})	0.50	0.68	0.24
Time-To-React (q_{TTR})	0.50	1.00	0.98
Action Point Distance (q_{APD})	0.50	0.32	0.97
Change Type (q_{Type})	0.30	0.55	0.81

Table 5.3 Objective function results by profile ⁽⁵¹⁾

Parameter	(Original)	Time Opt.	Fuel Imp.
Final error [s]	0.84	0.33	0.88
Fuel burn [kg]	1639.0	1641.1	1630.5
Command difference [-]	0.9	0.0	0.5
Critical commands [-]	1.0	0.5	0.7


Figure 5.7 Optimization results – final error vs. fuel burn ⁽⁵¹⁾

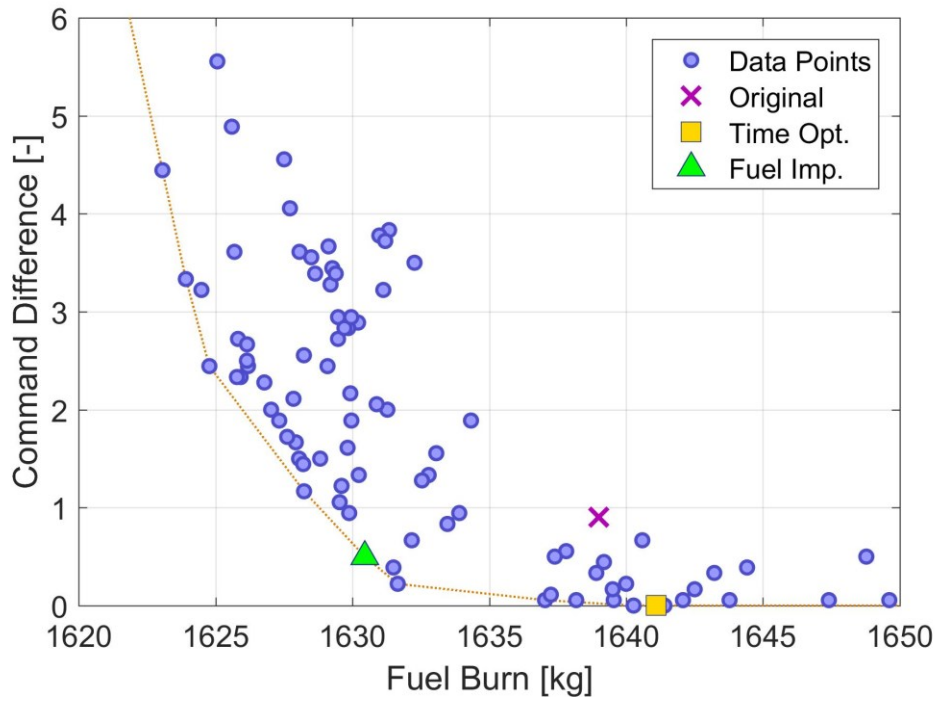


Figure 5.8 Optimization results – command difference vs. fuel burn ⁽⁵¹⁾

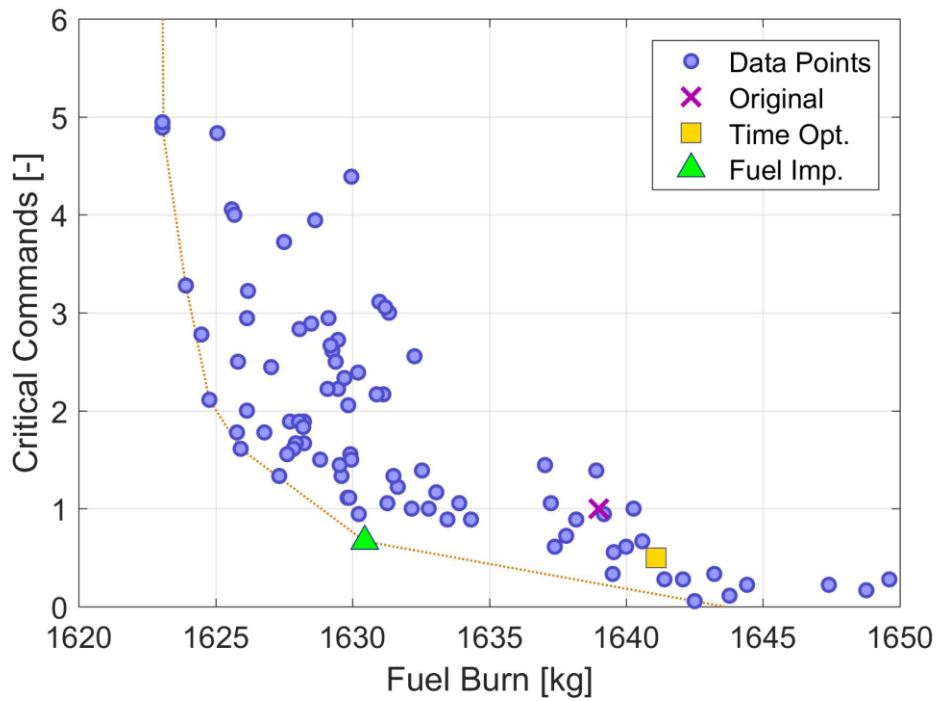


Figure 5.9 Optimization results – critical commands vs. fuel burn ⁽⁵¹⁾

5.5.2. Speed Profile Characteristics

Examples for the resulting speed profiles generated by IM-SP using the T+ and F+ settings are shown in Figures 5.10 and 5.11. The setup used in Figure 5.10 is the same as previously shown for the backloading phenomenon (Figure 5.3), whereas the setup in Figure 5.11 represents its inversion, meaning the same pattern but with opposite direction and negative initial spacing error.

As seen in in Figure 5.10, the T+ setting commands fewer speed changes, but with higher magnitudes. In contrast F+ commands more speed changes and an earlier initial acceleration (DTG of 119 NM vs. 94 NM) but reaches an overall lower top-speed (333 kt vs. 339 kt).

After the initial deceleration to 250 kt both profiles are almost identical, with a small difference for the second and third to last deceleration.

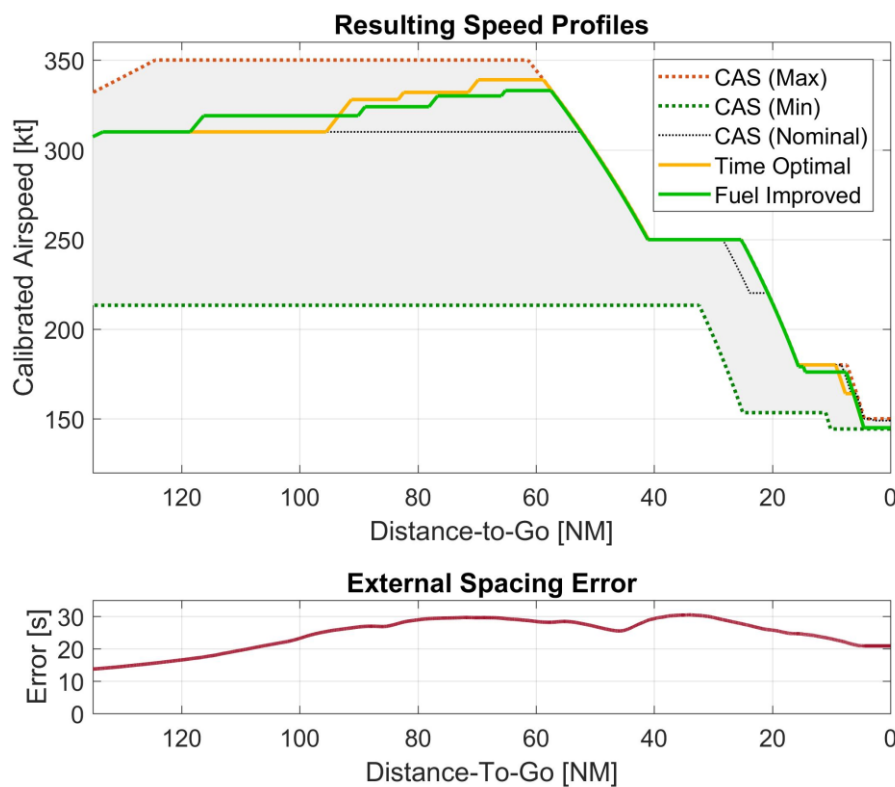


Figure 5.10 Comparison for T+ and F+ on the "SHTLE High+" setup with an initial positive error ⁽⁵¹⁾

In the example shown in Figure 5.11 both systems react with the same initial deceleration, but show different characteristics from the first planned deceleration on.

In detail, the F+ setting, using a higher q_{AEM} , tries to acquire more AEM earlier by advancing the planned deceleration to 220 kt (in case the arrival has to be expedited again). By contrast the T+ setting remains on the nominal profile for longer and instead the planned deceleration to 180 kt is reduced to 163 kt. However, because of the now rising error, the system has to react with a small acceleration to 166 kt.

As seen for both examples, the F+ setting has a tendency for earlier reactions, i.e., it is rather proactive, where in contrast the T+ setting is a little bit more reactive. Depending on the error progression, this gives either setting an advantage or disadvantage.

For example, the T+ setting's later reaction is beneficial for changing errors, where a prolonged time to combine and revert actions allows to issue less commands. However, this strategy also makes it more vulnerable to run out of error handling capabilities. Here, F+ displays a higher tolerance for sudden additional error

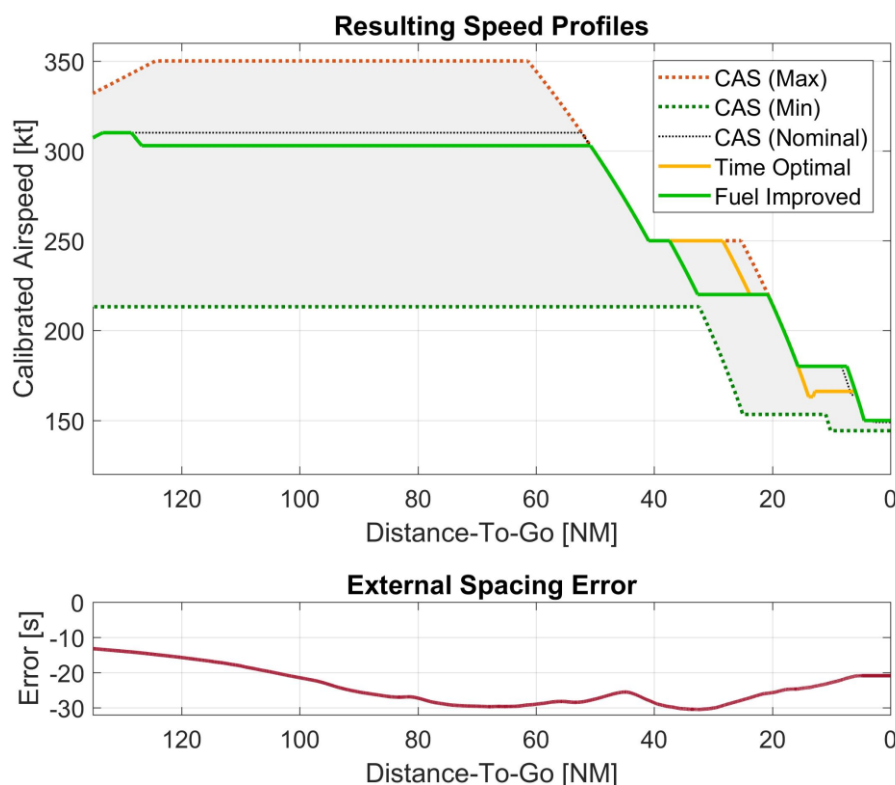


Figure 5.11 Comparison for T+ and F+ on the "SHTLE High-" setup with an initial negative error ⁽⁵¹⁾

5.5.3. Full Dataset Results

The results for all 175 simulations, grouped by the setting, are shown in Tables 5.4-5.6, and as boxplot graphs in Figures 5.12 and 5.13. The boxplots are illustrated the same way as in Chapter 4. A further analysis of the objective and non-objective parameters is given in the respective subsection.

Table 5.4 Overall results for the original settings (Orig.)⁽⁵¹⁾

Parameter	Median	Mean	SD
Final error [s]	0.19	0.84	2.00
Fuel burn [kg]	1635.1	1639.0	43.6
Total commands [-]	7	6.9	1.6
Critical commands [-]	1	1.0	1.1
Accelerations [-]	1	1.3	1.1
Speed brake use [s]	456.2	445.3	45.8
RPD [kt*NM]	809.3	815.0	432.2
Max. CAS Dev. [kt]	20.5	20.5	5.8

Table 5.5 Overall results for the time optimal setting (T+)⁽⁵¹⁾

Parameter	Median	Mean	SD
Final error [s]	0.29	0.61	1.90
Fuel burn [kg]	1639.2	1645.3	44.3
Total commands [-]	6	6.0	1.2
Critical commands [-]	0	0.5	0.7
Accelerations [-]	1	1.1	1.0
Speed brake use [s]	460.0	456.6	34.0
RPD [kt*NM]	774.5	744.1	452.1
Max. CAS Dev. [kt]	20.3	20.5	6.4

Table 5.6 Overall results for the fuel improved setting (F+)⁽⁵¹⁾

Parameter	Median	Mean	SD
Final error [s]	0.21	0.82	1.93
Fuel burn [kg]	1629.1	1633.2	37.8
Total commands [-]	7	6.8	1.6
Critical commands [-]	0	0.8	1.1
Accelerations [-]	1	1.4	1.3
Speed brake use [s]	456.4	440.7	54.9
RPD [kt*NM]	817.1	830.0	422.2
Max. CAS Dev. [kt]	20.5	21.8	5.7

5.5.3.1. Objective Parameter

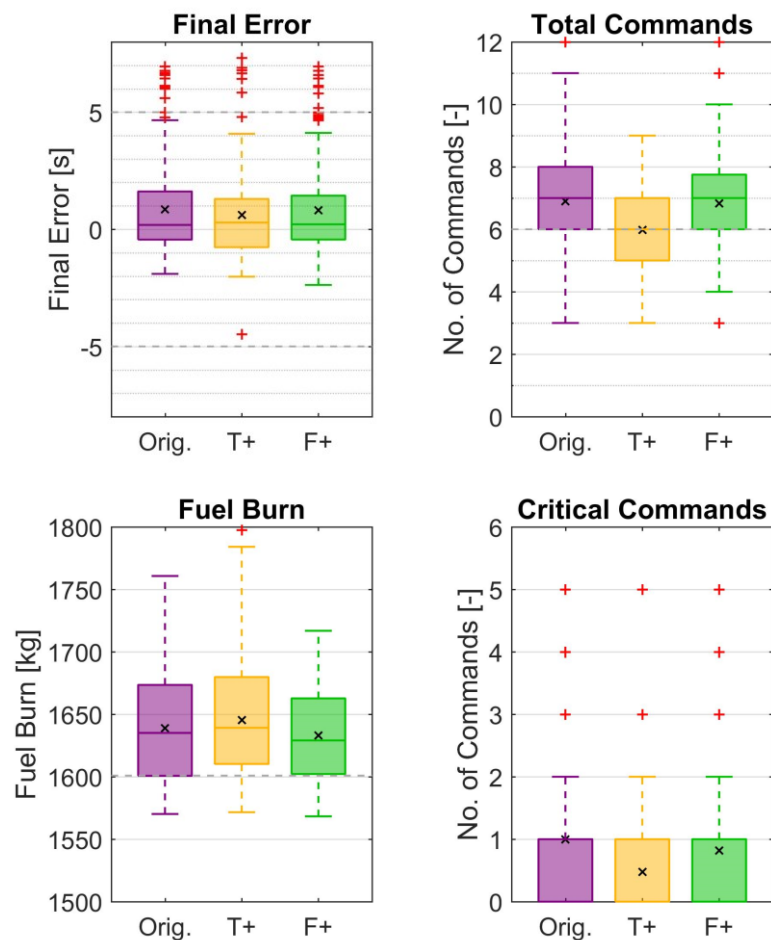


Figure 5.12 Boxplot for the objective functions divided by setting ⁽⁵¹⁾

The full data set results indicate that each setting has the forecasted effect on the objective functions, i.e., compared to the spacing performance of the original settings (0.84 ± 2.00 s) T+ shows an improvement (0.61 ± 1.90 s), whereas F+ delivers comparable performance (0.82 ± 1.93 s). Confirming the projected results of the optimization set with the actual results of the full data set, a decline for T+ (0.61 vs. 0.33), but a slight improvement for F+ (0.82 vs. 0.88) is observed. The former can be accredited to lack of initial offset for the error patterns in the optimization data set, which makes it more benign, or conversely the full data set more onerous.

Further, the extreme outliers of T+ support the previous observation, that, though the setting delivers a better performance overall, it is more susceptible to run out of error handling capability.

Using the F+ setting, the fuel economy was successfully improved (to 1633.2 ± 37.8 kg), lowering both the mean and standard deviation of the fuel burn by approximately 6 kg, compared to the original setting (1639.0 ± 43.6 kg). Further, as seen in the box plot, extremely high fuel burns were also lessened.

Accordingly, with the better fuel economy of F+, the drawback of a higher fuel burn compared to ASTAR in Section 4.6 is mostly eliminated.

In contrast, T+ shows an elevated fuel burn, increasing the mean value by approximately 6 kg.

In regard to the number of speed commands, T+ matches the predicted results at 6.0 ± 1.2 commands (median 6), indicating that this setting can achieve the required spacing performance without the need for more speed commands than originally planned. Here too, F+ delivers similar performance as the original settings (6.8 ± 1.6 vs. 6.9 ± 1.6).

A reduced number of critical commands was achieved with both settings, T+ again matching the predicted result at 0.5 ± 0.7 (median 0), and F_{opt} at 0.8 ± 1.1 (0), compared to the original results of 1.0 ± 1.1 (1). Here T+ benefits from the fact that a lower number of total commands, also implies a lower risk to encounter a critical command. Nevertheless, the boxplot indicates that, depending on the error growth, critical commands can be inevitable for successful FIM operation.

5.5.3.2. Non-Objective Parameters

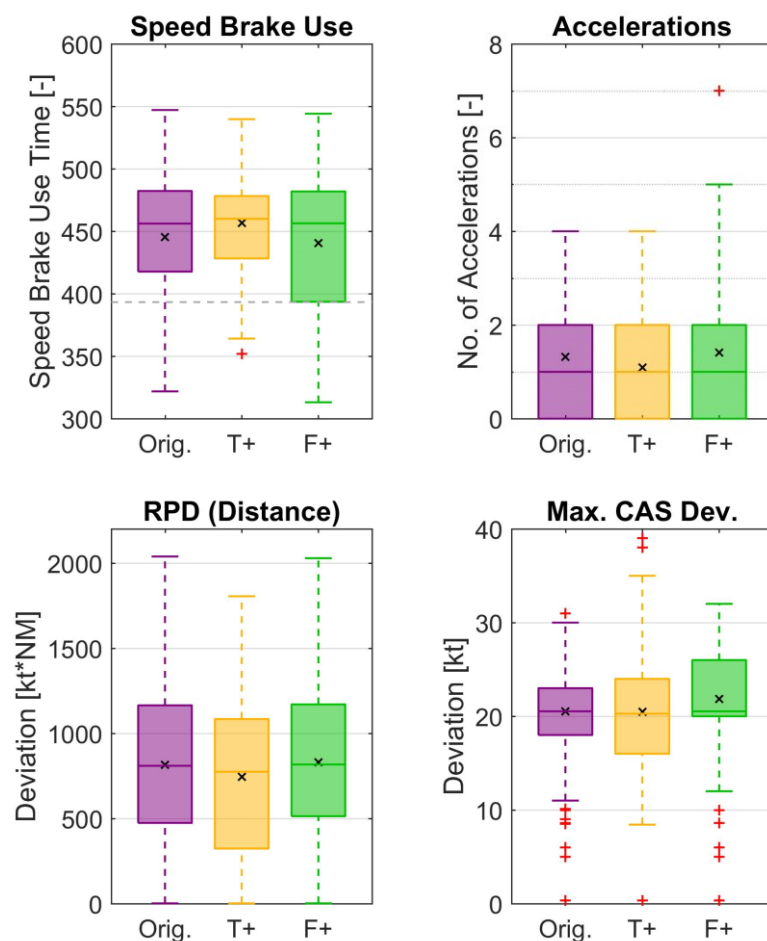


Figure 5.13 Boxplot for the non-objective functions divided by setting ⁽⁵¹⁾

For the speed brake use time, it can be seen that T+, reaching higher top speeds than the other profiles, as seen in Figure 5.10, also requires more application of the speed brakes on average, especially visible by the lower end of the box whisker.

In contrast, F+ shows a slight reduction giving it the best emission footprint, both in fuel and noise.

Compared to the number of accelerations of the original setting (1.3 ± 1.1), a reduction is observed for T+ (1.1 ± 1.0), whereas F+ shows a marginal increase (1.4 ± 1.3). More conspicuous is a single outlier in the boxplot, indicating seven accelerations.

Further examination of the resulting profile however showed that these seven accelerations were composed of two consecutively increasing accelerations, one in four steps (similar to Figure 5.10), and the other in three. The tendency for stepped accelerations is a side effect of the higher, “proactive” q_{AEM} setting of F+ and must not be mistaken as an indicator for reversals.

In terms of the RPD, T+ shows the smallest deviation. While it in contrast produces the highest absolute reference CAS deviation, these deviations are kept for a shorter duration, rendering the overall lower RPD. In contrast F+ shows the highest average reference CAS deviation, but a similar RPD, compared to the original settings. This combination can be explained by the setting’s tendency to shift decelerations more, as seen in Figure 5.11, so that more CAS deviation is generated in a lateral, rather than a vertical manner.

5.6. Discussion

5.6.1. Optimal Setting

Based on the 87 solutions found by the algorithm, and with respect to the four, partially conflicting, objective functions, it can be deduced that there is no single optimal setting. Accordingly, the choice of a practical setting depends somewhat on individual preferences.

Assuming that more solutions on the Pareto fronts are explored, i.e., settings in between T+ and F+ are established, one option could be to determine the setting based on the need for the individual flight, rather than using a fixed value. For example, the same way airlines use a cost index to optimize the profile of each individual flight.

Another option could be the use of dynamic, i.e., time or distance-variant, weights instead of fixed weights. For example, the system could start with a fuel performance improved setting when far from the airport or in front of the first planned deceleration, and then gradually shift toward a spacing performance priority during the later phases of flight (comparable to the distance dependent amplification factor $g1$ used in ASTAR). In contrast, the downside of a dynamic value

could be the changing system behavior which could affect the system's comprehensibility, that is the predictability of the next action, from a pilot's perspective.

When having to make a decision between T+ and F+ it could be argued that T+, showing better results in six out of eight categories (three objectives, and three non-objectives respectively) is the best setting.

However, looking at the detailed results, it is debatable that an improvement of 0.2 s in spacing performance, 1 command, and 0.5 critical commands, is a legitimate trade-off for 12 kg of increased fuel burn. Specifically, the difference of 0.2 s is unlikely to be perceived by either the flight crew, the ATCo, or the passengers.

In contrast, the reductions in commands is certainly desirable, however, one more command, and one more critical command every second flight is reasonable; especially when considering that this additional command, generated by F+, usually occurs during earlier phases of flight (as seen in Figures 5.10 and 5.11).

Last, as discussed previously and supported by the extreme outliers in the boxplots, T+, compared to F+, shows an increased risk in running out of adjustment margin.

Therefore, interpreting the results and considering all operational aspects, future iterations of IM-SP will use the "fuel improved" setting, F+.

5.6.2. Synergetic Effects of q_{AEM} and the Penalty Attributes

In the weight factor analysis (Section 5.4) it was strongly indicated that the penalty attributes fulfil their individual purpose. Further, the notably high settings of the individual factors for F+ ($q_{TTR} = 0.98$, $q_{APD} = 0.97$, $q_{Type} = 0.81$) support this claim.

By example, the q_{AEM} of F+ is 0.76; Looking at the progression of the total commands in Figure 5.2, an average 8 commands would be expected for F+, however, ultimately it only showed 6.8 commands. A similar abatement was observed with the critical commands, with 0.8 instead of 1.3. Therefore, it is concluded that the penalty attributes, especially in combination with high weight factor settings, successfully mitigate some of the negative effects of a high q_{AEM} .

Further, it was worried that very demanding setups, i.e., those with rapidly changing errors, would provoke especially F+ to issue commands in rapid succession, However, further examination of these profiles revealed that the penalty functions successfully inhibited a fast response and commands were issued with at least 60 s between them, similar to the profile in Figure 5.10. Thus, these profiles comply with the request made in Ref. (19) to have no more than one command per minute.

5.7. Conclusion of Chapter 5

The optimization study with SMPSO gave the following insight about the weight factors of IM-SP:

First, all weight factors have a significant impact on the systems performance, and the scoring parameters change the basic system response and the penalty functions suppress undesired behavior as intended by their respective design.

Some desired traits, represented by the objective functions, contradict each other, meaning they cannot be achieved or improved at the same time. Nevertheless, this study demonstrated that it is possible to improve the overall performance of IM-SP by just changing the weight factors.

Out of a total 87 solutions for the optimization problem, two distinctive solution, a “time optimal” and a “fuel improved” have emerged and their optimization results were validated with the full data set.

From those two solutions, the “fuel improved” setting, F+, was able to reduce the fuel burn by an average 6 kg relative to the original settings and demonstrated improved or comparable performance in all other categories, thereby alleviating previous deficiencies over ASTAR.

Finally, with respects to its improved fuel burn and overall operationally desirable characteristics, the “fuel improved” setting has been recommended as the new standard setting for IM-SP and its future studies.

6. FLIGHT SIMULATOR EVALUATION

The following Chapter describes the flight simulator evaluation of ASTAR and IM-SP. Results were partially included in Ref. (59), “Pilot-Centered Evaluation of Flight-deck Interval Management Control Laws using an A320 Simulator”, submitted to the AIAA – Journal of Aircraft, currently under review. Figures submitted are used with permission.

6.1. Introduction

The ATD-1 flight test has highlighted the importance of Human-in-the-Loop (HITL) testing to confirm if the assumed system performance is actually achievable under operationally realistic conditions.

From the beginning of the development of IM-SP, which was specifically designed to allow for a lower workload and higher acceptance with pilots, it was aspired to apply the same standards, i.e., also subject the proposed logic to HITL testing.

Therefore, to test if the hypothesized improvements would actually be perceived, the scenario introduced in Section 4.7 was designed specifically for a HITL evaluation and the respective simulator model.

The environment of the ATD-1 flight test was recreated, including the FIM avionics, GUIs and survey methods. Furthermore, a new GUI, designed for the enhanced capabilities of IM-SP was designed and integrated in the test.

The experiment was unique, not only in that it was the first evaluation of IM-SP in a HITL environment, but also the first HITL evaluation of ASTAR-based FIM in an Airbus A320 simulator.

In the following sections, the simulator environment and test plan are described in detail. Following, the results of the questionnaire are presented and an in-depth analysis of the findings are presented. Finally, recommendations for the future design of FIM and its GUIs are given.

6.2. Simulator

The experiment was conducted in a fixed-base Airbus A320 research simulator, located at the Institute of Flight Guidance (IFF) of the Technische Universität Braunschweig. The simulator, shown in Figure 6.1, features the same instrumentation and control panels as the original aircraft, albeit some switches and handles have a different feel. Other differences are discussed in Subsection 6.6.1.

The simulator's visual model and flight physics were supplied by Lockheed's Prepar3D in version 3.4, and the A320 systems (fly-by-wire, autopilot, etc.) were simulated using the Aircraft Simulation Technology (AST) build version 603. AST uses its own A320 model, i.e., the AST Project Airbus A320-214 (2007 Project Airbus Team) with CFM56-5B4 engines.

The data-logging and connection between the simulator and CGD was established by the SimConnect interface of Prepar3D. The FIM avionics were emulated on a laptop PC showing the EFB on the laptop's primary display and the CGD on an external 7-inch display.



Figure 6.1 Overview of the Airbus A320 simulator at the IFF ⁽⁵⁹⁾



Figure 6.2 Position of the CGD on the Captain's side ⁽⁵⁹⁾
(here displaying the GUI used with IM-SP)

The CGD was positioned on either the Captain's or First Officer's side as shown in Figure 6.2.

Originally, it was planned to position the CGD at the same location as in the ATD-1 flight test, i.e., above the glare shield panel (closer to the FCU), however, its position was changed by participants' request, as the shown location (outward of the PFD) fits better into the scanning pattern for the Airbus A320. In this configuration, the CGD is always in the (peripheral) field of view of the pilot; if flying head-down, i.e., focusing on the PFD or ND, the CGD is in the pilot's upper outward peripheral view, and conversely if looking outside, in the lower outward peripheral view.

6.3. GUI Design

6.3.1. ASTAR

The original design of the ASTAR GUI ⁽⁶⁰⁾, from here on referred to as "GUI A", was adapted to fit the screen of the used display, as shown in Figure 6.3.

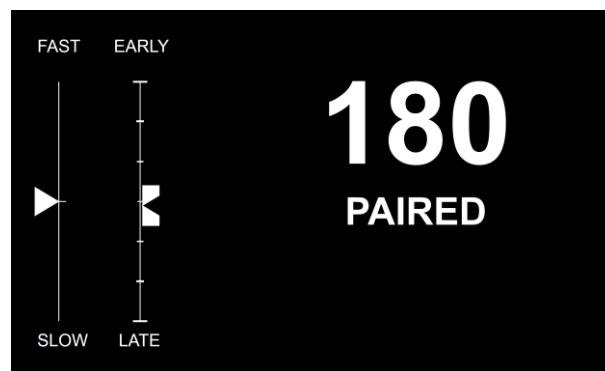


Figure 6.3 CGD layout for ASTAR (GUI A) ⁽⁵⁹⁾
(adapted to the screen used in the experiment)

The displayed elements function as described in Subsection 2.3.2, however without the set speed conformance monitoring. For example, on a speed command update the speed is displayed in reverse video (Figure 6.4), but does not start to blink if the speed was not set on the FCU.

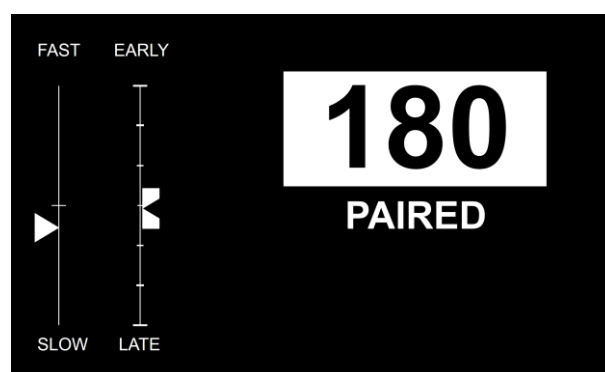


Figure 6.4 Reverse video on GUI A to indicate a speed command update

6.3.2. IM-SP

To make use of the additional information available with the IM-SP algorithm, e.g., the time until the next command (TTN), or the next speed, an alternative GUI was also designed. The new design, continuously referred to as “GUI B”, was developed through discussion with pilots and under consideration of the same general design guidelines for electronic flight displays as GUI A^(61,62). GUI B inherits certain features from GUI A, and its general layout is shown in Figure 6.5.

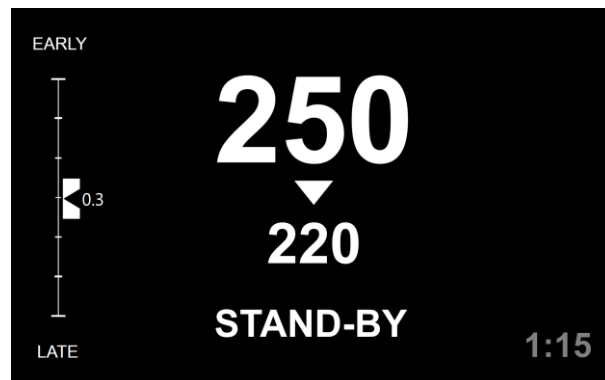


Figure 6.5 CGD layout for IM-SP (GUI B) ⁽⁵⁹⁾

Here the current FIM speed is shown as the upper, large font numeric value (250 kt). The next expected speed is indicated by the smaller sized value below (220 kt), pointed at by an arrow.

The TTN is shown in the bottom right corner in gray (1:15). Therefore, the situation shown in Figure 6.5, can be read as “expect to set 220 kt in 1 min and 15 s”.

To reduce the amount of changes, i.e., movements, on the display, the TTN for values higher than 10 s is updated in 5 s intervals, e.g., 1:15, 1:10, etc. Further its color was reduced to make it less prominent. The text below the next speed indication (STAND-BY) is a status and action indicator.

The ELI was retained from GUI A, with the current RSE now being displayed beside the arrow. The numerical value was added to give the crew an indication if the spacing task is still achievable, and as a mean of feedback to ATC, how much delay is to be expected. The FSI, i.e., the instantaneous speed conformation indication, is displayed in a different manner, explained later.

Ten seconds before a new speed should be set, the display changes, and shows a solid countdown bar on the right to obtain the crew's attention (Figure 6.6).

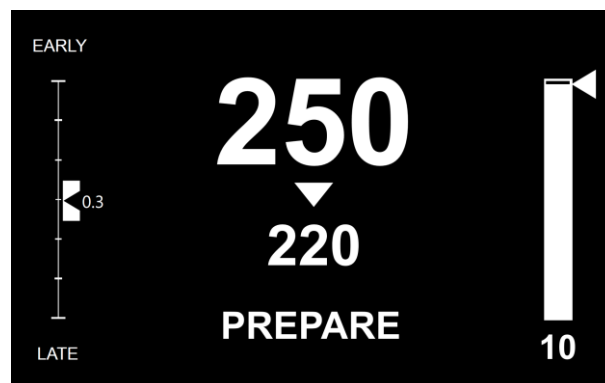


Figure 6.6 GUI B indicating an upcoming speed change ⁽⁵⁹⁾

The bar then empties and the numeric TTN is counting down in 1 s intervals. The crew is expected to set the new speed when the TTN reaches 0, i.e., the countdown bar has fully emptied.

During a speed change, the upper numeric value indicates the instantaneous FIM speed, that is the speed the systems expects the aircraft to fly on the deceleration curve, in a rotating-dial representation (here decelerating from 249 kt to 248 kt, Figure 6.7).

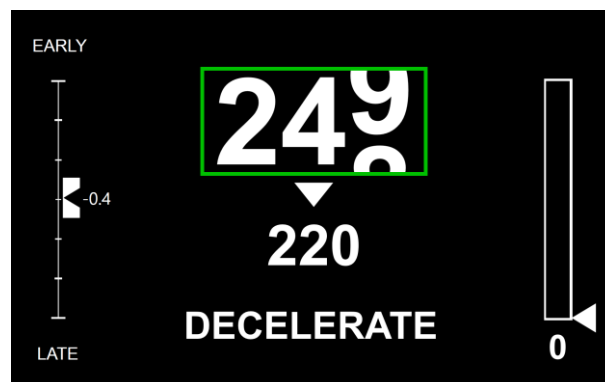


Figure 6.7 GUI B during a speed change ⁽⁵⁹⁾

In the event that an immediate reaction by the crew is required, the status text will flash, meaning alternate in reverse video, at 1Hz for 5 s as an additional attention-getter. Furthermore, the new target airspeed will be framed in a (magenta) box to highlight the changed element (Figure 6.8).



Figure 6.8 GUI B indicating a speed plan change that requires immediate crew reaction

In addition to the CGD page, an alternative for the EFB page was also designed. The EFB page contained four elements: a sized copy of the CGD, a graphical representation of the speed plan, a tabular representation of the speed plan, and a general information section, indicating items such as the TTG and DTG until the next AP and until the ABP.

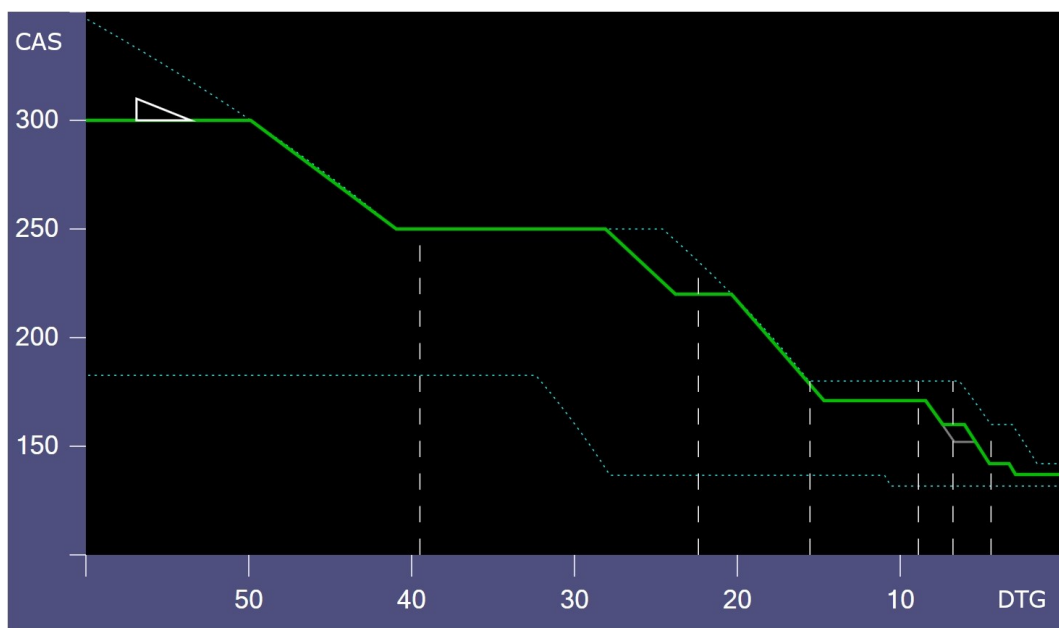


Figure 6.9 Graphical representation of the speed plan on the EFB page of GUI B⁽⁵⁹⁾

Figure 6.9 shows the graphical representation of the speed plan on the EFB page. The current plan, i.e., the progression of CAS over the DTG (or TTG if selected) is shown in green. Further, the last acknowledged speed plan is shown in gray to allow for an easier comparison. The speed envelope and waypoints ahead are indicated by dotted and dashed lines respectively.

The display was shown to the pilots upon request, i.e., it was not a mandatory scanning item. This method of presentation was chosen to count the number of times the pilot would make use of the information available on the EFB.

6.4. Test Plan

6.4.1. Operational Procedures

In typical modern-day airline operations, tasks in the flight deck are shared among the pilots. One pilot assumes the role of the pilot flying (PF) and the other one the role of the pilot monitoring (PM). The PF is in charge of all actions pertaining the control of the aircraft, i.e., here, setting the commanded FIM speed on the FCU, extending the speed brakes as necessary, and manipulating the flight controls and thrust levers during manual flight. The PM observes the instruments, double-checks the PF and configures the aircraft, e.g., sets flaps or manipulates the landing gear, as instructed by the PF.

In this experiment the participant, that is the rated pilot, always assumed the role of the PF, and a test administrator assisted with basic PM tasks. The participant was given the choice to sit either in the left or the right seat, and the test administrator occupied the other seat accordingly.

The aircraft was pre-configured with the A/P and A/THR set to the appropriate mode for the initial conditions, here SPEED at 300 kt CAS, FPA descent mode at -2.2° , and lateral navigation (LNAV) according to the route stored in the FMS.

An ATC clearance to engage in FIM operation was assumed, and the FIM avionics were also pre-configured and in “ARMED” mode, i.e., no setup work was required at the beginning of the scenario.

The system changed to “PAIRED” or “STAND-BY” mode at a DTG of 60 NM, where the first FIM command could occur. Upon reaching the PTP, the FIM displays automatically shut off.

6.4.2. Routing and Error Setups

The approach flown in the experiment is the same as for Scenario II (Section 4.7). From all error setups, four were chosen as listed in Table 6.1 with their respective error progression shown in Figure 6.10.

Table 6.1 Selected setups for the flight simulator evaluation

No.	Pattern	Amplification	Direction	Initial Offset
1	SHTLE	High	+	+ 10 s
2	Triangle	High	-	- 20 s
3	Square	High	+	0 s
4	SPICA	High	-	0 s

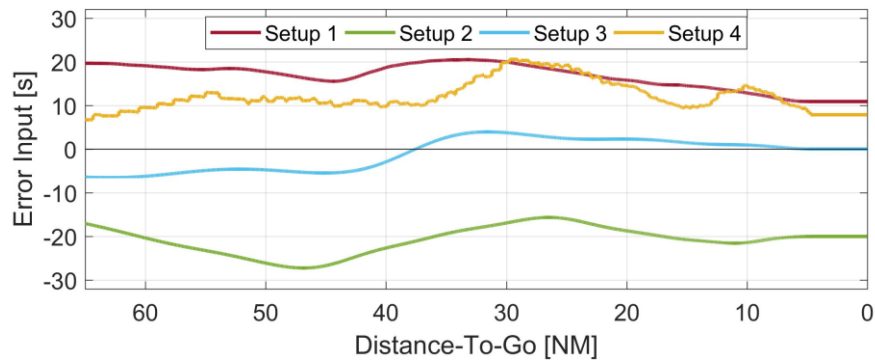


Figure 6.10 Error propagation of the selected setups ⁽⁵⁹⁾

Setups 1 and 2 were used with all configurations, Setup 3 was only used with IM-SP and GUI B, and Setup 4 was only used in the model verification trials (Subsection 6.5.4).

6.4.3. Participants

Participation in the experiment was voluntary and consensual, further no remuneration was paid.

A total of five pilots participated in the experiment, of which all hold at least a Commercial Pilot License (CPL) with an Instrument Rating (IR) and Multi-Engine (ME) privileges, or a comparable Multi-Crew Pilot License (MPL). Further, three of the participants hold an Airbus A320 type rating, two of them are in active airline duty on type. Furthermore, two of the participants hold a flight test rating. The participants' flight experience ranged from 300 to 9,000 hours.

The scope of FIM and its associated logics and applications were unknown to all participants prior to the experiment.

6.4.4. Pilot Briefing

All participant received an information package approximately two weeks prior to the experiment, explaining its scope, i.e., the "Evaluation of FIM control logics and GUIs", the instrument approach procedures to RJTT, and a brief description of the GUI layout. No explicit details were given about the logics' design or working principles. To avoid any bias toward either logic during the experiment, these details were not disclosed until the individual participant had completed all of his approaches.

On the day of the test, each pilot was briefed again for the approach procedure details and the questionnaire that was used during the evaluation, before starting with the actual experiment.

Pilots were asked to follow the commanded speed as close as possible, but were free in their decision when to use speed brakes or disengage the autopilot.

6.4.5. Test Sequence

The first flight was always a familiarization flight with GUI A to allow the pilots to get comfortable with the simulator, FIM avionics, and what they are expected to do. This flight used the reference profile with no error applied, i.e., all speed changes occurred as shown for the prebriefed approach (Figure 4.2). After the first, and each following approach, pilots were surveyed for their impressions and comments using the questionnaire (Subsection 6.5.1). However, familiarization flights have not been considered in the final results.

Following, four more approaches were flown with GUI A, two using ASTAR and two using IM-SP with setups 1 and 2 respectively.

The GUI was then changed to GUI B and at least three more flights were flown, all with IM-SP.

After the final flight pilots were once again surveyed for their general impression of FIM, i.e., what aspects they liked and in contrast what changes they would like to see made (comparable to the questions asked in the ATD-1 flight test).

6.5. Results

The results have been grouped into the three possible configurations, i.e., ASTAR with GUI A (A-A), IM-SP with GUI A (I-A), and IM-SP with GUI B (I-B). The color coding used throughout this chapter is blue (A-A), orange (I-A) and green (I-B). Given the equal number of data points for A-A and I-A the midpoint between the two renders the overall rating for GUI A. Conversely, the score for GUI B is equal to I-B.

6.5.1. Quantitative Results

The questionnaire used in this experiment was closely oriented to the questionnaire used in the ATD-1 flight test (Ref. (17) and Section 2.4). Furthermore, the same scoring method (7-point Likert scale, 1 = "Completely Unacceptable", 7 = "Complete Acceptable") and a priori hypothesis (score equal or better than '5') were applied.

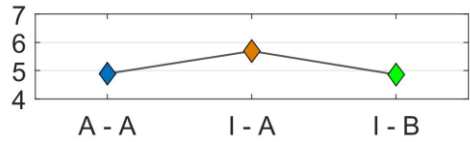
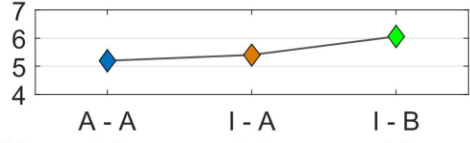
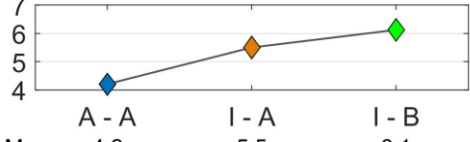
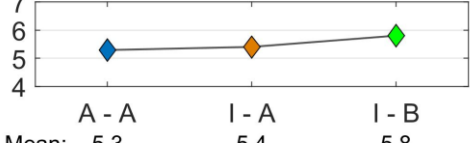
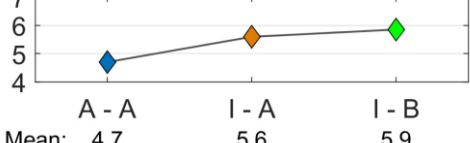
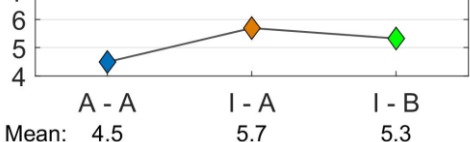
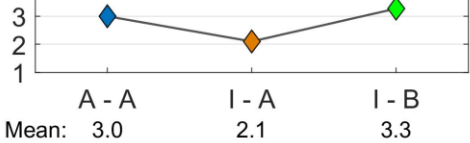
Questions that were added to the questionnaire primarily asked for details about the comprehensibility of the system's actions and its level of distraction.

Table 6.2 lists all the questions and their corresponding results, represented by the mean value and standard deviation, grouped by configuration. Additionally, a graphical representation of the mean is given for an easier comparison.

Owing to the small number of data points per configuration (10 or 15 respectively), the individual results were not statistically tested and should be regarded as a comparative indicator.

The individual questions and comments related to their scoring are discussed further below.

Table 6.2 Summary of the questionnaire responses ⁽⁵⁹⁾

Statement	A - A	I - A	I - B
Number of data points	10	10	15
1.) The overall FIM operation was acceptable	 <p>Mean: 4.9 5.7 4.9 SD: 0.7 0.8 1.2</p>		
2.) The resulting speed profile was acceptable	 <p>Mean: 5.2 5.4 6.1 SD: 1.5 1.0 0.5</p>		
3.) The timing of the FIM commands was comprehensible	 <p>Mean: 4.2 5.5 6.1 SD: 1.2 1.5 0.6</p>		
4.) The commanded FIM speeds were comprehensible	 <p>Mean: 5.3 5.4 5.8 SD: 1.3 1.3 0.6</p>		
5.) The total number of FIM commands was acceptable	 <p>Mean: 4.7 5.6 5.9 SD: 1.3 1.0 0.9</p>		
6.) Interruptions caused by FIM were at an acceptable level	 <p>Mean: 4.5 5.7 5.3 SD: 1.6 1.3 1.0</p>		
7.) I was fully focused on the FIM system (here low values are desirable)	 <p>Mean: 3.0 2.1 3.3 SD: 1.5 0.7 1.2</p>		

1.) The overall FIM operation was acceptable

The overall acceptability of the FIM operation was reported at 4.9 for A-A, an improved 5.7 for I-A, but just a comparable 4.9 for I-B, which also showed a higher standard deviation. Accordingly, neither A-A nor I-B would meet the a priori criterion.

In comparison, during the ATD-1 flight test the overall acceptability for IM Cross operations was rated at 5.9. However, in preparation for the test, the participating flight crews received an extensive training on FIM and the use of FIM avionics, whereas in this experiment the crew had no foreknowledge of the system. Therefore, it is assumed that higher ratings for all configurations would have been achieved with prior training.

Reasons given for the individual rating included: For A-A, the number of speed commands was too high and undesirable accelerations and reversals existed; For I-B, the amount of attention that needed to be diverted to the system was higher (further discussed in Subsection 6.5.2.3).

2.) The resulting speed profile was acceptable

The acceptability for the final speed profile was satisfactory for all configurations, reported at 5.2 (A-A), 5.4 (I-A), and 6.1 (I-B).

Comments for A-A again included the existence of accelerations. Interestingly, the rating with I-B was significantly higher than with I-A and had a lower standard deviation, despite the system reaction being identical. This could indicate that more information about the system's intention, i.e., more foreknowledge about the speed profile in general, as is presented with GUI B, could lead to a higher acceptance of the profile itself.

3.) The timing of the FIM commands was comprehensible

This question was asked in order to gauge the pilots' understanding of why a speed command was issued at the particular time. The results showed the most significant difference and improvement over all questions, being reported at 4.2 (A-A), 5.5 (I-A), and 6.1 (I-B).

It is assumed that the design of the IM-SP algorithm to summarize and apply IM actions to planned speed changes allowed for a better anticipation of a speed change, as its point of initiation might not have been changed at all or just marginally. Furthermore, the TTN indication on GUI B, which was generally regarded as helpful (Subsection 6.5.2.3), contributed to the high rating of I-B.

4.) The commanded FIM speeds were comprehensible

This question queried the pilots for their understanding of the numerical value, i.e., the target speed, the system has commanded.

Results were reported at 5.2 (A-A), 5.3 (I-A), and 5.8 (I-B), showing comparable results for GUI A and a slight improvement with GUI B.

Comments indicated that for I-B the display of the next speed was helpful. However, for both IM-SP configuration, a specific speed change of just 2 kt, that occurred during one setup, has caused for a degradation, as pilots commented that “the A/THR is not able to make such small changes”. Therefore, future iterations of IM-SP should consider a minimum speed step size of 5 kt.

5.) The total number of FIM commands was acceptable

This question focused on the acceptability of the number of speed changes, regardless of when they happened or to what speed they were. Scores were reported at 4.7 (A-A), 5.6 (I-A), and 5.9 (I-B), indicating that the reduction in the total number of speed changes with IM-SP was recognized and appreciated by the pilots. Further, the slightly better score with I-B could indicate that a better awareness of the upcoming speed changes might also increase the tolerance for the number of speed changes. In general, pilots commented that they would rather see fewer speed changes with a large speed difference, than the other way around.

6.) Interruptions caused by FIM were at an acceptable level

This question was aimed at the level of disturbance the pilots perceived when using the system and is therefore linked to the amount of interaction required and the way information is presented.

The reported values were 4.5 (A-A), 5.7 (I-A), and 5.3 (I-B). This also shows a significant improvement with IM-SP, especially for I-A, but since a higher disturbance was perceived with I-B, it also indicates some deficiencies with GUI B, which corresponds to the results of Questions 1 and 7, and Subsection 6.5.2.3.

7.) I was fully focused on the FIM system

This question queried for the amount of attention the pilots felt they had to divert to the system. Note that for this question low values are desirable and the a priori assumption was “equal to or lower than ‘3’ “.

Results were reported at 3.0 (A-A), 2.1 (I-A), and 3.3 (I-B). Again, showing a significant improvement with I-A, but here a higher focus required with I-B, compared to A-A.

Comments made by pilots in regard to GUI B included that it “required a larger amount of attention than GUI A did”, because it contained more information, moving elements and because of the different speed conformance monitoring (further discussed in Subsection 6.5.2.3).

Summarizing, IM-SP with GUI A showed equal or improved performance in all categories, indicating no obstacle in its use from a pilot’s perspective. IM-SP with GUI B showed a significant improvement and the best results in the comprehensibility of the systems intentions, but could not receive a better overall acceptance, due to its higher demand and attention required.

6.5.2. Qualitative Survey

This subsection contains comments and further detailed explanations that were given repeatedly, i.e., given by multiple pilots, grouped into general and GUI specific statements. The subsections list the statements first, followed by a detailed explanation.

6.5.2.1. General FIM Operation

- ➔ “Accelerations and reversals generally undesirable”
- ➔ “Earlier termination preferable”
- ➔ “Increased use of speed brakes feels odd”
- ➔ “Conflicting speed settings / next speed below lowest selectable speed (V_{LS})”

Commands to accelerate, especially after the initial deceleration always created some irritation with the pilots and caused for some uncertainty in the future intentions of the system, which had an impact on the pilots behavior (further described in Subsection 6.5.2.2).

A factor unique to this approach was the late merging waypoint at the FAF AZURE (1,500 ft, DTG 4.4 NM) and subsequently late ABP and PTP. Although pilots commented that they would accept one last command at the FAF in this scenario, they also added that they rather prefer an earlier FIM termination to have more time to stabilize the aircraft for the approach.

Stabilization means fulfilling certain condition, e.g., established on the glide slope, speed within limits, etc., to assure a safe approach. The stabilization gate, i.e., the altitude where the conditions must be met, can differ by operator and meteorological conditions, but is usually found at 1,000 ft (approx. 3 NM to the runway) or 500ft above field elevation. Non-conformance requires a go-around, i.e., abandoning the landing and setting up for a new approach.

As very late FIM commands could cause high-energy states, conflicting with the stabilization criteria, as was observed in the ATD-1 flight test⁽¹⁷⁾, an earlier termination gives the pilots more time to achieve stabilization.

An operational aspect mentioned by the airline pilots was the required use of speed brakes. Even though the pilots were advised that the use of speed brakes is encouraged and necessary for the approach design and to achieve the required deceleration rate, the airline pilots mentioned that they were not accustomed to the prolonged use of speed brakes or the use of speed brakes for smaller decelerations (e.g., 5-10 kt). Furthermore, concerns about potential discomfort for the passengers and that the use of speed brakes could be regarded as a sign of poor descent planning, caused a certain hesitation in using the speed brakes, which was mentioned by and observed for the airline pilots. Another contributing factor could be the operator’s standard operating procedures (SOP) that might require a pilot to have his hand on the speed brake lever for the entire

duration of use, which also adds to the overall workload.

In contrast, the test pilots did not show any reluctance using the speed brakes. Therefore, it is hypothesized that once CDOs have become more common, and pilots are trained for FIM, that the observed hesitation will eventually be eliminated.

Though the final comment is aircraft type and approach specific, it highlights an item for future consideration in FIM operation and logic design.

For example, the Airbus A320 has five flap settings (0, 1, 2, 3, FULL), each for which a lowest selectable speed (V_{LS}) for the A/P exists. In other words, no lower speed can be set on the FCU with the A/P and A/THR engaged. Furthermore, each flap setting has a maximum flap extension speed (V_{FE} , Figure 6.11), and flaps are usually extended at preferred speeds, that is $V_{FE} - 10$ kt.

LIMIT SPD (IAS)	
VLE	280KT/M67
VLO	EXT 250KT RET 220KT
VFE	1 230KT
	1 + F 215KT
	2 200KT
	3 185KT
	FULL 177KT

Figure 6.11 Maximum speed placard of an Airbus A320⁽³⁸⁾
(© Cockpit Revolution, used with permission)

In the approach used here, a speed constraint is enforced at KAIHO (180 kt), causing a deceleration on the nominal speed profile from 220 kt to 180 kt.

With $V_{FE,1} = 230$ kt, i.e., preferred extension speed: 220 kt, and $V_{LS,0} = 190$ kt, it can be seen that 180 kt cannot be selected if the aircraft is still in clean configuration (FLAPS 0).

If the previous speed is the nominal speed of 220 kt or below, this is of no concern, however if due to a FIM command, the speed was higher, e.g., 230 kt or above, this means that the new speed must be set in three steps:

First, set target speed on FCU to $V_{LS,0}$ (190 kt).

Second, while in deceleration, configure for FLAPS 1 once the appropriate speed is reached.

Last, correct target speed on FCU to actual target speed (180 kt).

Obviously, this procedure is much more workload intensive and the last step could be easily executed too late or missed, especially if any interruption happens during the procedure.

This aspect is also crucial for conformance logics, that compare the FIM commanded speed with the speed set on the FCU, to not cause a false-positive indication.

Therefore, it might be advisable to integrate certain aircraft type specific aspects into the individual FIM avionics logics (discussed in further detail in Subsection 6.6.5).

6.5.2.2. GUI A

- “More knowledge about the system intention would be desirable”
- “Hesitation to extend flaps because of potential speed up command”

The simplicity of the original GUI was generally appreciated by the pilots, however most of them would have desired more information regarding the system intentions, i.e., upcoming changes.

In combination with the possibility of an upcoming acceleration, this caused some pilots to be reluctant in configuring the aircraft to the next flap setting, especially in the lower speed regimes; As mentioned in Section 2.4, raising extended flaps again is “operationally unacceptable”. Unfortunately, this behavior is conducive to causing the previously explained situation in which the next speed is below V_{LS} .

The FSI was regarded as intuitive and helpful by most pilots. However, because of its qualitative indication, meaning no numerical value is shown, smaller deviations were frequently ignored.

The ELI was not as intuitive and sometimes misinterpreted by the pilots. For example, some pilots wanted to act ahead of the system, i.e., if an early arrival was indicated, they felt it was appropriate to fly slower than indicate by the system, or ignore seemingly contradicting commands.

6.5.2.3. GUI B

- “Time to next command indication helpful”
- “Next speed indication helpful”
- “Expected deceleration rate indication helpful”
- “Larger amount of attention required”
- “Rotating dial type indication too distracting”

Most pilots identified the additional information available with IM-SP, i.e., the TTN and next speed indication as helpful in planning crew resources and conducive to comprehend the systems intentions; as indicated by the high scores of Questions 3 and 4 in the quantitative survey.

However, all pilots indicated that the rolling-dial type indication of the instantaneous FIM speed was too distracting as it caused continuous, i.e., too much, movement on the screen. Furthermore, the need to compare two numerical values, that is the instantaneous FIM speed on the CGD vs. the CAS on the PFD, was more demanding than the relative indication of the FSI.

Controversially, both airline pilots appreciated that this type of indication did inform them of the expected deceleration rate, which is often not clear with voice-transmitted speed instructions.

Furthermore, it was independently observed and mentioned by some pilots, that they felt more motivated to follow the instantaneous FIM speed with the rolling-dial indicator than with the FSI.

The validity of this statement was further examined by consulting the data logged by the simulator. In detail, the flight data record for the same pilot, flying the same error setup, however once with GUI A (Figure 6.12) and once with GUI B (Figure 6.13) were compared.

The difference between the instantaneous FIM speed and the actual CAS (Δ CAS) has been highlighted by the shaded area in orange (GUI A) and green (GUI B) respectively and is also presented as an extracted graph in Figure 6.14. Especially when considering the deceleration segments from 300 kt to 250 kt and from 250 kt to 180 kt, it can be seen that the statement made by the pilot was indeed correct, and a better conformance was achieved with GUI B.

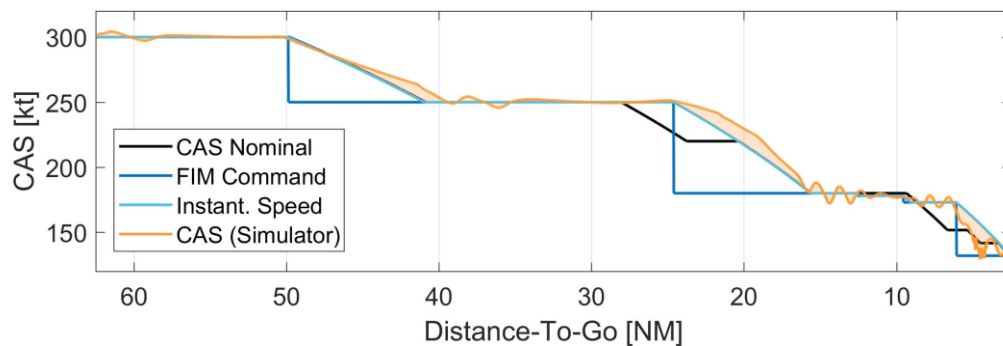


Figure 6.12 Flight data record for GUI A ⁽⁵⁹⁾

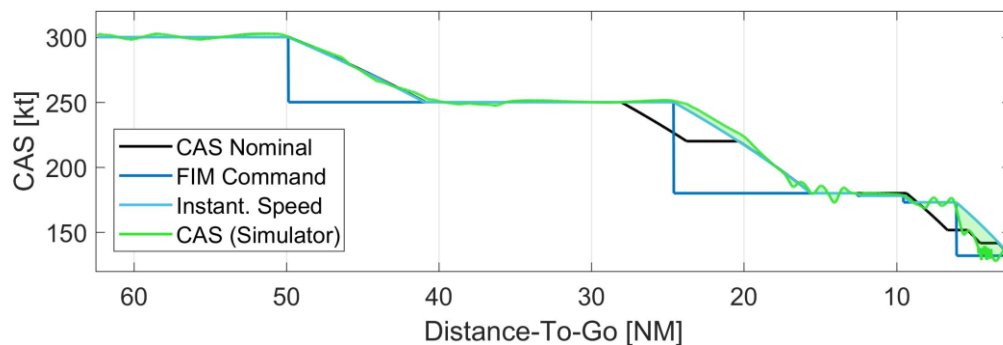


Figure 6.13 Flight data record for GUI B ⁽⁵⁹⁾

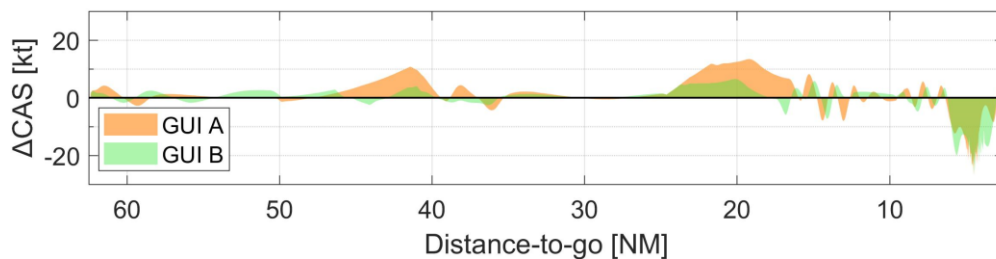


Figure 6.14 Comparison of the Δ CAS progression for GUI A and GUI B ⁽⁵⁹⁾

6.5.3. Reaction Times

Owing to the different speed change annunciation concept of GUI B, it was a prerequisite condition that speed commands are applied with at least the same precision, i.e., predictability, as with GUI A.

In ASTAR and MOPS-FIM the expected crew reaction time, that is the time between a speed command is annunciated by reverse video and this speed is actually set in the FCU, is 7 s.

In contrast, with GUI B, the crew is expected to set the command at the moment when the TTN countdown bar has reached 0, the exact timing when the declaration, plus engine delay, is planned.

Therefore, the reaction times were measured and the results for all participants, excluding the familiarization flights, are shown in Table 6.3 and Figure 6.15

Table 6.3 Reaction times and input time differences, grouped by GUI ⁽⁵⁹⁾

GUI	N	Mean [s]	Expected [s]	Diff. [s]	SD [s]
A	137	6.19	7	-0.81	3.07
B	69	-0.46	0	-0.46	2.14

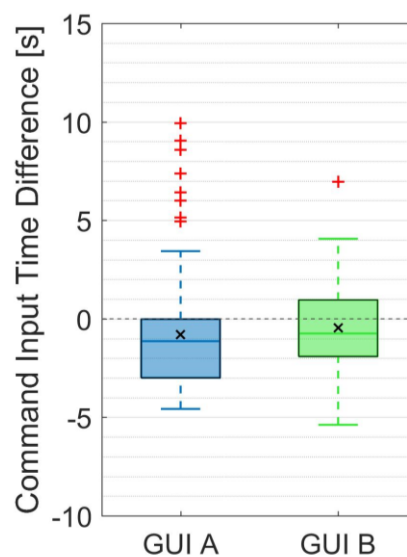


Figure 6.15 Boxplot of the command input time differences, grouped by GUI ⁽⁵⁹⁾

For both GUIs the speed commands have been entered marginally earlier than expected, i.e., 0.81 s earlier with GUI A and 0.46 s with GUI B. However, GUI A recorded a SD of 3.07 s, whereas GUI B showed a smaller, thus improved, value of 2.14 s, indicating that the prerequisite is met.

In a real word scenario, i.e., with more distractions on the flight deck, it is hypothesized that the mean for GUI A will see a shift toward higher values, possibly closer to 7 s, however no improvement in the SD is expected. In contrast, with GUI B it is assumed that this will have less of an effect and therefore a representation like GUI B might render less pilot input error.

6.5.4. Model Verification Trial

Independent of the data taken with the invited participants, another trial was conducted to evaluate the flight simulator's simulation model to the model of the numerical simulation used in Section 4.7.

This trial used all four setups on all three configurations, in addition to the reference profile for configurations A-A and I-B. Here, the A/P remained in command throughout the entire flight and was subsequently configured for autoland. The A/THR also remained engaged; but deviations from the instantaneous FIM command speed, e.g., a mismatching deceleration rate, were assertively corrected, taking into account the consideration in Section 6.6.

Figure 6.16 shows the difference between the ETA of the numerical model to the ATA of the flight simulator, measured at the runway threshold. Results are grouped by the configuration and the conformance area, here ± 10 s, as in the ATD-1 flight test, is indicated.

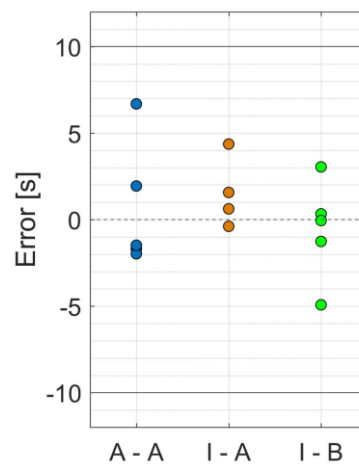


Figure 6.16 Final error for the model verification trials, grouped by configuration ⁽⁵⁹⁾

As seen in Figure 6.16, all data points are within the conformance range, recording an overall final error of 0.5 ± 2.9 s, and thus showing that the results of the numerical model were achievable in the flight simulator.

6.6. Discussion

6.6.1. Simulator Characteristics

With respect to the research-use nature of the simulator, some handling differences compared to the actual aircraft or a certified training-use simulator were expected; However, the following noticeable differences were independently identified by the test administrators and the type rated pilots.

First, the A/THR and engine response delay, i.e., the time between when a command was entered in the FCU, and when the A/THR and subsequently engines reacted, was longer than expected. Compared to the expected 3 s⁽⁹⁾, the actual delay was closer to 8 s. Consequentially, instead of transitioning into the target speed smoothly, the A/THR sometimes overshoot the target causing a periodic increase and decrease in thrust, prominently seen for the CCS at 180 kt in Figure 6.12.

Further, approximately at the FAF (1,500 ft), the indicated CAS started to vibrate heavily. While this had no immediate effect on any systems, it is visible in Figures 6.12 and 6.13 (DTG 5 NM).

The second major abnormality was a lower than expected deceleration rate of the aircraft when using idle thrust, peculiarly when considering the reduced mass of the aircraft and despite of the fixed FPA. As a result, more and prolonged use of the speed brakes was required. This phenomenon became especially prominent in the regime between 250 kt and 180 kt, when speed brakes had to be deployed to their highest available setting, i.e., 1/2 with the A/P engaged, to achieve the required deceleration rate.

6.6.2. Deceleration Rate

Independent of the too low deceleration rate produced by the simulator, as described in Subsection 6.6.1, the assumed fixed deceleration rate of -0.5 kt/s was not always appropriate or easily settable, thus supporting similar observations made in the ATD-1 flight test⁽¹⁷⁾.

Owing to the fixed FPA descent and the efficiency of the aircraft, idle thrust in a clean configuration often rendered a lower than required deceleration rate (notably between 250 kt and 180 kt). In contrast, once configured (here FLAPS 2) and with the landing gear extended, the actual deceleration rate was significantly higher than assumed. Both can be seen in Figures 6.12 and 6.13.

While the former is easily corrected by applying the speed brakes, correcting the latter would require the pilots to disengage the A/THR and increase the thrust manually; a maneuver that is much more workload intensive, especially during the later phases of flight.

Therefore, in lieu of using a uniform deceleration rate for all aircraft, applying aircraft type and approach phase specific variables, that project a deceleration rate closer to the actually achievable value, could prevent these workload intensive situations. (Further discussed in Subsection 6.6.5.)

6.6.3. Use of the EFB Page

As described in Section 6.2, the EFB page was emulated on the laptop and available upon pilot's discretion, however, with GUI A, no pilot asked to see the EFB page. Nevertheless, as pilots mentioned they would appreciate further information about the systems intention during the use of GUI A, it was hypothesized that the additional information with GUI B, i.e., the visual representation of the speed plan, would be used more frequently.

Controversially, out of the five pilots, only one asked to see the EFB page and only twice, indicating that the EFB page was of no concern for the pilots. However, since all participants assumed the role of the PF, it must be investigated if the information on the EFB is made more use of by the PM.

6.6.4. GUI Recommendations

In general pilots indicated that they prefer only essential information to be displayed on the CGD and have all the other information moved to the EFB page. The items that have proven to be crucial for FIM operation have been identified during the experiment as:

- ➔ An indicator for the FIM-commanded speed
- ➔ An attention getter (when a FIM command must be set)
- ➔ An instantaneous speed conformance monitor

The preferred type of attention getter differed between pilots, however an unobtrusive pre-warning, i.e., an indication that did not require immediate attention was generally appreciated. In contrast, in a situation that requires immediate action, especially for safety critical reasons, pilots would accept more prominent indications.

The conformance monitoring is a vital element to prevent significant deviations from the FIM instantaneous speed, possible jeopardizing the intentions of FIM. Notably, the results in Subsection 6.5.2.3 suggest that the type of indication has an influence on the conformance quality.

As the survey (Subsection 6.5.1) showed an overall better acceptance rating for GUI A but a better comprehensibility of the system's intention with GUI B, future GUIs for IM-SP should be oriented closer to GUI A, but include the TTN and next speed in a discreet, non-intrusive manner, possibly shaded as shown in Figure 6.5.

One pilot also suggested to have the CGD entirely blank during idle, i.e., stand-by, states and only have a command displayed when differing from the speed set on the FCU.

Another suggested way to represent the speed plan for IM-SP is to enhance the copy of the ND, as used on the EFB page of GUI A, with symbols indicating the APs (planned decelerations) en-route.

Other suggestions made by pilots were out of the scope of a retrofit, federated implementation, but gave hints for possible design strategies of future integrated systems.

6.6.5. Consideration of Aircraft Type Specific Parameters

For future iterations of FIM, considering aircraft type specific variables, other than the nominal speed profile, might help to overcome the issues of mismatching deceleration rates (Ref. (17), (44), Subsection 6.6.2), unsettable speeds (Subsection 6.5.2.1) and other undesired conditions.

In detail, pilots mentioned that preferred FIM speeds, oriented on configuration relevant speeds (e.g., V_{FE} , etc.), could be used instead of fixed speed step intervals. Furthermore, once a flap extensions speed has been passed, it could be considered to inhibit the system from issuing speed commands higher than V_{FE} . By example of the A320, if a speed command $< V_{FE,1} - 10\text{kt}$ (220 kt) was issued, the highest command that can be issued from thereon would be $V_{FE,1}$ (230 kt), so that pilots do not have to worry about a potentially flap retraction situation (Subsection 6.5.2.2).

In regards to the fixed deceleration rate, an alternative strategy, especially for fixed FPA descents, for which the deceleration rate is easier to predict, could be to use calculated, average idle thrust declaration rates, that better represent the actual performance. For simplification and predictability these could also be staggered in certain intervals (e.g. 20 kt). Another potential benefit of this method would be a lower speed brake use time, which is desirable for pilots as well.

Nevertheless, the obvious benefit of a fixed rate, if observed, is the better predictability for ATC and the easier calculation of the trajectory for the TTF.

6.6.6. Training Procedures for FIM

During the experiment it was observed and mentioned by the pilots that the learning curve for the FIM system was very steep, i.e., pilots got used to the system very quickly. Nevertheless, the operation, especially the execution of FIM commands as intended, does require a certain amount of training. Since in the ATD-1 flight test, pilots received both computer-based and simulator training, it is envisioned that line pilots will also receive a similar amount of training before conducting FIM in actual day-to-day operations.

Furthermore, SOPs for FIM must be defined that assign specific tasks to the PF and PM respectively and to ensure a control loop. For example, the PF might call out a newly issued speed command, and the PM checks that the call out and set speed is correct. Likewise, procedures for the event that FIM fails, in form of a loss of separation or as a system as a whole, must be established.

6.7. Conclusion of Chapter 6

Concluding, all pilots determined FIM to be a useful and feasible addition for actual operations, regardless of the used logic, provided that proper procedures for a two-man cockpit are established.

Furthermore, it was demonstrated that the reduced number of speed commands with IM-SP was perceived and welcomed by the pilots. Survey responses also highlighted a better comprehensibility of the system's intentions, especially when the next command will occur and to what speed it will be, with the newly designed GUI for IM-SP. However, added information and the different speed conformance monitoring strategy demanded for more attention, causing a malus in the overall acceptance; indicating that further research on the design of an appropriate GUI is advised.

The experiment also showed that the different speed annunciation concept of IM-SP achieved a slightly better predictability of the time the crew enters a speed command, suggesting an improvement in potential pilot input error.

Finally, a model verification trial confirmed that the speed profiles generated in the numerical simulation, and thus the resulting changes in the arrival time, were achievable in the flight simulator with sufficient precision.

Concluding, both logics work as desired, and the envisioned improvements with IM-SP were successfully demonstrated in an actual HITL environment.

7. CONCLUSION

7.1. Research Summary

The main purpose of the thesis was to facilitate a solution that improves the speed command behavior in Flight-deck Interval Management (FIM) in order to mitigate the concerns raised by pilots in the ATD-1 flight test and to promote the further development of FIM.

To achieve this, a new control system, by the name of Interval Management – Speed Planning (IM-SP), that uses a speed planning concept, based on a rule-based selection algorithm, was introduced in this thesis. IM-SP was tested in various conditions on different arrival scenarios and, compared to the original FIM logic ASTAR, showed a reduction in speed commands by almost half, while ensuring sufficient spacing performance in a speed constrained environment.

Taking the results of the original IM-SP benchmark study, the algorithm's underlying cost function was optimized using Speed-constrained Multi-objective Particle Swarm Optimization (SMPSO) with the aim to further improve its convenience from a pilot's perspective and improve its fuel-efficiency. Two solutions of the optimization, a spacing-performance optimal and a fuel-economy improved solution have been presented and compared. The fuel-economic solution rendered a good trade-off between required crew interaction and fuel burn and allowed to save an average 6 kg per flight. Accordingly, this setting is suggested as the future standard for IM-SP.

A flight simulator study, in which airline and test pilots gauged the acceptance of ASTAR and IM-SP in an operational environment, was conducted to investigate if the reduced number of speed command would actually be positively perceived. A quantitative survey confirmed that the reduction was indeed noticed and appreciated by the pilots, and design changes to the existing GUI were able to increase the comprehensibility of the system's intentions. The experiment suggested that with further development of a suitable GUI, IM-SP will be able to achieve a high user acceptance rate.

Summarizing it can be said that IM-SP has successfully addressed the issues identified in the NASA ATD-1 flight test, providing a valid solution with less speed commands and reversals, and a better understanding of the system's intentions, as confirmed in numerical simulations and flight simulator experiments.

7.2. Other Contributions and Findings

This research contributed to the domain of FIM, locally and globally in many ways:

Foremost, as summarized above, IM-SP provides the FIM research community with an alternative, human operator oriented, control logic. The selection algorithm and cost function have been documented and can be enhanced in future iterations to allow for other modes of operation

than just the here shown TBO for merging traffic. Further, the working principle of IM-SP is not limited to FIM application, and could easily be adapted for GIM applications as well.

The simulator experiment has been unique in its kind, as it was the first experiment using ASTAR based FIM in an Airbus A320 simulator. Pilots' comments highlighted some aircraft type specific aspects that indicate possible complications in the use of FIM, such as undesirable FIM and flap extension speed combinations. Accordingly, possible solutions for this and other issues, alongside recommendations for operating and training procedures, were given. Other observations made in the ATD-1 flight test, that were not within the scope of this thesis, like the mismatch between the fixed and actual deceleration rate, also emerged during this experiment and emphasize the need for additional research.

Locally, the numerous approaches to RJTT have shown that there is no hindrance to the application of FIM by the arrival route design. However, it was pointed out that some long-distance aircraft pairings, especially those on opposing east-west directions in winter times, should rather be avoided, as prevailing wind conditions cause for too high differences in the ground speed, jeopardizing the success of FIM. This phenomenon is not limited to Japan or RJTT, but applicable to all airports worldwide that are situated in Jetstream and trading wind affected areas. It is therefore suggested that arrival routes are analyzed for their probability for IM to be successful, and support by ATC is provided to select appropriate aircraft pairings.

For the above-mentioned case, IM-SP's AEM can also provide a mean to detect an unattainable spacing goal and prevent chasing after it.

7.3. Future Research

7.3.1. Numerical Testing

Naturally, there are many more scenarios for which IM-SP should be tested, that were outside of the scope of this thesis due to time and resource constraints. Among those are performance evaluations with wind error, or in chained operations, or using other aircraft models, or descent operation methods. With a potential operational implementation in mind, further simulations will be required to ensure the system's performance and discover possible limitations of the current version.

Further it should also be investigated if allowing a 15% tolerance for speed constraints, similar to ASTAR, will have a positive effect on IM-SP or not.

7.3.2. HITL Testing

While the ATD-1 flight test and flight simulator evaluation in this thesis were aimed to investigate the pilots' experience using FIM, it also crucial to conduct evaluation studies involving Air Traffic

Controllers, to obtain their impression on IM-SP's performance and their acceptance of the resulting speed profiles, as ultimately, the responsibility to maintain the separation is still with them.

The aircraft specific comments given by pilots in Chapter 6 also indicate that type specific HITL test should be conducted to avoid situations in which general control logic assumptions conflict with the maker's or aircraft's individual operation philosophy.

Last, it should be investigated how much the hypothesized workload reduction for the ATCo is in proportion to the potentially increased workload for the pilots.

7.3.3. FIM Avionics and GUI Design

In line with the above, further design research on appropriate GUIs and the final positioning of the CGD (as discussed in Chapter 6) is another task, that concerns especially the makers of future FIM avionics products. As certain elements of the CGD have changed during the prototype development of FIM, clear standards to ensure unity among all providers must yet be defined.

7.3.4. Long-term Vision

In regard to the calculation of the TTF's TTG or ETA, any FIM logic's performance could greatly be improved if the TTF would transmits its self-calculated trajectory or speed profile information via ADS-B.

The simplest option would be the transmission of the TTG, or especially during in-trail operation the time until the next planned deceleration and target speed. Both information could potentially be encoded with sufficient precision in a two-byte, i.e., 16-bit, message.

Given that IM operations are a GANP target and the quality of IM operations could be significantly raised with intent information, it is highly advisable and envisioned that IM supporting data blocks will be implemented in future extensions of the ADS-B standard.

Provided that the first retrofitted versions of FIM will prove successful in service, it is without doubt that eventually an integrated solution will be pursued. This might happen in gradual steps, for example first by integrating the function of the CGD into existing displays and then ultimately by full A/P and A/THR integration, with dedicated FIM modes.

BIBLIOGRAPHY

- (1) Japan Aircraft Development Corporation. Worldwide Market Forecast 2019-2038. [Online, Accessed on 15 Oct. 2019]. http://www.jadc.jp/files/topics/143_ext_01_en_0.pdf
- (2) Boeing. Boeing Commercial Market Outlook 2019-2038. [Online, Accessed on 15 Oct. 2019]. <https://www.boeing.com/resources/boeingdotcom/commercial/market/commercial-market-outlook/assets/downloads/cmo-sept-2019-report-final.pdf>
- (3) Airbus S.A.S. Global Market Forecast 2019-2038. [Online, Accessed on 15 Oct. 2019]. <https://www.airbus.com/content/dam/corporate-topics/strategy/global-market-forecast/GMF-2019-2038-Airbus-Commercial-Aircraft-book.pdf>
- (4) International Civil Aviation Organization, "Global Air Navigation Plan - Fifth Edition," ICAO, Montréal, QC, Doc 9750-AN/963, 2016.
- (5) Federal Aviation Administration. NextGen Implementation Plan 2016. [Online, Accessed on 31 Mar. 2019]. https://www.faa.gov/nextgen/media/NextGen_Implementation_Plan-2016.pdf
- (6) SESAR Joint Undertaking. European ATM Master Plan 2015 Edition. [Online, Accessed on 31 Mar. 2019]. <https://www.atmmasterplan.eu/downloads/202>
- (7) Study Group for the Future Air Traffic System. Long-term Vision for the Future Air Traffic Systems CARATS, Collaborative Actions for Renovations of Air Traffic Systems. [Online, Accessed on 31 Mar. 2019]. <https://www.mlit.go.jp/common/000128185.pdf>
- (8) B. Randall and K. Long, "Air traffic controller utilization of voice and Data Link Communications during Interval Management," in *2016 Integrated Communications Navigation and Surveillance (ICNS)*, Herndon, VA, 2016, pp. 2D1-1-2D1-16.
- (9) RTCA/EUROCAE, "Minimum Operational Performance Standards (MOPS) for Flight-deck Interval Management (FIM)," Washington, DC, RTCA DO-361/EUROCAE ED-236, 2015.
- (10) RTCA/EUROCAE, "Safety, Performance and Interoperability Requirements Document for Airborne Spacing - Flight Deck Interval Management (ASPA-FIM)," Washington, DC, RTCA DO-328/EUROCAE ED-195, 2011.

- (11) L. Spinoso, G. Coville, and C. Roberts, "Analysis of the excess Inter-Arrival Time distribution," in *2014 Integrated Communications, Navigation and Surveillance Conference (ICNS) Conference Proceedings*, Herndon, VA, 2014, pp. 1-15.
- (12) R. S. Bone and A. S. Mendolia, "Pilot and Air Traffic Controller use of Interval Management during Terminal Metering Operations," The MITRE Corporation, McLean, VA, MITRE Technical Report MTR170570, Jan. 2018.
- (13) B. T. Baxley, W. C. Johnson, J. Scardina, and R. F. Shay, "Air Traffic Management Technology Demonstration-1 Concept of Operations (ATD-1 ConOps), Version 3.0," NASA Langley Research Center, Hampton, VA, NASA/TM-2016-219213, 2016.
- (14) T. S. Abbott, "An Overview of a Trajectory-Based Solution for En Route and Terminal Area Self-Spacing: Seventh Revision," NASA Langley Research Center, Hampton, VA, NASA/CR-2015-218794, 2015.
- (15) T. S. Abbott and K. S. Swieringa, "An Overview of a Trajectory-Based Solution for En Route and Terminal Area Self-Spacing: Eighth Revision," NASA Langley Research Center, Hampton, VA, NASA/TM-2017-219662, 2017.
- (16) T. S. Abbott, "A Trajectory Algorithm to Support En Route and Terminal Area Self-Spacing Concepts: Third Revision," NASA Langley Research Center, Hampton, VA, NASA/CR-2014-218288, 2014.
- (17) B. T. Baxley, K. A. Swieringa, S. R. Wilson, R. D. Roper, T. S. Abbott, C. E. Hubbs, P. Goess, and R. F. Shay, "Air Traffic Management Technology Demonstration-1 (ATD-1) Avionics Phase 2 Flight Test and Results," NASA Langley Research Center, Hampton, VA, NASA/TP-2018-219814, 2018.
- (18) B. T. Baxley, K. A. Swieringa, R. D. Roper, C. E. Hubbs, P. Goess, and R. F. Shay, "Recommended changes to interval management to achieve operational implementation," in *2017 IEEE/AIAA 36th Digital Avionics Systems Conference (DASC)*, St. Petersburg, FL, 2017, pp. 1-10.
- (19) B. T. Baxley, K. A. Swieringa, S. R. Wilson, R. D. Roper, C. E. Hubbs, P. Goess, and R. F. Shay, "Flight Crew Survey Responses from the Interval Management (IM) Avionics Phase 2 Flight Test," in *17th AIAA Aviation Technology, Integration, and Operations Conference*, Denver, CO, 2017.
- (20) K. A. Swieringa, S. R. Wilson, B. T. Baxley, R. D. Roper, T. S. Abbott, I. Levitt, and J. Scharl, "Flight Test Evaluation of the ATD-1 Interval Management Application," in *17th AIAA Aviation Technology, Integration, and Operations Conference*, Denver, CO, 2017.

- (21) B. T. Baxley, M. T. Palmer, and K. A. Swieringa, "Cockpit Interfaces, Displays, and Alerting Messages for the Interval Management Alternative Clearances (IMAC) Experiment," NASA Langley Research Center, Hampton, VA, NASA/TM-2015-218775, 2015.
- (22) B. T. Baxley, S. R. Wilson, K. A. Swieringa, W. C. Johnson, R. D. Roper, C. E. Hubbs, P. Goess, and R. F. Shay, "Human-in-the-Loop Assessment of Alternative Clearances in Interval Management Arrival Operations," NASA Langley Research Center, Hampton, VA, NASA/TP-2016-219362, 2016.
- (23) N. de Gelder, F. J.L. Bussink, E. G. Knapen, and A. C. in't Veld, "Interval Management Operations in the Terminal Airspace of Amsterdam Airport Schiphol," in *AIAA Guidance, Navigation, and Control Conference*, San Diego, CA, 2016.
- (24) F. J.L. Bussink, J. J. van der Laan, and P. M.A. de Jong, "Combining Flight-deck Interval Management with Continuous Descent Approaches in high density traffic and realistic wind conditions," in *AIAA Guidance, Navigation, and Control Conference*, Minneapolis, MN, 2012.
- (25) E. Itoh, K. Uejima, H. Chida, K. Nishinari, M. M.C. Everdij, G. J. Bakker, and H. A.P. Blom, "An Overview of Airborne Time-Spacing Research in the JADE Program," in *International Conference on Application and Theory of Automation in Command and Control Systems, ATACCS*, London, United Kingdom, 2012.
- (26) E. Itoh, K. Uejima, Y. Kakichi, and S. Suzuki, "Modeling and Simulation Study on Airborne based Energy Saving Arrivals to Tokyo International Airport," in *AIAA Guidance, Navigation, and Control (GNC) Conference*, Boston, MA, 2013.
- (27) E. Itoh and K. Uejima, "Applying Flight-deck Interval Management based Continuous Descent Operation for Arrival Air Traffic to Tokyo International Airport," in *10th USA/Europe Air Traffic Management Research and Development Seminar (ATM2013)*, Chicago, IL, 2013.
- (28) X. Bai and L. A. Weitz, "Exploring a Model Predictive Control Law to Design Four-Dimensional Trajectories for Interval Management," in *AIAA Information Systems-AIAA Infotech @ Aerospace*, Grapevine, TX, 2017.
- (29) L. A. Weitz and X. Bai, "Using Model Predictive Control for Trajectory Optimization and to Meet Spacing Objectives," in *2018 AIAA Guidance, Navigation, and Control Conference*, Kissimmee, FL, 2018.

- (30) J. Banke and L. Gipson. NASA Presents FAA with New Air Traffic Management Technology. [Online, Accessed on 8 Oct. 2019]. <https://www.nasa.gov/aero/nasa-presents-faa-with-new-air-traffic-management-technology>
- (31) Japan Civil Aviation Bureau. Capacity Expansion Program for Tokyo Metropolitan Airports. [Online, Accessed on 19 Oct. 2019]. http://www.schedule-coordination.jp/news/pdf/1_capacity_expansion_program_for_tokyo_metropolitan_airport.pdf
- (32) International Civil Aviation Organization, "Procedures for Air Navigation Services Air Traffic Management Sixteenth Edition," ICAO, Montréal, QC, Doc 4444, 2016.
- (33) A. L. Haines, "Parameters of Future ATC Systems Relating to Airport Capacity/Delay," Federal Aviation Administration, Washington, DC, FAA-EM-78-8A, 1978.
- (34) W. J. Swedish, "Evaluation of the Potential for Reduced Longitudinal Spacing on Final Approach," Federal Aviation Administration, Washington, DC, FAA-EM-79-7, 1979.
- (35) B. T. Baxley, B. E. Barmore, T. S. Abbott, and W. R. Capron, "Operational Concept for Flight Crews to Participate in Merging and Spacing of Aircraft," in *6th AIAA Aviation Technology, Integration and Operations Conference (ATIO)*, Wichita, KS, 2006.
- (36) J. L. Murdoch, B. E. Barmore, B. T. Baxley, T. S. Abbott, and W. R. Capron, "Evaluation of an Airborne Spacing Concept to Support Continuous Descent Arrival Operation," in *8th USA/Europe Air Traffic Management Research and Development Seminar (ATM2009)*, Napa, CA, 2009, pp. 1-9.
- (37) B. E. Barmore, R. S. Bone, and W. J. Penhallegon, "Flight Deck-Based Merging and Spacing Operations," *Air Traffic Control Quarterly*, vol. 17, no. 1, pp. 5-37, 2009.
- (38) Cockpit Revolution. (2019) Airbus A319/A320/A321 [LCD] CEO & NEO. Cockpit Poster for Training Use. <http://www.cockpitrevolution.com>
- (39) Eurocontrol, "Surveillance Data Exchange - Part 12 ADS-B Reports," Eurocontrol, SUR.ET1.ST05.2000-STD-12-01, 2010.
- (40) D. Toratani, N. K. Wickramasinghe, and H. Hirabayashi, "Evaluating Energy-Saving Arrivals of Wide-Body Passenger Aircraft via Flight-Simulator Experiments," in *2018 Winter Simulation Conference (WSC)*, Stockholm, Sweden, 2018, pp. 2249-2260.

- (41) E. Itoh, S. Fukushima, H. Hirabayashi, and N. K. Wickramasinghe, "Evaluating Energy-Saving Arrivals of Wide-Body Passenger Aircraft via Flight-Simulator Experiments," *AIAA Journal of Aircraft*, vol. 55, no. 6, pp. 2427-2443, 2019.
- (42) E. Itoh, H. Hirabayashi, N. K. Wickramasinghe, and S. Fukushima, "Feasibility study on fixed flight-path angle descent for wide-body passenger aircraft," *CEAS Aeronautical Journal*, vol. 10, no. 2, pp. 589-612, 2019.
- (43) Eurocontrol Experimental Centre, "User Manual for the Base of Aircraft Data (BADA) Revision 3.12," Eurocontrol, 2014, Project BADA - EEC Technical/Scientific Report No. 14/04/24-44, 2014.
- (44) T. Riedel, M. Takahashi, T. Tatsukawa, and E. Itoh, "Evaluating Applied Flight-deck Interval Management using Monte Carlo Simulations on the K-Supercomputer," *Transactions of the Japan Society for Aeronautical and Space Sciences*, vol. 62, no. 6, pp. 299-309, 2019.
- (45) T. Riedel, E. Itoh, M. Takahashi, and T. Tatsukawa, "Preliminary Study on Interval Management for Improving Aircraft Speed Command Behavior," in *55th JSASS Aircraft Symposium*, Matsue, Japan, 2017, pp. 1-12.
- (46) T. Riedel, E. Itoh, and M. Takahashi, "Investigating Aircraft Speed Control Logics for Interval Management targeting Arrival Traffic to Tokyo International Airport," in *2017 Asia-Pacific International Symposium on Aerospace Technology (APISAT)*, Seoul, South Korea, 2017, pp. 1-10.
- (47) H. Miyazaki, Y. Kusano, S. Naoki, F. Shoji, M. Yokokawa, and T. Watanabe, "Overview of the K computer System," *FUJITSU Scientific & Technical Journal*, vol. 48, no. 3, pp. 255-265, 2012.
- (48) T. Riedel, M. Takahashi, and E. Itoh, "Reducing Speed Commands in Interval Management using Speed Planning," *The Aeronautical Journal*, vol. 124, no. 1272, pp. 189-215, 2020.
- (49) T. Riedel, M. Takahashi, E. Itoh, T. Feuerle, and P. Frost, "Evaluating Speed Logics for Flight-deck Interval Management," in *6th ENRI International Workshop on ATM/CNS*, Tokyo, JP, 2019, pp. 1-7.
- (50) Japan Civil Aviation Bureau, "Aeronautical Information Publication AD2-24, RJTT Charts Related to an Aerodrome," eAIP Japan, 2018.
- (51) T. Riedel, M. Takahashi, and E. Itoh, "Cost Function Optimisation of Interval Management - Speed Planning using SMPSO," *The Aeronautical Journal*, under Review, pp. 1-28, 2020.

- (52) J. Kennedy and R. Eberhart, "Particle Swarm Optimization," in *Proceedings of ICNN'95 - IEEE International Conference on Neural Networks*, Perth, Australia, 1995, pp. 1942-1948.
- (53) A. J. Nebro, J. J. Durillo, J. García-Nieto, C. A. Coello Coello, F. Luna, and E. Alba, "SMPSO: A New PSO-based Metaheuristic for Multi-objective Optimization," in *2009 IEEE Symposium on Computational Intelligence in Multi-Criteria Decision-Making (MCDM)*, Nashville, TN, 2009.
- (54) H. Rahil, B. Abou El Majd, and M. Bouchoum, "Optimized Air Routes Connections for Real Hub Schedule Using SMPSO Algorithm," in *Recent Developments in Metaheuristics, Operations Research/Computer Science Interfaces Series*. Cham: Springer, 2018, vol. 62, pp. 369-384.
- (55) Y. Shi and R. Eberhart, "A Modified Particle Swarm Optimizer," in *1998 IEEE International Conference on Evolutionary Computation Proceedings. IEEE World Congress on Computational Intelligence*, Anchorage, AK, 1998, pp. 69-73.
- (56) M. R. Sierra and C. A. Coello Coello, "Improving PSO-Based Multi-objective, Optimization Using Crowding, Mutation and ϵ -Dominance," in *Evolutionary Multi-Criterion Optimization, Third International Conference, EMO 2005, Guanajuato, Mexico, March 9-11, 2005. Proceedings*. Berlin, Heidelberg: Springer, 2005, pp. 505-519.
- (57) M. Clerc and J. Kennedy, "The Particle Swarm—Explosion, Stability, and Convergence in a Multidimensional Complex Space," *IEEE Transactions on Evolutionary Computation*, vol. 6, no. 1, 2002.
- (58) D. Hadka. MOEA Framework – A Free and Open Source Java Framework for Multiobjective Optimization. [Online, Accessed on 1 May 2019]. <https://moeaframework.org>
- (59) T. Riedel, M. Takahashi, E. Itoh, P. Frost, and T. Feuerle, "Pilot-Centered Evaluation of Flight-Deck Interval Management Control Laws using an A320 Simulator," *AIAA Journal of Aircraft*, under Review, pp.1-33, 2020.
- (60) G. F. Wilber, "ATM Technology Demonstration-1 Phase II Boeing Configurable Graphical Display (CGD) Software Design Description," NASA Langley Research Center, Hampton, VA, NASA/CR-2017-219594, 2017.
- (61) Federal Aviation Administration, "Electronic Flight Displays," Washington, DC, AC 25-11B, 2014.
- (62) M. Yeh, Y.J. Jo, C. Donovan, and S. Gabree, "Human Factors Considerations in the Design and Evaluation of Flight Deck Displays and Controls," Washington, DC, 2013.

APPENDIX A (EQUATIONS)

1. Route Calculation

According to MOPS-FIM ⁽⁹⁾ the route calculation is simplified to Cartesian coordinates. This is achieved by first converting the en-route waypoints' geodetic coordinates (Latitude and Longitude, as with GPS), via Earth-centered Earth-fixed (ECEF) to relative East-North-Up (ENU) coordinates.

The waypoints are then connected point-to-point, and afterwards the turn segments are calculated. Finally, the remaining straight and turn segment distances are calculated to give the final routing. The process is described below.

Geodetic Coordinates to ECEF coordinates:

ϕ : Latitude [rad] λ : Longitude [rad] i : Waypoint index
 $a = 6378137$ [m] $e^2 = 6.69437999014 \times 10^{-3}$ (World Geodetic System 1984)

First, the distance of the surface of the earth to the equatorial plane (N) is calculated:

$$N = \frac{a}{\sqrt{1 - e^2 \sin^2 \phi_i}}$$

which is then used to calculate the ECEF coordinates:

$$\begin{aligned} X_i &= N \cos \phi_i \cos \lambda_i \\ Y_i &= N \cos \phi_i \sin \lambda_i \\ Z_i &= N (1 - e^2) \sin \phi_i \end{aligned}$$

ENU Distances from ECEF coordinates:

The ENU distances of waypoint $i-1$, relative to waypoint i , can then be calculated by:

$$\begin{bmatrix} dx_{i-1} \\ dy_{i-1} \\ dz_{i-1} \end{bmatrix} = \begin{bmatrix} -\sin \lambda_i & \cos \lambda_i & 0 \\ -\sin \phi_i \cos \lambda_i & -\sin \phi_i \sin \lambda_i & \cos \phi_i \\ \cos \phi_i \cos \lambda_i & \cos \phi_i \sin \lambda_i & \sin \phi_i \end{bmatrix} \begin{bmatrix} X_{i-1} - X_i \\ Y_{i-1} - Y_i \\ Z_{i-1} - Z_i \end{bmatrix}$$

Assuming that the last waypoint in the flight sequence ($i=N$) has the coordinates $(x_N, y_N, z_N) = (0,0,0)$, the position of the previous waypoints ($i=N-1, \dots, i=1$) can be obtained by calculating backwards:

$$\begin{bmatrix} x_i \\ y_i \\ z_i \end{bmatrix} + \begin{bmatrix} dx_{i-1} \\ dy_{i-1} \\ dz_{i-1} \end{bmatrix} = \begin{bmatrix} x_{i-1} \\ y_{i-1} \\ z_{i-1} \end{bmatrix}$$

Turn computation:

Based on the previously calculated route, turns are now calculated by computing the course change, here defined by the backtrack (θ), opposite to the direction of flight:

$$\theta_i = \tan^{-1} \left(\frac{y_i - y_{i+1}}{x_i - x_{i+1}} \right)$$

defined in the range of $[-\pi, \pi]$ to prevent turns greater than 180° :

$$\Delta\theta = \theta_i - \theta_{i-1}, [-\pi, \pi]$$

The turn radius is then estimated as a function of the groundspeed (V_{GS}) and the aircraft's bank angle (ϕ) during the turn:

$$R = \frac{V_{GS}^2}{g \tan \phi}$$

Where the bank angle is defined by:

$$\phi = \min \left(\frac{\Delta\theta}{2}, 23 \text{ degrees} \right)$$

Following, the turn end points of the turn segment are calculated:

$$x_{turn_end} = x_{i+1} + \left[L - R \tan \left(\frac{|\Delta\theta|}{2} \right) \right] \cos \theta_i$$

$$y_{turn_end} = y_{i+1} + \left[L - R \tan \left(\frac{|\Delta\theta|}{2} \right) \right] \sin \theta_i$$

And depending on the direction of the turn, i.e., counter-clockwise ($\Delta\theta < 0$), or clockwise ($\Delta\theta > 0$), the turn center and turn start points are computed:

For $\Delta\theta < 0$:

$$\begin{aligned} x_{turn_center} &= x_{turn_end} + R \cos\left(\theta_i - \frac{\pi}{2}\right), & y_{turn_center} &= y_{turn_end} + R \sin\left(\theta_i - \frac{\pi}{2}\right) \\ x_{turn_start} &= x_{turn_center} + R \cos\left(\theta_{i-1} + \frac{\pi}{2}\right), & y_{turn_start} &= y_{turn_center} + R \sin\left(\theta_{i-1} + \frac{\pi}{2}\right) \end{aligned}$$

For $\Delta\theta > 0$:

$$\begin{aligned} x_{turn_center} &= x_{turn_end} + R \cos\left(\theta_i + \frac{\pi}{2}\right), & y_{turn_center} &= y_{turn_end} + R \sin\left(\theta_i + \frac{\pi}{2}\right) \\ x_{turn_start} &= x_{turn_center} + R \cos\left(\theta_{i-1} - \frac{\pi}{2}\right), & y_{turn_start} &= y_{turn_center} + R \sin\left(\theta_{i-1} - \frac{\pi}{2}\right) \end{aligned}$$

Finally, if any of the turn start or turn end points would be located behind the midpoint of the previous or following leg, i.e., the turn start or end are closer to the previous or next waypoint than to the waypoint the turn was generated at, then the turn radius is recalculated in the following manner:

$$R = \frac{\frac{L}{2}}{\tan\left(\frac{|\Delta\theta|}{2}\right)}$$

2. Trajectory Calculation

The trajectory of each aircraft was calculated based on MOPS-FIM ⁽⁹⁾.

Definitions:

The trajectory is defined as the Along-path Position (s), Altitude (h), True Airspeed (V_{TAS}), as a function of time

$$\begin{aligned} s(t + \Delta t) &= s(t) + \frac{ds}{dt} \cdot \Delta t \\ h(t + \Delta t) &= h(t) + \frac{dh}{dt} \cdot \Delta t \\ V_{TAS}(t + \Delta t) &= V_{TAS}(t) + \frac{dV_{TAS}}{dt} \cdot \Delta t \end{aligned}$$

With their derivatives defining the Ground Speed (V_{GS}), Rate of Climb/Descent ($ROCD$), and TAS Acceleration Rate (a_{TAS}):

$$V_{GS} = \frac{ds}{dt}$$

$$ROCD = \frac{dh}{dt}$$

$$a_{TAS} = \frac{dV_{TAS}}{dt}$$

Depending on if the aircraft is in level and/or unaccelerated flight the equations are defined as follows:

General Equation:

V_{\parallel} : Wind component, parallel to course V_{\perp} : Wind component, perpendicular to course
 γ : Aerodynamic Flight-Path Angle Γ : Geometric Flight-Path Angle
 $\gamma^{(+/-)}$: Exponent indicates previous iteration (-) or next iteration (+)

$$\frac{ds}{dt} = \sqrt{(V_{TAS} \cos \gamma)^2 - V_{\perp}^2} + V_{\parallel}$$

$$\frac{dh}{dt} = -V_{TAS} \sin \gamma$$

$$\frac{dV_{TAS}}{dt} = \frac{dV_{TAS}}{dh} \cdot \frac{dh}{dt}$$

Constant Geometric FPA Descent, Maintain CAS

$$\frac{ds}{dt} = \sqrt{(V_{TAS} \cos \gamma^-)^2 - V_{\perp}^2} + V_{\parallel}$$

$$\frac{dh}{dt} = -V_{TAS} \sin \gamma^-$$

$$\frac{dV_{TAS}}{dt} = \frac{dV_{TAS}}{dh} \cdot \frac{dh}{dt}$$

Estimation of the next aerodynamic FPA (γ^+)

$$\gamma^+ = \sin^{-1} \left(\frac{- \left(\sqrt{(V_{TAS}^+ \cos \gamma^-)^2 - V_{\perp}^2} + V_{\parallel} \right) \tan \Gamma}{V_{TAS}^+} \right)$$

Constant FPA, Deceleration

$$\frac{ds}{dt} = \sqrt{(V_{TAS} \cos \gamma^-)^2 - V_{\perp}^2} + V_{\parallel}$$

$$\frac{dh}{dt} = - \left(\sqrt{(V_{TAS} \cos \gamma^-)^2 - V_{\perp}^2} + V_{\parallel} \right) \tan \Gamma$$

$$\frac{dV_{TAS}}{dt} = -decel$$

3. Atmospheric Calculation

Atmospheric calculations and conversions were made based on the BADA Manual ⁽⁴³⁾, here all shown for International Standard Atmosphere (ISA) conditions

ISA Conditions at Mean Sea Level (MSL) and other Definitions:

Temperature at MSL:	T_0	=	288.15 [K]
Pressure at MSL:	p_0	=	101325 [Pa]
Air density at MSL:	ρ_0	=	1.225 [kg/m ³]
Speed of sound:	a_0	=	340.294 [m/s]
Adiabatic index of air:	κ	=	1.4
Real gas constant for air:	R	=	287.05287 [m ² /(K s ²)]
Gravitational acceleration:	g_0	=	9.80655 [m/s ²]
Temperature gradient below tropopause	$\beta_{T,<}$	=	- 0.0065 [K/m]
Pressure altitude of the tropopause:	$H_{p,Trop}$	=	11000 [m]

Determination of Temperature (for ISA Conditions at MSL $\Delta T = 0$)

General:	$T = f(H_p, \Delta T)$
Below tropopause:	$T_{<} = T_0 + \Delta T + \beta_{T,<} H_{p,<}$
At tropopause:	$T_{Trop} = T_0 + \Delta T + \beta_{T,<} H_{p,Trop}$
Above tropopause:	$T_{>} = T_{Trop}$

Determination of Air Pressure (for ISA Conditions at MSL $\Delta p = 0$)

$$\begin{aligned} \text{General:} \quad p &= f(T, \Delta T) \\ \text{Below tropopause:} \quad p_{<} &= p_0 \left(\frac{T_{<} - \Delta T}{T_0} \right)^{\frac{g_0}{\beta_{T,<} R}} \\ \text{At tropopause:} \quad p_{\text{Trop}} &= p_0 \left(\frac{T_{\text{Trop}} - \Delta T}{T_0} \right)^{\frac{g_0}{\beta_{T,<} R}} \\ \text{Above tropopause:} \quad p_{>} &= p_{\text{Trop}} \exp \left[-\frac{g_0}{R T_{\text{ISA,Trop}}} (H_{p,>} - H_{p,\text{Trop}}) \right] \end{aligned}$$

Determination of Air Density

$$\rho = \frac{p}{RT}$$

Determination of Speed of Sound

$$a = \sqrt{\kappa R T}$$

CAS/TAS Conversion

$$\begin{aligned} V_{\text{TAS}} &= \left[\frac{2p}{\mu\rho} \left\{ \left(1 + \frac{p_0}{p} \left[\left(1 + \frac{\mu\rho_0}{2p_0} V_{\text{CAS}}^2 \right)^{\frac{1}{\mu}} - 1 \right] \right)^{\mu} - 1 \right\} \right]^{\frac{1}{2}} \\ V_{\text{CAS}} &= \left[\frac{2p_0}{\mu\rho_0} \left\{ \left(1 + \frac{p}{p_0} \left[\left(1 + \frac{\mu\rho}{2p} V_{\text{TAS}}^2 \right)^{\frac{1}{\mu}} - 1 \right] \right)^{\mu} - 1 \right\} \right]^{\frac{1}{2}} \end{aligned}$$

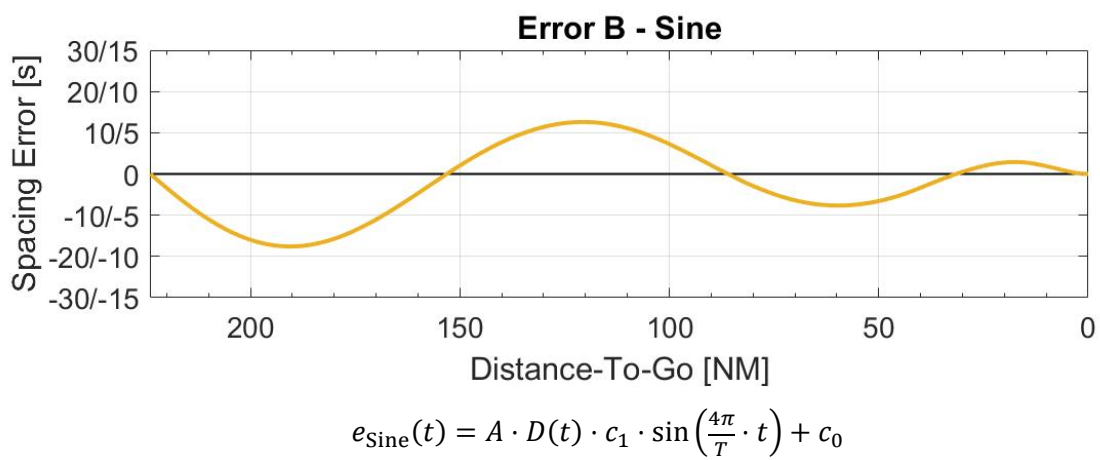
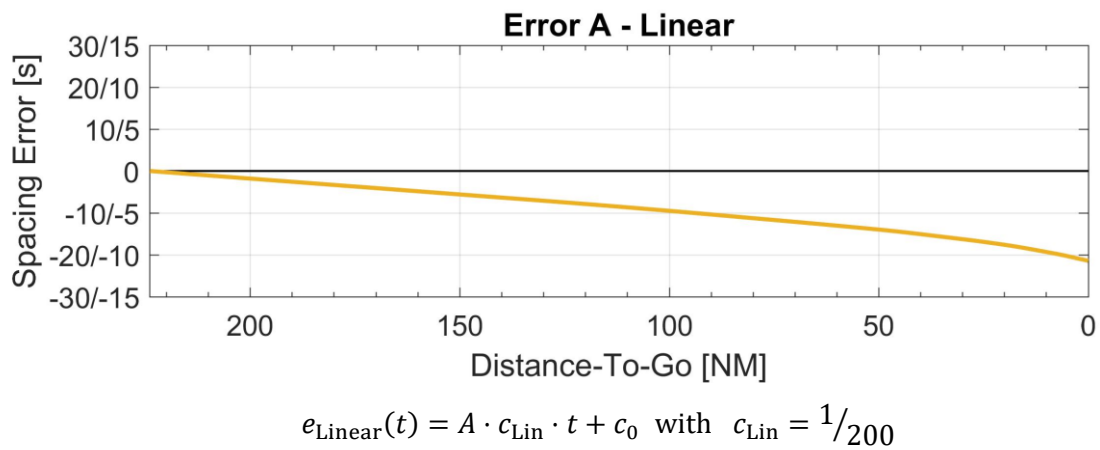
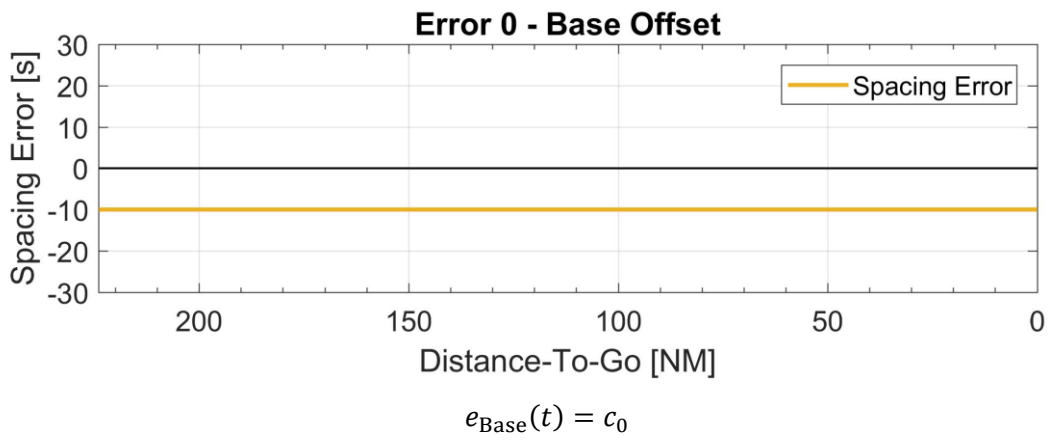
with

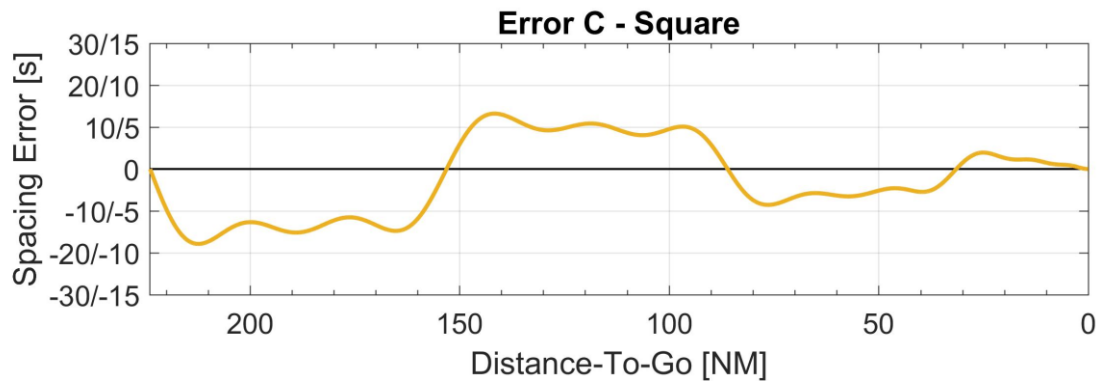
$$\mu = \frac{\kappa - 1}{\kappa}$$

Mach/TAS conversion

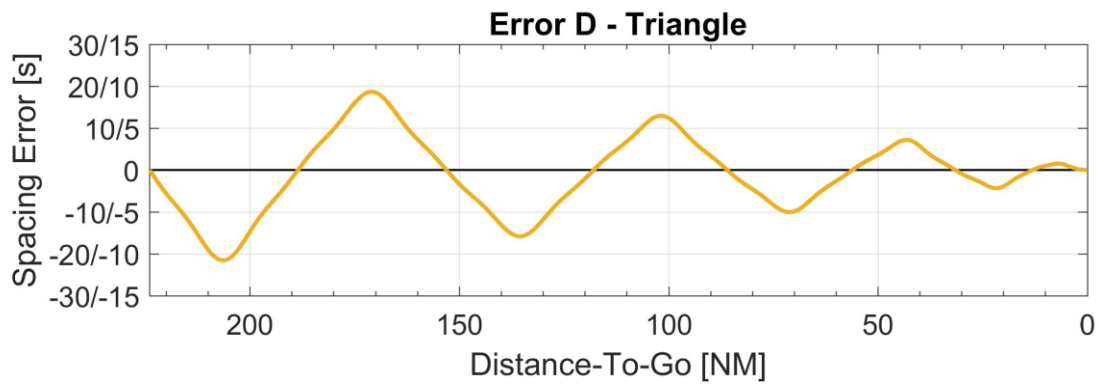
$$V_{\text{TAS}} = M \times \sqrt{\kappa R T}$$

APPENDIX B (ERROR PATTERNS)

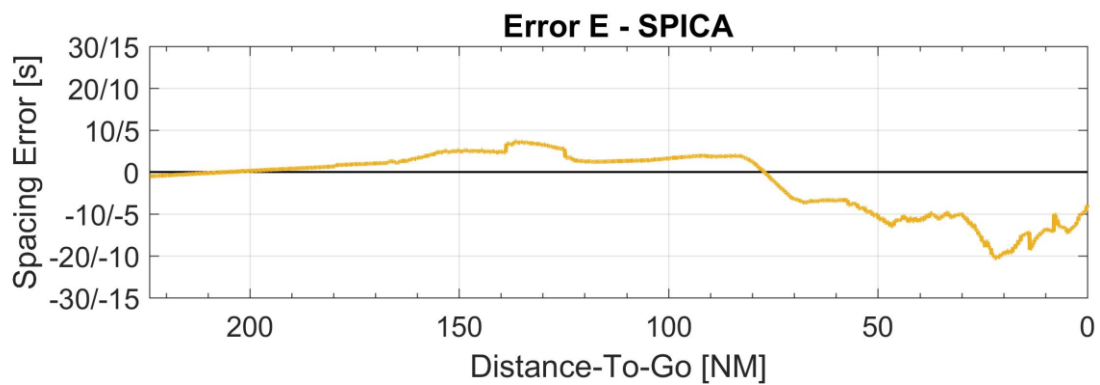




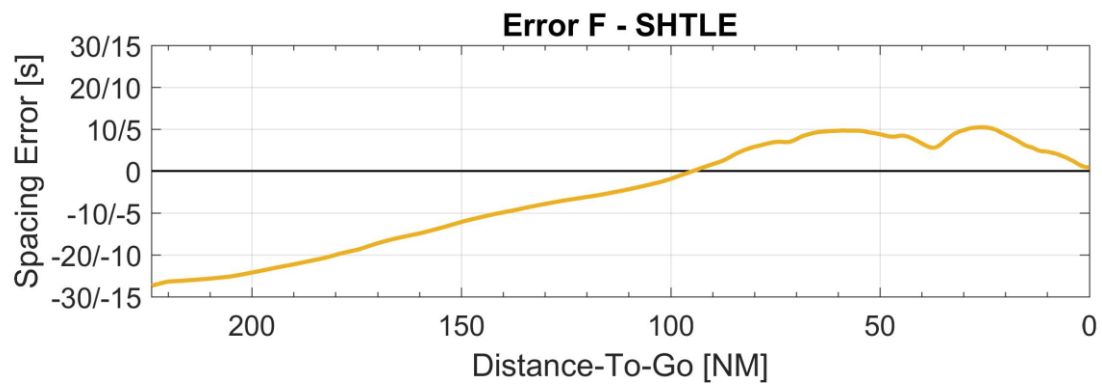
$$e_{\text{Square}}(t) = A \cdot D(t) \cdot c_1 \cdot \sum_{k=0}^2 \left[\frac{1}{2k+1} \sin \left((2k+1) \cdot \frac{4\pi}{T} \cdot t \right) \right] + c_0$$



$$e_{\text{Triangle}}(t) = A \cdot D(t) \cdot c_1 \cdot \sum_{k=0}^2 \left[\frac{1}{(2k+1)^2} \cdot (-1)^k \cdot \sin \left((2k+1) \cdot \frac{8\pi}{T} \cdot t \right) \right] + c_0$$



$$e_{\text{SPICA}}(t) = A \cdot e_{\text{Data}}(t) + c_0$$



$$e_{\text{SHTLE}}(t) = A \cdot e_{\text{Data}}(t) + c_0$$

with

$$c_0 = [-30, -20, -10, 0, +10, +20, +30][s] \text{ (Scenario I)}$$

$$c_0 = [-20, -15, -10, -5, 0, +5, +10, +15, +20][s] \text{ (Scenario II)}$$

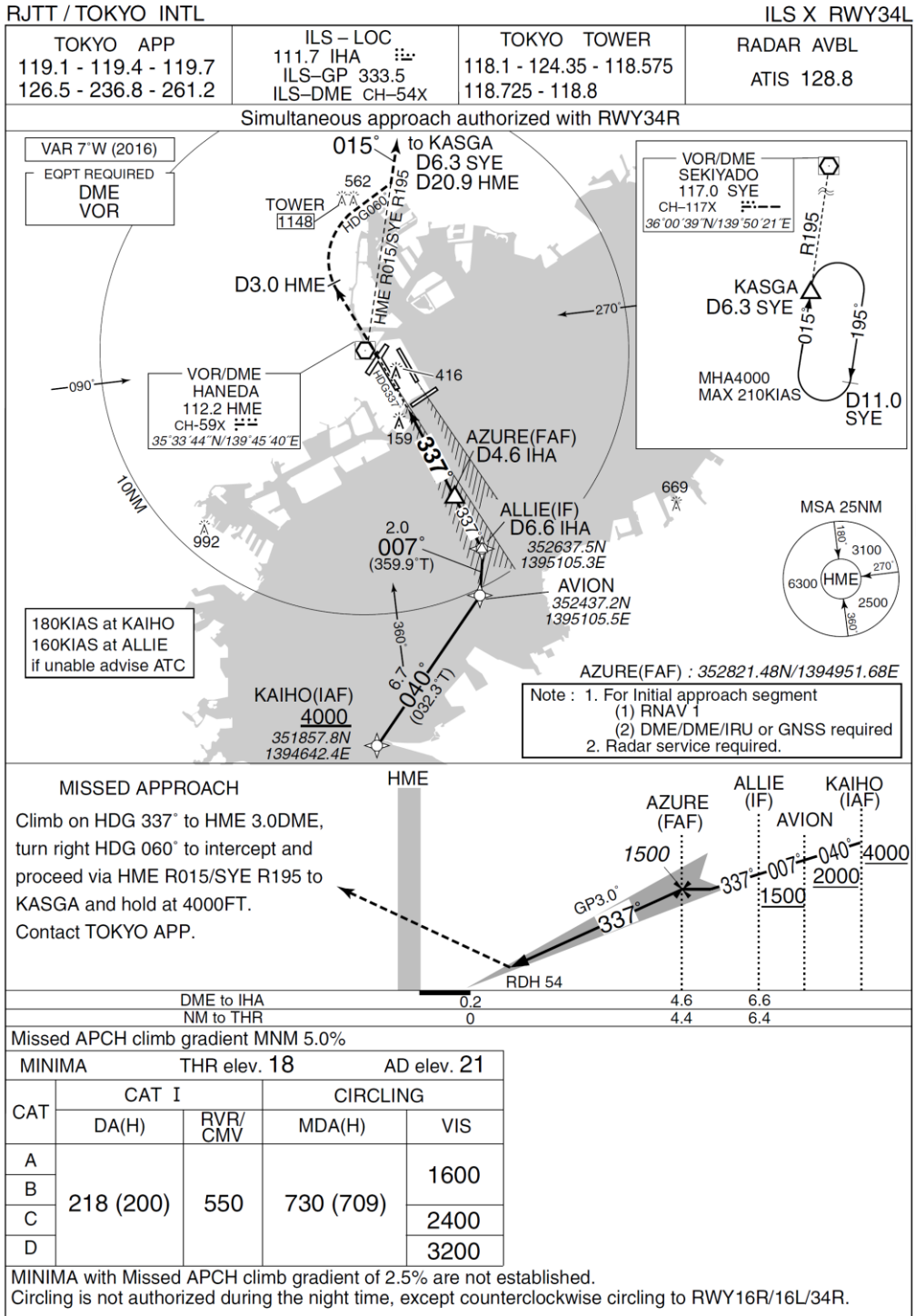
$$A = [-2, -1, +1, +2], c_1 = 10 \text{ s}, D(t) = \frac{T-t}{T}, T = 2146 \text{ s}$$

APPENDIX C (APPROACH PLATE RJTT ILS X RWY 34L) (50)

RJTT-AD2-24.61

AIP Japan
TOKYO INTL

INSTRUMENT APPROACH CHART



EXPIRED - DO NOT USE FOR ACTUAL NAVIGATION

APPENDIX D (INDEX)

A/P	(Autopilot)	7
A/THR	(Autothrust, Autothrottle)	7
A13	(ASTAR – Intended Implementation)	56
ABP	(Achieve-by Point)	8
ADS-B	(Automatic Dependent Surveillance – Broadcast)	7
AEM	(Arrival Expedition Margin)	42
ANSP	(Air Navigation Service Provider)	65
AP	(Action Point)	37
APC	(Action Point Dataset – Candidates)	41
APD	(Action Point Distance)	44
APM	(Action Point Dataset – Modifications)	41
ASG, Δ	(Assigned Spacing Goal)	10
ASPA	(Airborne Spacing)	1
AST	(Aircraft Simulation Technology)	89
ASTAR	(Airborne Spacing for Terminal Arrival Routes)	2, 11
ATA	(Actual Time of Arrival)	5
ATC	(Air Traffic Control)	5
ATCo	(Air Traffic Controller)	1
ATD-1	(Air Traffic Management Technology Demonstration 1)	2
BADA	(Base of Aircraft Data)	19
CARATS	(Collaborative Actions for Renovation of Air Traffic Systems)	1
CAS	(Calibrated Airspeed)	12
CCS	(Constant CAS Segment)	37
CDA	(Continuous Descent Approach)	18
CDO	(Continuous Descent Operations)	18
CGD	(Configurable Graphics Display)	8
CPDLC	(Controller Pilot Data Link Communication)	1
CPL	(Commercial Pilot License)	96
CRS	(Course)	32
CTD	(Constant Time-Delay)	12
DTG	(Distance-To-Go)	12
EFB	(Electronic Flight Bag)	8, 94
ELI	(Early/Late-Indicator)	15
ENRI	(Electronic Navigation Research Institute)	20
ESL	(End Speed Logic)	29
ETA	(Estimated Time of Arrival)	5

FAA	(Federal Aviation Administration)	2
FAF	(Final Approach Fix)	15
FAS	(Final Approach Speed).....	5
FCU	(Flight Control Unit).....	8
FDMS	(Flight Deck-based Merging and Spacing)	7
FIM	(Flight-deck Interval Management).....	1
FL	(Flight Level)	25
FMS	(Flight Management System).....	8
F+	(Fuel Improved Solution).....	78
FPA	(Flight-Path Angle)	18
FSI	(Fast/Slow-Indicator).....	15
ft	(Feet, 1 ft = 0.3048 m)	25
GANP	(Global Air Navigation Plan).....	1
GIM	(Ground-based Interval Management).....	1
GS	(Ground Speed).....	8
GUI	(Graphical User Interface).....	8, 14, 91
HITL	(Human-in-the-Loop)	2, 89
IAT	(Inter Arrival Time)	5
IATA	(International Air Transport Association)	3
ICAO	(International Civil Aviation Organization)	1
IFF	(Institute for Flight Guidance – Technische Universität Braunschweig)	89
IFR	(Instrument Flight Rules)	5
ILS	(Instrument Landing System).....	48
IM	(Interval Management).....	1
IMAC	(Interval Management Alternative Clearances)	14
IM-SP	(Interval Management – Speed Planning)	2, 35
IR	(Instrument Rating).....	96
ISA	(International Standard Atmosphere).....	50
kt	(Knot 1 kt = 1 NM/h)	5
LTD	(ASTAR – Limited Implementation, speed constraints enforced)	56
MCP	(Mode Control Panel).....	8
ME	(Multi Engine).....	96
MOEA	(Multi-objective Evolutionary Algorithm)	69
MOPS	(Minimum Operational Performance Standards).....	10
MPL	(Multi-Crew Pilot License)	96
MSL	(Mean Sea Level).....	61
NAS	(National Airspace System).....	1
NASA	(National Aeronautics and Space Administration)	2
ND	(Navigation Display)	7

NextGen	(Next Generation Air Transportation System)	1
NM	(Nautical Mile 1 NM = 1.852 km)	5
OMOPSO	(Optimized Multi-objective PSO)	68
OWN	(Ownship)	10
PF	(Pilot Flying)	95
PFD	(Primary Flight Display)	7
PM	(Pilot Monitoring)	95
PSO	(Particle Swarm Optimization)	67
PTP	(Planned Termination Point)	9
RJTT	(Tokyo International Airport – Haneda Airport)	3
RPD	(Reference Profile Deviation)	51
RSE, $e()$ *	(Remaining Spacing Error)	41
RWY	(Runway)	23
SD, σ	(Standard Deviation)	5
SESAR	(Single European Sky ATM Research)	1
SMPSO	(Speed-constrained Multi-objective Particle Swarm Optimization)	67
SOP	(Standard Operating Procedures)	101
SP	(IM-SP – Intended Implementation)	56
SPICA	(Spacing Time Intervals of Arrival Aircraft Conducting ASPA IM)	20
STA	(Scheduled Time of Arrival)	5
STAR	(Standard Terminal Arrival Route)	21
TAS	(True Airspeed)	19
TBO	(Trajectory-based Operation)	12
TMA	(Traffic Management Advisor)	5
TOD	(Top of Descent)	18
T+	(Time Optimal Solution)	78
TTF	(Traffic-To-Follow)	8
TTG	(Time-To-Go)	9, 43
TTN	(Time-To-Next Command)	92
TTR	(Time-To-React)	43
UPS	(United Parcel Service)	7
UTC	(Coordinated Universal Time)	27
V_{FE}	(Velocity – Flap Extension Maximum Speed)	102
V_{LS}	(Velocity - Lowest Selectable)	101
W_x	(Wind)	32